The effect of aeration on the maximum pressure during wave impacts on a horizontal overhang

K. P. van Gent

July 6, 2023

TU Delft

The effect of aeration on the maximum pressure during wave impacts on a horizontal overhang

An experimental and numerical study of the effect of aeration on the maximum impact on a horizontal overhang.

K.P. van Gent

to obtain the degree of Master of Science at the
Delft University of Technology

Student number:	4975219
Thesis committee	Dr.ir. P.R. Wellens
	Dr.ir. R.L.J. Helmons
	G. Bufalari
Date	July 6, 2023

Abstract

When waves break, air and water mix and small air bubbles are formed in the water, creating aeration. The mixture of air and water alters the behavior of the fluid. Traditionally, it has been assumed that aeration has a damping effect on impact, as exemplified by the use of air bubbles in the swimming pool below the Olympic 10m platform and during synchronized 10m platform jumps to reduce the force exerted on the swimmer's body.

However, in recent years, it has been found that this assumption does not hold true in all situations involving aeration. When treating aerated water as a non-compressible fluid, it does exhibit a damping effect on impact. However, when treating aerated water as a compressible fluid, the speed of sound of the mixture can actually change with implications for the propagation of density waves. This means that an aerated water impact can feature pressure oscillations that increase the force instead of reducing it. Consequently, hydraulic structures that have been or will be constructed with the assumption that aeration only has a damping effect, may be affected.

Understanding the effect of wave-induced aeration on a horizontal platform is crucial for the design of new hydraulic structures in a more efficient and cost-effective manner. This research aims to determine the maximum force experienced by a horizontal surface during an aerated wave impact. The investigation involves using a numerical method, followed by a series of self-conducted small-scale sloshing experiments. The simulations contribute in two ways: they aid in understanding the problem and the magnitude of forces acting on the experimental setup, and they assist in verifying the experimental results once the experiments are completed. For the experiments, a new tank layout has been designed to facilitate the creation of aerated water inside the tank. The tank is used for conducting experiments where aerated wave impacts are compared to non-aerated wave impacts for different wave impacts. The experimental results confirm both the effect of pressure reduction due to aeration when the aeration level is near to 4%, as well the effect that the maximum pressure can increase for aeration levels between 1 and 2%.

Preface

The completion of this master's thesis marks the culmination of an extensive journey of exploration into the fascinating field of aerated wave impacts on a horizontal structure. It has been a challenging yet immensely rewarding endeavor, made possible with the invaluable support and assistance of numerous individuals.

I would like to begin by expressing my sincere gratitude to Peter, my supervisor, for his unwavering support and dedication throughout this thesis. He consistently made time for me, even during unconventional hours, and his guidance has been invaluable in shaping the direction of my research.
I am also incredibly grateful to my girlfriend for her endless patience, willingness to listen to my dilemmas, and assistance with proofreading. Her unwavering support has been a constant source of motivation and inspiration.
Furthermore, I would like to extend my heartfelt thanks to all the individuals working at the towing tank facility. First and foremost, their warm hospitality in providing access to their testing facility has been greatly appreciated. Additionally, their involvement in the construction process, collaborative brainstorming for designs, and overall engagement during the experiments have significantly contributed to the success of this research.
Lastly, I would like to express my appreciation to my housemates, family and friends. Their understanding, encouragement, and support have been instrumental in enabling me to focus on this thesis and overcome the challenges that arose along the way.

The contributions of these remarkable individuals have played an integral role in the completion of this thesis. Their unwavering commitment, assistance, and encouragement have been invaluable, and I am truly grateful for their involvement. It is my sincere hope that this thesis contributes to the existing body of knowledge, stimulates further research, and fosters a deeper understanding of aerated wave impacts on horizontal structures. May it serve as a stepping stone for future studies and inspire others to delve into this captivating field.

Koen van Gent
Delft, July 2023

Contents

List of Figures

List of Tables

1 Introduction

For multiple centuries man-made objects are exposed to waves. Over the years, these objects have become significantly larger. Furthermore, extreme weather events happen more frequently and have become more severe. Severe weather events often result in bigger waves. The change in weather and size of the exposed structures requires better insight into the strength of these structures and the forces on the object caused by the waves.

A set of structures that is already extensively studied in the context of wave forces, is the set of structures that can be simplified to a vertical wall. This set contains for example dikes, locks, platform legs or a ship hull. Research on this set of simplified structures provides, for example, the maximum force on a vertical wall under different circumstances.

However, not all structures can be simplified to vertical wall. Take for example offshore platforms, flood gates, coastal protection, and platforms of offshore wind turbines. These structures not only exist of a vertical wall but also contain a horizontal overhang. The force caused by a wave on such a structure consists of two parts: a horizontal force on the vertical wall and a vertical force on the horizontal overhang. A study on wave forces that is limited to the force on a vertical wall does not provide sufficient results for such a structure. For that reason, another simplification is used for structures with a horizontal overhang. This simplification is a reversed L-shape (Γ) and is called: a vertical wall with a horizontal cantilever slab.

In contrast to the vertical walls, the amount of research on vertical walls with a horizontal cantilever slab is limited. The main reason for this is that research on a structure with an overhang is a relatively new research topic from only the last two decades. This thesis focuses on the vertical walls with horizontal cantilever slab, with a special interest in the vertical force acting on this horizontal overhang.

Although it is not much, there is certainly literature available that focuses on vertical walls with horizontal cantilever slab [27]. The main difference between the real situation and the models or the laboratory scale experiments on vertical walls with horizontal cantilever slab, is that the aeration created by breaking waves is not taken into account. The assumption is often made that the effect of aeration could be neglected due to the damping effect. Research of the past decade proved [46] that incorporating the effect of aeration in research on wave impacts is crucial to ensure a comprehensive understanding of the forces, pressures, and structural response that a structure experiences. By accounting for aeration, researchers can enhance the accuracy of their studies and make informed decisions regarding the design and performance of coastal or offshore structures.

For this study the specific focus is the influence of aeration on the maximum wave force on the horizontal overhang. This is relevant because breaking waves can contain up to 14% aeration[7]. The influence of aeration on a wave impact can vary, depending on the specific conditions and characteristics of the waves and the aerated environment. Generally speaking, aeration can have both positive and negative effects on wave impacts.
On the positive side, aeration can help to reduce the impact of waves by introducing air into the water, which can absorb some of the wave energy and reduce the force of the impact. This effect can be particularly beneficial in coastal environments where structures such as seawalls or breakwaters are used to protect against wave impacts.[2] [31].
On the negative side, aeration can also create turbulence and instability in the water, which can actually increase the force and impact of waves in certain conditions. For example, in areas where large amounts of air are entrained into the water by waves breaking over rocks or reefs, the turbulence created by the aeration can increase the force of the waves and lead to more intense impacts.[19] [44]

In this research, the interest is on the negative influence of aeration on the maximum wave force. Namely, how aeration will have an increasing effect on the maximum wave fore. In the past decade, the effect of aeration was not known. Therefore, man made the assumption that aeration would have a cushioning effect. Because it has been proven that aeration does have a negative side as well [19], there is relevance for this research on the effect of an aerated wave impact on a horizontal overhanging cantilever slab.

1.1 Literature study

The research on the effect of aeration on the maximum wave force on a vertical wall with a horizontal cantilever slab starts with a summary of the related work. Because of the novelty of the combination of these subjects, there is no literature that covers all subjects in one. The related work is therefore separated into four subjects that cover the earlier main research topics. These four subjects, or pillars, are: Impacts on vertical walls , Impacts on Horizontal overhangs, Impacts with aeration and scaling with aeration.

By splitting the research topic into 4 different pillars, the most knowledge will be efficiently gathered during this thesis. At the end of the chapter the literature will be summarised into the knowledge gap from which the novelty statement and the research question will be formulated.

1.1.1 Literature impact on a vertical wall

Forces on vertical walls are the most simple versions of forces on a surface caused by waves. This situation is interesting for this research by the extensive amount of literature that is available on the topic. The qualitative and quantitative determination of wave loads on vertical walls has already been examined intensively in the past decades [10]. Research on vertical walls uses different types of research methods, such as modeling [50], analytical solution [39], full-scale test [23], and lab-scale test [30]. Besides that, also different types of waves are investigated, such as breaking waves [35], flip-through waves [30], irregular waves [47], and violent breaking waves [3].

This shows that many different types of research have been performed since Bagnold (1939) [41] proved that wave impacts can be evaluated with pressures. This was also the first time that peak pressures were shown and the total wave impact was known since then as the integral of pressure over the duration of the impact. Although pressure measurements vary between identical wave impacts, the integral of pressure over the duration of the impact the pressure-impulse, is a more consistent measure of wave impact.

When examining the impact of air on wave behavior, it was noticed that the greatest pressure magnitudes occur when the air cushion is small, but not completely absent. Secondly, despite significant variations in maximum peak pressures, the region enclosed by the pressure-time curve, referred to as pressure-impulse, remains remarkably consistent. The pressure impulse-impulse can be expressed by $P = \int_{t_d} p\,dt$, with P the pressure impulse [Pa s] , p the pressure in [Pa] and t_d the impact duration [17]. Regarding the vertical structure, a notable characteristic is that the wave's kinetic energy is halted at the wall's surface. As a result, this energy is either reflected or transformed into vertical motion, which can cause overtopping [26]. Over the past few decades, researchers have extensively studied the qualitative and quantitative aspects of wave loads on vertical structures. Oumeraci [35] has compiled previous work on wave loads and proposed a method for assessing both quasi-static and impulsive loads. This study aims to verify the applicability of the pressure impulse theory to vertical hydraulic structures that possess overhangs.

1.1.2 Literature impact on a horizontal overhang

The current state of the art lacks research on structures with an overhang. In the previous century a paper was published on forces beneath a horizontal surface [49]. This was one of the first papers that covers the topic of horizontal overhang. Further a few experimental studies on vertical forces on a horizontal overhang have been performed [28] [25]. And validation research has been done on the applicability of pressure-impulse theory [17] [18].

Von Karman (1929) [45] is the founder of the fluid-structure interaction. With his research about landing seaplanes, his work was also the first in the vertical impacts on a flat horizontal surface. Not only a full-scale test has been performed, but also a first try of an analytical formula was made. This is the basis of all the following fluid-structure interactions. This fluid-structure interaction in the years that followed was mainly about ship hulls-wave interactions and wave impacts on a vertical wall structure. Due to a lack of good estimates of upward impacts D.J.Wood and D.H.Peregrine [49] considered an article about upward impacts on a horizontal plate. This is the first research that considers a combined problem of structure that consists of a vertical and a horizontal part. They used an analytical approach that consists of a pressure impulse method vertically structure. Using existing and previously tested pressure impulse method that was already validated and theoretically approved [39] [11] [12] [13]. They found that when the water becomes more shallow, the impulse is more violent.

G. Cuomo (2009) [15] focus was on vertical forces on a horizontal plate. Whereas previous research on wave-in-deck loads mainly concentrated on wave forces on structural members of offshore structures [1]. The main focus point here is the coastal bridges instead of the previously researched jetties and piers, that had a relatively small horizontal surface. Using a scaled test in a wave basin, it was the first time that wave loads on the longitudinal beams were also measured. Cuomo developed an ad-hoc prediction method. This method should be valid for static and impulsive loads on the horizontal deck of bridges. The compression law of Bagnold–Mitsuyasu [41] is used to complete this research on waves underneath the bridge deck when air is involved in the impact. This takes the importance of the role of air entrapment into account when scaling is used. Serinaldi (2011) [43] continued the research of Cuomo and added to this previous research the interaction between the impact frequency of the incoming wave and the natural period of the bridge structure. This is because the interaction is often neglected. Serinaldi concludes that with impulsive deck loads, the vertical force on the horizontal deck can exceed the weight of the bridge deck itself. causing uplift forces that can lift the deck and cause damage to the whole structure. Assuming a uniform pressure distribution did result in an overestimation of the vertical loads.

Kisacik (2011) [26] Wanted to find a design tool for violent water wave impacts on a vertical wall with a horizontal overhang. The first big result was that the largest peak pressure on the vertical part was at mean sea level, and the largest peak pressure of the horizontal overhang was in the corner with the vertical support. The assumption that Serinaldi [43] used that there is a uniform pressure distribution is no longer valid. Due to the irregular waves, Kisacik found that the impact pressures are non-repeatable under identical conditions. This is due to the turbulence that is left behind by a wave, The interaction with the reflecting wave, and its due to the air that is trapped in the wave.

Adversely to the previous papers, the follow-up research of Kisacik [27] did not only include the vertical part but research on both the vertical and the horizontal impact. The only research that has combined the two topics before are Wood and Peregrine [49]. In this research, the wave height, water depth, and wave period were varied and compared. This research concludes that the effect on the maximum pressure of the wave period is negligible compared to the effect of change in wave height and water dept. In the experimental follow-up research, Kisacik [28] did an experimental study to extend the knowledge of the pressure distribution. In this paper, the location and the magnitude of the maximum pressure are determined. Kisacik introduced non-dimensional terms. This is so the analysis could be done dimensionless. For the vertical part, the term is z_{max}/h_s and H/h is wave height/ water dept. The result of this analysis is that the p_{max} is still located at the closed corner. This research shows that the magnitude of the maximum pressure is sharply below $10\rho gH$ between $x/h_s = 0.8 - 1$.

The two most relevant results for this thesis of Kisacik are that the maximum pressure underneath a horizontal overhang is near the vertical support (the closed corner). The second most relevant finding is that the variation in period has significantly less effect on the maximum pressure than the water dept and wave height.

Chen (2019) [10] developed a method to design hydraulic structures exposed to impulse wave impact. With the aim to come up with a standard prediction method. The reason behind this is that a lot of hydraulic structures have to be replaced or restored in the coming years. This not only emphasizes the research of Chen but also the relevance of this thesis. Using the Weibull curve to extrapolate the water levels, these expected values could be analyzed. Concluding the research not only the peak impact force must be used for the extreme value distribution, but also the Impact-related impulse. They can be recombined to get an even better prediction for the impact forces on an overhanging structure. resulting in a method with a good estimation of the forces, when the structure is exposed to a wave impact. Almeida (2020)[17] aims to fill the knowledge on the impact of a non-breaking standing wave. Vertical structures with an overhang have only been studied with breaking waves.

1.1.3 Impacts with aerated water

Air phenomena like Aeration or entrained air, are known for their cushioning effects on impact. This has been proven by D.H. Peregrine[16]. He did one of the first researches to the cushioning effect of aeration. From this research, it became clear that there will be an reduction of peak pressure, due to the comprehensibility of the air water mixture. Even with a very small air percentage the reduction of impact pressure is large[40].
Peregrine also mentions that the standard choice of scaling will be Froude scaling, but this does results in extremely large prototype forces.

This knowledge has been extended by G.N. Bullock [7] who made an relationship between the violence of the impact and the level of aeration and has proved the previous work of Peregrine with experimental results. This relation ship was made with both laboratory and field test. This were one of the first field test with aeration, and the experiments of Bullock where thereby the first to confirm the results of Peregrine [16], with matching results for the field and theory tests. This means that they both showed that the cushioning effect of air becomes more relevant if the violence of the waves getting bigger.
Further Bullock discovered that air will escape quicker from fresh water than from sea water.

The role of air in water was only treated as a cushioning effect, where Wood [50] was the first to show that it can increase the pressure near the wall as well. Later this turned out to be scale dependent as well. M. van der Eijk [22] continued with this research and confirmed these findings. According to van der Eijk [19] the cushioning effect is not the only effect to encounter for. The compressibility that is neglected in previous researchers made only the cushioning effect possible. If the compressibility is included, this makes it possible that the acting forces will increase, because the impact pressure has now a longer lasting time. Also the resonance between the oscillating air pockets and generated pressure waves. Additionally, due to the extension of the area, created by the deformation of an air bubble, the forces can increase in magnitude to [5] [8] [34]. The current state of the art for aerated wave impacts is a combination of the different papers of Bredmose[5]. The novelty of these papers is the different breaker types in combination with a low and a high level of aeration. This is tested on a vertical wall from perfectly vertical to a 27-degree incline. They found that the putting the vertical wall at the maximum slope, a reduction of 50% can be found in the impact.[9]

1.1.4 Literature scaling of aerated water

For many coastal and offshore structures scaled model tests are used. By default, these model tests are performed according to Froude Scaling. In the case of Froude Law scaling, the same scale between the experiment and real size will be used for the dimensions and the pressures. For these conversions between a model test and a full-scale test, where gravity will be the dominant force, Froude law scaling will be used. The Froude Law can be used for 2 objects with the same geometry. For those scaling, objects with the same relation between the inertia force and the gravitational force, also have the same Froude number. [7]

$$\frac{u_A}{\sqrt{\lambda_A * g}} = \frac{u_B}{\sqrt{\lambda_B * g}} \tag{1}$$

Here, U is the characteristic velocity, λ is the characteristic length and g is the external field. For calculating the pressures in the new system, according to the Froude scaling will be:

$$p_A = \frac{\rho_A * \lambda_A}{\rho_B * \lambda_B} * p_B \tag{2}$$

For some situations, Froude Law scaling will not be sufficient and will lead to huge results. One of these cases, when it will not be sufficient, is when the max pressure $P_{max} > 318kPa$. In this case, the Bagnold-Mitsuyasu scaling law will be suggested[3]. For aerated water impacts and a maximum pressure $P_{max} < 318kPa$ Froude scaling will be sufficient. [16][15] [14]

For wave impacts with entrained air and a $P_{max} > 318kPa$, the scaling could be a bit more complex. For these types, Cauchy law scaling can also be used. Because of the scale of a bubbly liquid the speed of sound is not constant. Hence the speed of sound in aerated water is the frequency and is dependent on the bubble shape. So Pereregrine and Thais [16] made the assumption to treat the aerated water as a homogeneous aerated medium. To include the comparability of the homogeneous aerated water the elasticity factor K, is introduced in the Cauchy scaling law.

$$K = -\frac{dp}{dV/V} \tag{3}$$

Here V is the original volume and dV is the increase in volume after introducing aeration to the medium. The Cauchy law scaling will use the ratio between the inertia force and the elastic force.

$$\frac{\rho_A * {u_A}^2}{K_A} = \frac{\rho_B * {u_B}^2}{K_B} \tag{4}$$

This scale relation will lead to a pressure formula:

$$p_A = \frac{K_A}{K_B} * p_B \tag{5}$$

For aerated wave impacts the Froude law can be used, but it would be likely to have an overestimation in the pressures. For this reason, Bullock [7] suggests the Cauchy scaling law if the pressures will exceed a $P_{max} > 318kPa$

1.2 Knowledge gap

For a long time, aeration was known as a medium that had a cushioning effect on wave impacts against hydraulic structures. Due to the simplification, that aerated water was treated as an incompressible medium. This made previous research conclude that aerated water had only a cushioning effect.

Treating aerated water as a compressible medium had an impact on the dynamics of structures. This makes it possible that the frequency of the medium can change. A changing frequency can interfere with the eigenfrequency of the structure, resulting in increasing forces. Recent research [20] shows that there can be an increase in pressure when treating aerated water as a compressible medium. Also on a vertical wall and for the phenomena of green water on ships[19], aerated water impacts have been investigated.
Now for the case of a structure with an overhang, the effect of treating an aerated wave impact as a compressible medium on the maximum impact is not clear. After numerical simulations [5][19], experiments [44] on the effect of impact with aerated water, analytical investigation on vertical walls [3], simulations [37] and experiments [23] in overhang impacts. The knowledge gap is defined as the impact of an aerated wave on a structure with a horizontal overhang.

The need for this research is summarised that it is shown for different types of structures, that the simplification of incompressibility can lead to underestimated peak pressures and forces. For all the offshore located structures with a horizontal overhang, this research will contribute to a better understanding of the pressures and forces, and prevent designing unsafe designed structures. Also preventing that structures have to undergo major refits before the end of their designed lifetime or have to be designed with too large safety factors. Which in both cases will lead to an extreme amount of costs. Taking offshore wind turbines, are one of the most used structures with a horizontal overhang. At the end of 2020, 25GW offshore wind power was generated with 5402 wind turbines[48]. To reach the climate goals, just The Netherlands, aims to reach 70GW of offshore wind in 2050[36]. Taking the total offshore wind power of Europe to 300GW. This will mean that over 60000 wind turbines have to be placed offshore. Not all these turbines will be installed with mono-piles, also floating wind turbines will most lily be used. But still, the relevance to getting a better understanding of how aerated wave impact will have an effect on the maximum pressure is very useful.

1.3 Novelty

The novel part of this research is filling the gap of the missing research on aerated wave impacts on a structure with a horizontal overhang. Where Peregrine(1996)[16] did research about the effect of treating aerated water as a compressible medium on a vertical wall to see what the maximum pressure would be on this vertical wall. Bredmose [3] added to this the dimensionless approach, but tested it again on a vertical wall to see what the pressure development would be on a vertical wall. This research will treat the aerated water, as the previous two, like a compressible medium. But the experiments will be on a horizontal overhang instead.

The most recent developments in the research of aeration were at the TU Delft. Van der Eijk [19] did research on a falling object in homogeneous aerated water.

The follow-up research on this last development is filling the knowledge gap of what will happen to the maximum pressure when a wave hits an object instead of an object hitting stationary water.

So this research will aim to add the location and the maximum pressure of an aerated wave impact on a horizontal overhang construction.

Due to the complexity, numerical simulations can, and will help to understand the problem, but experiments will be needed to validate these results.

The laboratory experiments will be done with a new design. Adding aeration to a sloshing experiment is not done before. This in combination with focusing on a wave impact on a vertical overhang makes not only the research, but also the experimental setup contribute to the novelty of this research.

1.4 Research question

What is the effect of aeration on the maximum vertical force on a horizontal overhanging cantilever slab, caused by wave impacts?

1.4.1 Sub questions

For answering the main research question, the following sub-questions are formulated.

- How are the frequency, water height, wave height, and wave pressure related to each other?
- What is the expected maximum pressure on the overhang without the effect of aeration based on the simulations?
- What is the maximum pressure on the overhang without the effect of aeration?
- What is the effect of aeration on the maximum pressure on the overhang?

2 Numerical simulations

In order to address the research inquiry, we intend to conduct both simulations and experiments. This section will be dedicated to the simulations. A simulation study aims to replicate real-world situations where a wave enters the vertical wall with a horizontal cantilever slab.

Simulations are relevant for several reasons. First of all, a simulation study is used to estimate the forces on the structure. This gives insight into the scale of the forces for the experiment. Also, with multiple simulations, it is possible to find the relation between the input parameters such as the frequency, and the output parameters such as the wave forces. It is easy and fast to obtain multiple results from a simulation, relative to a real-life experiment. The results from the simulation study will be used to choose the optimal setup for the real-life experiment. This makes the combination of a simulation study and a scaled experiment efficient and prevents the experiment setup from damage from too large a force on the structure.
The mathematical model employed to represent the fluid motions is based on governing equations. This mathematical model is an approximation of the reality. The results of the simulations are theoretical results that serve as validation for the experiment. While the mathematical model provides a strong representation of reality, it is important to acknowledge that it will never perfectly emulate the actual situation. That is the reason why the simulations are combined with the experiment.

The first part of this section encompasses comprehensive background theory concerning the mathematical models intended for simulation purposes. In Section 2.1 it is explained that the dynamics of fluids can be described by the governing equations. The execution of this mathematical model is feasible using a program called ComFLOW. The general explanation of ComFLOW is included in Section 2.2.
In Section 2.3, the specific simulation setup that will be used for all experiments in this thesis is presented. Using this specific setup, the input parameters and the input signal are explained in depth in Section 2.3.1 and Section 2.3.2 respectively.
Section 2.4 contains the theory about the Transfer function, which relates the frequency to the maximum wave height. The final theoretical topic to be elucidated is the return period in Section 2.5, which contains the probabilistic computation of a wave height with a certain return period.

The second part of this section states and explains the specific simulations that will be executed in this thesis. In Section 2.6, each of the five sets of simulations is described in terms of their objectives, configuration, and relation to theory. In Section 2.7, the intermediate results of certain specific simulations are presented. These obtained results serve as the basis for defining the experimental setup and input parameters. For that reason, the intermediate conclusion is also included in **??**..

2.1 Governing equations

The numerical method in ComFLOW is based on governing equations for a one or two-phase flow. In general, fluid motions are governed by the Navier-stokes equation. The Momentum and continuity equations are used to describe a Newtonian fluid's behavior. For calculations, the Navier-Stokes equations will be reduced by assuming some simplifications. In the simulations, a two-phase flow will be used. The main difference between the one and two-phase flow for the used simulation is that ComFLOW sees the air as an empty medium in the first case, or it sees the air as a gas with a density and viscosity in the second case.

2.1.1 Mathematical model for 1-phase flow

The Navier-Stokes equation describes the fluid motion in domain Ω, with the boundary S and a normal vector $\mathbf{n}$. This forms the three-dimensional domain where mass conservation is applied. The mass conservation for a 1-phase flow is given by the formula:

$$\nabla * \mathbf{u} = 0, \tag{6}$$

where u is the three-dimensional velocity vector. The conservation of momentum for a 1-phase flow is given by

$$\frac{\partial \mathbf{u}}{\partial t} + \mathbf{u} * \nabla \mathbf{u} = -\frac{1}{\rho}\nabla p + \frac{\mu}{\rho}\nabla * \nabla \mathbf{u} + F. \tag{7}$$

In this formula, the density is ρ, the pressure is denoted by p, the dynamic viscosity is denoted by μ and the F represents the external forces [33]

Boundary conditions are needed to solve the Navier-Stokes equation. For a 1-phase flow, the boundary conditions needed are those for the solid boundaries and the free surface. For the solid boundaries it is said that no fluid can go through this boundary and due to the viscosity it will stick to the wall. This gives the fluid particles at the wall no speed $\overrightarrow{u} = \overrightarrow{0}$. This is not only valid for solid boundaries, also solid objects, like the horizontal overhang, will have these boundary conditions.

For the free surface boundary conditions the position can be given by $s(x,t) = 0$. Using this representation for the position, the free surface displacement is given by:

$$\frac{Ds}{Dt} = \frac{\partial s}{\partial t} + (u * \nabla)s = 0 \tag{8}$$

Taking the continuity of normal and tangential stresses, this leads to the boundary conditions for the free surface for a 1-phase flow of

$$-p + 2\mu\frac{\partial u_n}{\partial n} = -p_0 + 2\sigma H \tag{9}$$

$$\mu(\frac{\partial u_n}{\partial t} + \frac{\partial u_t}{\partial n}) = 0 \tag{10}$$

with u_n as the normal velocity component and u_t the tangential velocity component

Inside the domain, the force on an object can be determined. In real-life situations, the force component of a fluid-structure interaction exists in two parts: a shear force part and a pressure force part. In ComFLOW, only the pressure force part is used, because the shear force is almost negligible in most cases. hence the formula for the force calculation is given by

$$\mathbf{F}_p = \int_S p\,\mathbf{n}\,dS, \tag{11}$$

where F_p denotes the pressure force, S is the boundary of the object, and p is the pressure.

2.1.2 Mathematical model for 2-phase flow

The difference between a 1-phase flow and a 2-phase flow is that a 2-phase flow does not only have a *incompressible* viscous fluid e.g. water. But also a *compressible* viscous gas e.g. air. The conservation of mass is given by

$$\int_{\Omega} \frac{\partial \rho}{\partial t} d\Omega + \oint_{S} (\rho \mathbf{u}) * \mathbf{n} dS = 0 \tag{12}$$

All the bold symbols are representing a vector. For the case of $\mathbf{u}$ it is: $\mathbf{u} = (u, v, w)^T$. By applying the Gauss theorem, the conservation of mass for a 2-phase flow can be rewritten as

$$\frac{\partial \rho}{\partial t} + \nabla * (\rho \mathbf{u}) = 0 \tag{13}$$

This is called the conservative partial differential form of Equation 12. Here $\mathbf{u}$ is still the vector $\mathbf{u} = (u, v, w)^T$.

A procedure similar to the mass conservation procedure can be applied to the momentum equation. The conservation of momentum can be written as

$$\frac{\partial (\rho \mathbf{u})}{\partial t} + \nabla * (\rho \mathbf{u}\mathbf{u}) + \nabla p - \nabla * (\mu \nabla \mathbf{u}) - \rho \mathbf{F} = 0 \tag{14}$$

In which μ is the dynamic viscosity, p represents the pressure and $\mathbf{F}$ denotes the external forces e.g. the gravitational force. In the case of a 1-phase flow, the assumption is made that the density is constant.

The boundary conditions for a 2-phase flow are in comparison to the 1-phase flow not near the fixed boundaries and the free surface, but only at the fixed boundaries. Since a 2-phase flow is about an incompressible fluid and a compressible gas, there will not be a boundary but an interaction between the two. At the fixed boundaries the conditions will be the same as the one for the 1-phase flow. That is, no flow can go through the boundary and due to the viscosity, the fluid particles at the wall will stick and therefore have no velocity: $u = 0$ at fixed boundaries. But at the free surface, the forces describing the action between the two are described in the $\mathbf{F}$ component of Equation 14.

The force calculation with a 2-phase flow is equal to the calculation described in Mathematical model for 1-phase flow. This results in the same equation as for a 1-phase flow, repeated below for convenience,

$$\mathbf{F}_p = \int_S p \, \mathbf{n} \, dS, \tag{15}$$

where again, F_p denotes the pressure force, S is the boundary of the object, and p is the pressure.

2.2 ComFLOW

For the numerical simulations, the program ComFLOW is used. ComFLOW is a user-friendly and validated finite volume method. This numerical tool is originally developed to study the sloshing effects of spacecraft fuel [33]. This research was performed by the University of Groningen. Later the numerical tool was further extended with a more detailed way to model the free surface effect in collaboration with the Maritime Research Institute Netherlands (MARIN)[32]. Currently, the numerical tool is not only suitable for fuel sloshing but it can now also be used in the offshore market to model green water and wave impacts. The method that is used by ComFLOW solves the momentum and continuity equation while using a viscous incompressible liquid free-surface flow discussed in Governing equations.
A limitation of the numerical approach is that it is an approximation of reality, which always includes numerical errors. Additionally, the use of ComFLOW has one main limitation for this research: aeration can not be modeled in ComFLOW. Hence the results will only verify the non-aerated wave impacts of the experiments. This means that the ComFLOW will verify the non-aerated wave test and the aerated wave test will be compared only to other aerated wave impact tests.

2.3 Simulation set up

The setup for the simulation is designed to represent the sloshing rig, which will be used for real experiments. This setup consists of a rectangular tank filled with water. In the tank stands a vertical wall with a horizontal cantilever slab, see Figure 1. The size of the tank is equal to the size of the sloshing tank. The size in each dimension is presented in Table 1.
The domain of the tank is closed, which means that the boundary conditions at the outside borders of the domain are the no-slip conditions and the fluid velocity is zero at the boundary relative to the wall. Also, it is defined that no water can enter or exit the tank via the four domain walls by assuming the no-leak condition.

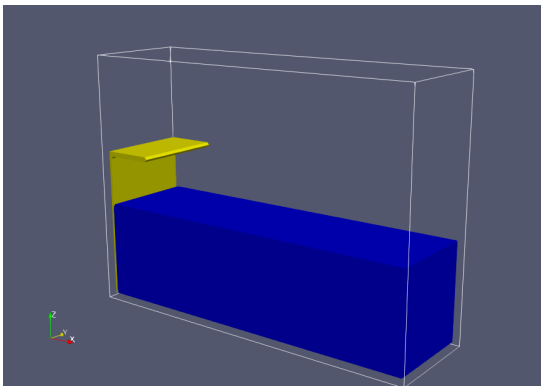

Figure 1: In this 3D image, the ComFLOW setup is visualized. The horizontal overhang is placed at a height of 300mm and has a length of 100mm. The water height will be variable during the simulations and is currently at 200mm

x_{min}	x_{max}	y_{min}	y_{max}	z_{min}	z_{max}
0.000	0.700	-0.500	0.500	0.000	0.496

Table 1: The position of the vertices of the simulation tank domain in meters.

The horizontal overhang is placed at a height of 0.300 meters and has a length of 0.100 meters, see Figure 1. The overhang consists of two building blocks. These blocks are defined in ComFLOW as 3D bricks via the file *geometry.in*. The first and second bricks represent the vertical and horizontal parts of the structure respectively. The structures are defined such that the boundaries are closed. As a consequence, the fluid interacts with the structure as it is one solid structure.

In order to obtain wave forces on the horizontal overhang, the water needs to hit the overhang. This is obtained by moving the tank in the x direction. When the tank is moved in the x direction, the water will be moving as well and waves will appear. With certain specific movements, these waves will hit the horizontal overhang and thereby will cause a force on the overhang of the structure.
The movements of the tank and the fluid dynamics depend on certain input parameters. Based on these input parameters, the movements of the tank are computed in ComFLOW. This will be explained in Figure 26b. The dynamics of the fluid in the tank are computed in ComFLOW through a finite volume method that is related to the governing equations. Therefore, by defining all the input parameters, the simulations can be conducted using ComFLOW.

Simulation set up with the aeration stones The objective of this thesis is to determine the effect of aeration on the wave force on the horizontal overhang. Unfortunately, it is not possible to simulate the aeration using ComFLOW and it is only possible to investigate this effect with the experiments.
To aerate the water for the experiment, aeration stones are placed at the bottom of the sloshing tank, see Figure 2b. The size of the aeration stones is presented in Table 2.

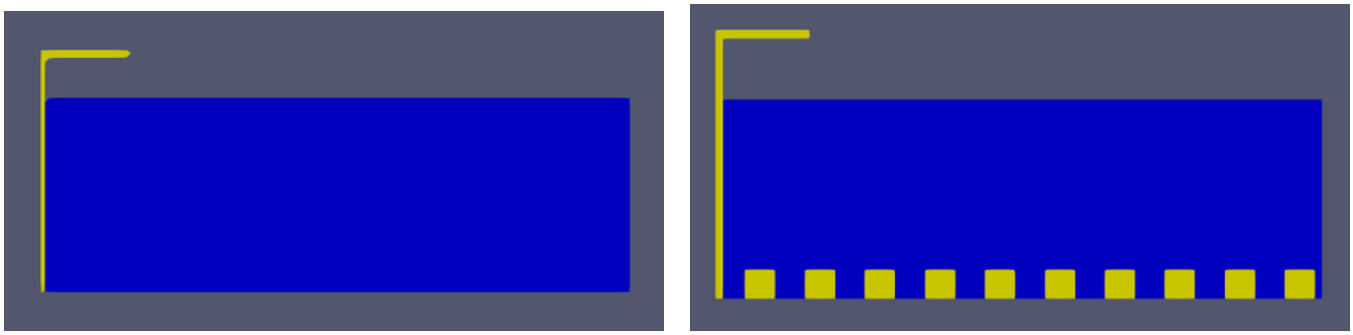

(a) Simulation set up excluding the aeration stones (b) Simulation set up including the aeration stones

Figure 2: Different test setup used in the simulations

x [m]	y [m]	z [m]
$3.8 \cdot 10^{-2}$	$15 \cdot 10^{-2}$	$3.8 \cdot 10^{-2}$

Table 2: Size of the aeration stones in each dimension

2.3.1 Input parameters

There are three categories of input parameters: the input parameters that influence the fluid properties, the input parameter that influences the accuracy, and the input parameters that define the movements of the sloshing tank.

Fluid properties The first category is the parameters that influence the fluid properties, which are the viscosity and the density of the fluid, and the water height. The first two parameters depend on the type of fluid that is used for the experiment. Ideally, salt water is used for the experiment, because that makes the results directly applicable to offshore structures. However, the experiment cannot be conducted using saltwater due to the harm it would cause to the measurement equipment. Therefore, fresh water will be utilized for both the simulations and the experiment. The fluid properties are also influenced by the water height. Further explanation about the water height will be provided later in this thesis.

Accuracy The second category is the parameter that influences the accuracy, which is the grid size. The simulation computes the fluid motion at certain points in the domain, called grid points. The space between two grid points is called the grid. The grid size defines the size of the grids.
Increasing the grid size in one direction means that there are fewer grid points in that direction, hence the results are less precise. However, a grid size that is too small results in too many grid points and too many computations, which leads to too long computational time. The minimum number of grids for a wave simulation is 60 grids per wavelength and 6 grids per wave height [33].

Tank movements The third category are the parameters that define the movements of the sloshing tank, which are the frequency and the amplitude. The sloshing tank will be moving in the x direction in order to cause a wave. These movements are specified by the frequency, which is the number of times the tank moves per second, and the amplitude, which is the maximum extent of the displacement. The wave height is expected to be maximum at the natural frequency and increasing the amplitude is expected to increase the wave height as well. The relation between the frequency and amplitude and the movement of the sloshing tank will be explained in the next paragraph.

2.3.2 Input signal

The movements of the sloshing tank are modeled by a regular motion. A regular motion is defined at each moment t by the positions in $[m]$, the velocities in $[m/s]$, and the accelerations in $[m/s^2]$ in the x, y, and z directions and by the positions in [deg], the velocities in [deg/s] and the accelerations in $[\text{deg}/s^2]$ for roll, pitch, and yaw. For the regular motion in this thesis, the position, velocity, and acceleration are fixed except for the x direction. That means

that the tank will only move in the x dimension.

The relation between the position, velocity, and acceleration in the x direction and the frequency and amplitude is given by

$$x(t) = r \cdot \sin(2\pi \cdot f \cdot t) \tag{16}$$
$$\dot{x}(t) = r \cdot (2\pi \cdot f) \cdot \cos(2\pi \cdot f \cdot t) \tag{17}$$
$$\ddot{x}(t) = -r \cdot (2\pi \cdot f)^2 \cdot \sin(2\pi \cdot f \cdot t) \tag{18}$$

where $x(t)$, $\dot{x}(t)$ and $\ddot{x}(t)$ are respectively the position, velocity, and acceleration of the tank in the x direction at time t, r the amplitude, f the frequency in [Hz] and t the time.

Within ComFLOW, there exist two options for acquiring position, velocity, and acceleration. The first option is to use the build method. For this method, you only need to specify the frequency and amplitude in your ComFLOW settings. Then ComFLOW generates the position, velocity, and acceleration values using

$$x = x_o + u_0 t + \frac{1}{2} a_0 t^2 + r \cdot \cos\left(2\pi t^2 + \frac{\pi\phi}{180}\right) \tag{19}$$
$$\dot{x} = u_0 t + a_0 t - r \cdot \sin\left(2\pi t^2 + \frac{\pi\phi}{180}\right) \cdot 2\pi f \tag{20}$$
$$\ddot{x} = a_0 t - r \cdot \sin\left(2\pi t^2 + \frac{\pi\phi}{180}\right) \cdot (2\pi f)^2, \tag{21}$$

which are the same as Equation 16-17 but transformed into polar coordinates with a phase shift of 0.5π and including the initial position x_0, velocity u_0 and acceleration a_0.

The second option to acquire the position, velocity, and amplitude is by defining the values for the position, velocity, and acceleration in an external input file. Such an input file has the following structure.

t	$x(t)$	$y(t)$	$z(t)$	$R(t)$	$P(t)$	$Y(t)$	$\dot{x}(t)$	$\dot{y}(t)$	$\dot{z}(t)$	$\dot{R}(t)$	$\dot{P}(t)$	$\dot{Y}(t)$	$\ddot{x}(t)$	$\ddot{y}(t)$	$\ddot{z}(t)$	$\ddot{R}(t)$	$\ddot{P}(t)$	$\ddot{Y}(t)$
0	x_1	0	0	0	0	0	$\dot{x}_1$	0	0	0	0	0	$\ddot{x}_1$	0	0	0	0	0
0.1	x_2	0	0	0	0	0	$\dot{x}_2$	0	0	0	0	0	$\ddot{x}_2$	0	0	0	0	0
0.2	x_3	0	0	0	0	0	$\dot{x}_3$	0	0	0	0	0	$\ddot{x}_3$	0	0	0	0	0
⋮	⋮	⋮	⋮	⋮	⋮	⋮	⋮	⋮	⋮	⋮	⋮	⋮	⋮	⋮	⋮	⋮	⋮	⋮
10	x_n	0	0	0	0	0	$\dot{x}_n$	0	0	0	0	0	$\ddot{x}_n$	0	0	0	0	0

where for each moment t, the values for the position x_t, velocity $\dot{x}_t$ and acceleration $\ddot{x}_t$ are computed using Equation 16-17. Notice that all values for y, z, R, P, and Y are zero, which corresponds to the zero movements in those directions.

The main difference between the build-in method and the external input file is that the build-in method uses a continuous signal. The external input file is a discrete approximation of the continuous signal, which makes the results less precise. However, the accuracy of the discrete signal can be improved by decreasing the step size.

2.4 Transfer function

In the introduction of this chapter, it was explained that the simulations are used to obtain insight into the scale of the forces on the horizontal overhang. The scale of the forces depends on the wave height and the wave height depends on the motion of the sloshing tank. In the previous paragraph, it was explained that the motion of the sloshing tank depends on the input parameters frequency and amplitude. In this paragraph, the focus will be on the relation between the frequency and the wave height, which will be referred to as the 'transfer function'.

The transfer function can be computed theoretically for one frequency: the natural frequency. The transfer function at the natural frequency can be computed using the dispersion relation. The dispersion relation uses the fact that waves with different lengths travel at different speeds. The relation between the radian frequency ω and the wave number k is given by

$$\omega^2 = g \cdot k \cdot \tanh(k \cdot d), \tag{22}$$

where g is the gravitational constant and d is the water depth. This equation holds for any water depth and therefore also holds for the simulation setup.
The wave number k is computed by

$$k = \frac{2\pi}{\lambda}, \tag{23}$$

where λ is the wavelength. The wave in the sloshing tank adopts the shape of the first mode, which is visualized in Figure 3. This means that the wavelength equals to rimes the effective length of the sloshing tank.
So, if we know the effective length of the sloshing tank and the water depth, it is possible to compute the natural frequency using Equation 22 and Equation 23. The transfer function, which will be explained later, will be validated using this natural frequency.

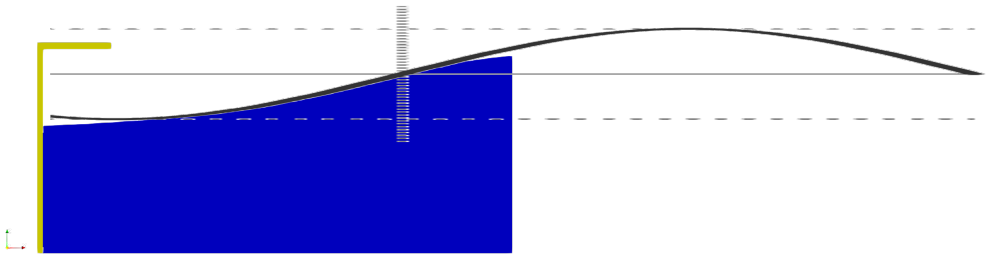

Figure 3: The first mode that is visible during the sloshing

2.5 Return period

The experiments in this thesis will be a representation of a real-life situation at the Oosterscheldekering. The goal is to simulate a wave that has a maximum wave height equal to the wave with a five-year return period at the Oosterscheldekering. This makes the result in this thesis directly relevant to the real-life scenario.
To simulate a wave with a return period of five years, it is necessary to know the height of the maximum wave with a return period of five years. The height is then scaled to the size of the experiment. Finally, the frequency that causes this wave height will be chosen using the transfer function.

The first step is to estimate the maximum wave height with a return period of 5 years. This height will be estimated using a sample of significant wave heights $H_{1/3}$. The significant wave height is defined as the average of the highest 1/3 of the waves in a certain time interval. The significant wave height is related to the maximum wave height by [24]

$$H_{max} \approx 1.86 \cdot H_{1/3}. \tag{24}$$

So, if we know the significant wave height with a return period of 5 years, we can estimate the maximum wave height by this relation.

To obtain the significant wave height with a return period of 5 years, the assumption is made that the significant wave height follows a Weibull distribution. This assumption will be confirmed by a Weibull plot. If the observed significant wave heights in the Weibull plot can be approximated by a linear line, it may be assumed that the significant wave heights are Weibull distributed.
If the significant wave height is Weibull distributed, the probability that a certain significant wave height $H_{1/3}$ happens once every 5 years is [24]

$$F\left(H_{1/3}\right) = 1 - \frac{1}{N_5}. \tag{25}$$

This implies that the significant wave height with a return period of 5 years can be computed using

$$H_{1/3} = F^{-1}\left(1 - \frac{1}{N_5}\right), \tag{26}$$

where N_5 is given by

$$N_5 = \frac{(\text{Number of observations}) \cdot (5\ [years])}{(\text{Period of observing}\ [years])}. \tag{27}$$

To compute the Weibull inverse, the built-in function `wbinv` in Matlab will be used.

2.6 Simulations

So far in this section, the theory that serves as the background for the simulations and computations in this thesis has been presented. In this subsection, the simulations that are performed for this thesis will be defined and explained.

2.6.1 Input parameters for grid size, density, and viscosity for all simulations

Throughout all simulations, the grid size, density, and viscosity of the fluid are fixed. Their fixed values are based on the characteristics of the fluid that will be used in the real experiments. Therefore, all simulations are based on fresh water. The density and viscosity of fresh water are given in Table 3.

	Density (kg/m^3)	Viscosity (NS/m^2)
Freshwater	1000	1.002

Table 3: Input parameters density and viscosity

To determine the grid size, the minimum number of grids is used as explained in Section 2.3.1. The wavelength is expected to be two times the length of the tank, as seen in Figure 3. This implies that half a wavelength is expected in the tank. Using the minimum number of grids, this results in a minimum of 30 grids in the x direction. For grids in the z direction, we will look at the wave height. The wave height that is needed at minimum is equal to the air gap to be useful for the experiments. The air gap is 0.1[m], so this is the minimum wave height needed. Resulting in 30 grids in z direction. For simplification, the number of grids will be changed to 70 and 50. This is due to the tank dimensions, this simplification does increase the accuracy of the simulation. The minimum grid sizes and the number of grids are summarized in Table 4. For two reasons, the grid size that will be used in the simulation is smaller than

Dimension	Minimum number of grids	simplified number of grids	Number of grids for simulation	Grid size for simulation ($m \times 10^{-3}$)
x	30	70	280	2.5
y	1	1	1	200
z	30	50	200	2.5

Table 4: The minimum number of grids and the maximum grid size in each dimension.

the minimum required grid size. The first reason is that for the best results, the first grid against a structure is not used for placing monitoring points. So the smaller the grid size, the closer the first monitoring point can be to the structure. This is beneficial because the largest pressure is expected near the wall. Subsequently, the simulation is a replica of the real experiment. In the real experiment, pressure sensors are located close to each other. If the grid size is too large, multiple sensors fall within the same grid and the simulation can not compute the pressure differences. Hence the grids must be chosen such that all sensors fall within a different grid. The values for the grid size that are used in the simulation are given in Table 4.

2.6.2 Simulation to validate the motion of the sloshing tank

The objective of the first simulation is to compare the two distinct methods that can be used to define the input signal in ComFLOW. In Section 2.3.2 it was explained that the input signal can be defined with an external input file or with a build-in method in ComFLOW. This simulation aims to validate the built-in method of ComFLOW in order to ensure reliable simulations.

To validate the built-in method of ComFLOW, the wave height of two simulations with the same input variables is compared. One of the simulations utilizes the built-in method of ComFLOW to determine the motion of the tank. For the other simulation, an input file is generated using Equation 16.-18. The duration of the simulation is 10 seconds. The amplitude is fixed at 0.03 [m], the frequency is fixed at 0.5 [Hz] and the water depth is 0.20 [m]. The input file is generated using a time interval of 0.1 seconds. Also, the values in the input file are compensated for the

phase shift by a rotation of 2π radians.

Throughout the simulation, the wave heights of both simulated fluids are measured at two locations in the sloshing tank. The results of both these measurements will be presented in Section 2.7.1.

2.6.3 Simulations to find the transfer function

The second simulation study aims to obtain the relation between the frequency and amplitude input values to the maximum wave height in the tank. To establish these relationships, Multiple simulations will be conducted, each with varying frequencies and amplitudes assigned to them.

The initial set of simulations comprises six simulations in which the amplitude is systematically varied across the values 0.03, 0.06, 0.09, 0.12, 0.15, and 0.18 [m]. The Frequency is fixed at 0.5 [Hz].
The subsequent set of simulations also consists of six simulations. In this set, the frequency is varied across the values 0.3, 0.4, 0.5, 0.6, 0.7, and 0.8 [Hz]. The amplitude is fixed at 0.09 [m]. The duration of each simulation is 10 seconds and the water depth is 0.20 [m]. The results of this set will be used in later simulations and therefore these intermediate results will be presented in Section 2.7.2.

The simulations described so far in this paragraph give an idea of the relation between the input parameters and the wave height. However, the step size for the amplitude and frequency is too large to obtain a result that can be used as a transfer function. Due to mechanical limitations in the experimental setup, the amplitude must be fixed at one value. Therefore, it is only in our interest to find the transfer function of the frequency.

The transfer function of the frequency is obtained using 150 simulations in which the frequency is systematically varied across the values 0.01 [Hz] to 1.5 [Hz], using a step size of 0.01 [Hz]. The amplitude in this simulation is fixed at 0.01[m]. The duration of this simulation is 10 seconds. During the simulation, the wave height is measured at two locations in the sloshing tank. Location x_1 is near the wall under the horizontal overhang. Location x_2 is near the free wall of the tank. The results of this set will be used in later simulations and therefore these intermediate results will be presented in Section 2.7.2.

Natural frequency In Section 2.4 it was explained that it is possible to validate the transfer function using the natural frequency. Using the theory in that paragraph, this natural frequency will now be computed for a water depth of 0.2 meters, corresponding to the simulation set up for the transfer function simulations.

The effective length of the sloshing tank is 0.68[m]. Using Equation 23, the effective wavelength is

$$\lambda = 2 \cdot 0.68[m] = 1.36[m].$$

Using Equation 23, the wave number equals

$$k = \frac{2\pi}{1.36[m]} = 4.61[rad/m].$$

For a water depth of 0.2[m] and a gravitational constant of $9.81[Nm^2/kg^2]$, the natural frequency is computed using Equation 23,

$$\omega^2 = 9.81 \cdot 4.61 \cdot \tanh\left(4.61 \cdot 0.2\right).$$

Thus the natural frequency for this simulation setup is $\omega = 0.97[Hz]$. The results in Section 2.7.2 will be validated using this value for ω.

2.6.4 Maximum wave with a return period of 5 years

Until now, the focus of the simulation was to obtain the relation between the input parameters and the wave height. From now on, the starting point for the simulation setup will be the maximum wave height that will be obtained within the simulation.

To obtain relevant results, the wave height in these simulations is based on the maximum wave height, H_{max}, with a return period of 5 years in the Oosterscheldekering. The value for H_{max} is estimated following the procedure in Section 2.5. For the estimation, I use a data set that is published by Rijkswaterstaat, consisting of 17,150 observations of the significant wave height $H_{1/3}$. These observations are obtained by Hydro Meteo Centrum Zeeland, over a time period of 1 year collected at location OS4. The Weibull plot of this data is given in Figure 4.In this plot, it can be observed that the data can indeed be approximated by a straight line, suggesting that the significant wave heights may be assumed to follow a Weibull distribution.

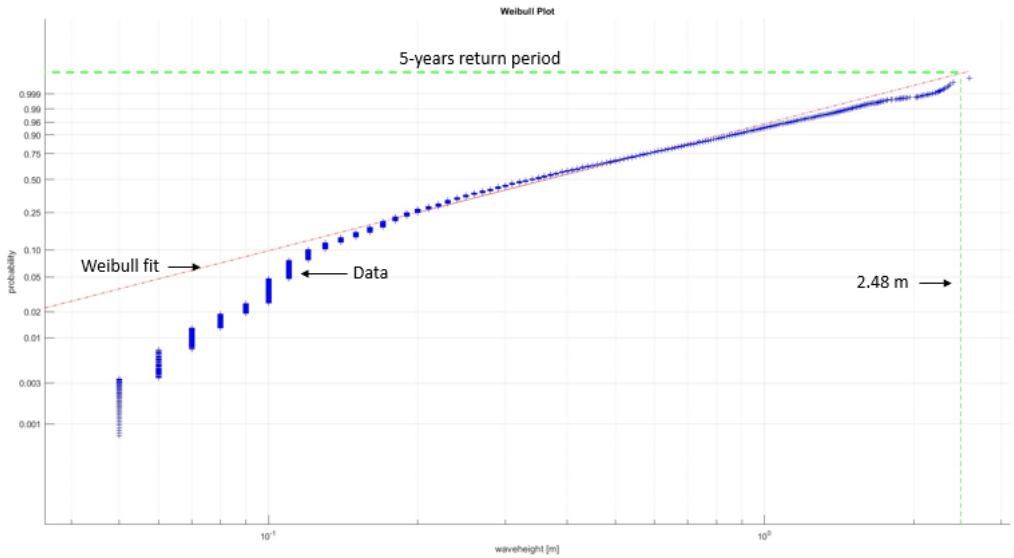

Figure 4: The Weibull plot of the 17,150 observations obtained at the Oosterscheldekering, published by Rijkswaterstaat. This plot shows that the data is Weibull distrubuted because it can be approximated by a straight line. The 5-year return period is indicated by the green dashed horizontal line.

Following the procedure described in Section 2.5, the computation for N_5 is performed as follows:

$$N_5 = \frac{17,150 \cdot 5}{1} = 85,750.$$

Therefore, the probability that $H_{1/3}$ occurs once every 5 years is

$$F(H_{1/3}) = 0.9999883382. \tag{28}$$

Using Equation 27, the significant wave height $H_{1/3}$ with a return period of 5 years is [24]

$$H_{1/3,5} = F^{-1}\left(0.9999883382\right) \approx 2.48[m].$$

Then using Equation 27, the maximum wave height H_{max} with a return period of 5 years is

$$H_{max,5} = 1.86 \cdot 2.48[m] = 4.62[m],$$

which results in a scaled maximum wave height of $H_{max,5} = 0.077$[m]. From now on, this value $H_{max,5}$ will be used as the maximum wave height for all simulations.

2.6.5 Simulation to find the relation between the wave height and the pressure

This simulation focuses on the relation between the wave height and the pressure. This simulation study consists of five simulations in which the wave height is systematically varied. The wave heights in this simulation is varied between $0.9{\cdot}H_{max}$, $0.95{\cdot}H_{max}$, $\cdot H_{max}$, $1.05{\cdot}H_{max}$, $1.10{\cdot}H_{max}$, where H_{max} is computed in the previous paragraph.

For this set of simulations, a water depth of 0.20 [m] will be used. This depth is related to the data of the Oosterscheldekering, where the average water depth near the structure is 12 [m].

To perform the simulations described in this paragraph, the input parameters that cause the waves to be tested must be known. The input parameter for the amplitude is fixed, and thus the transfer function of the frequency will be used to determine the frequency input parameter that will cause a wave spectrum where the maximum wave has height H_{max}.
The frequencies that cause H_{max} are intermediate results from the previous simulation and are presented in Section 2.7.2. The results for the simulation described in this paragraph are presented in Section 5.1 as well.

2.6.6 Simulation to find the relation between the water height and the pressure

This simulation focuses on the relationship between the water height and the pressure. This simulation study consists of ten simulations in which the water height is systematically varied over ten different values. The relation between the water height is specifically relevant for the Oosterscheldekering. The Dutch coast has a semidiurnal tide cycle, which means that it is not realistic that the largest pressure is caused by the setting with the average water height.

Throughout this set of simulations, the water depth is only increased relative to the average water depth. The reason for this is that a lower water level results in a maximum wave that is not large enough to hit the overhang of the structure. The frequency for this simulation is the frequency that corresponds to the maximum wave H_{max}, according to the transfer function. The frequency is an intermediate result of the previous simulation, which is presented in Section 2.7.2. The results of this simulation are presented in Section 5.2.

2.6.7 Aeration stones

The aim of this simulation is to see what the effect of the aeration stones will be, compared to the simulation without aeration stones. The simulation compares the pressure on the overhang for the simulation with the aeration stones (Figure 2b) to the pressure for the simulation without the aeration stones (Figure 2a).
The reason this test isn't performed up until now is the change in the experimental setup. During the simulations, the test setup was designed. When all the simulations were finished, a design change was made such that the aeration stones were exposed directly to the water in the tank. So this additional test is done to investigate the effect of the stones on the maximum wave pressure.

For these simulations, the same input parameters as those used in the two previous simulation studies are employed. The results of this set of simulations are presented in Figure 21.

2.7 Intermediate results

In this section, the intermediate results of the simulations explained in Section 2.6 are presented. These results are needed to determine some of the settings of the experiment.

2.7.1 Motion of the sloshing tank

In Figure 5, the results of the simulation described in Section 2.6.2 are presented. The plot aims to visualize the similarity of the wave heights corresponding to one of the methods to generate the regular motion. In the plot, you can see the relation between the time [s] at the x-axis, and the wave height [m] at the y-axis.

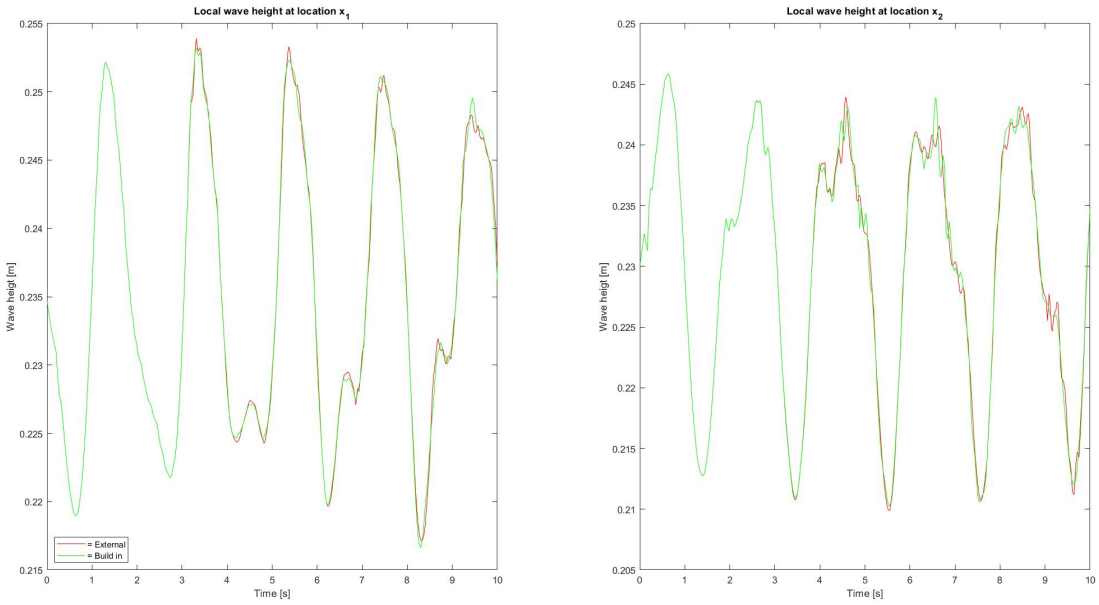

Figure 5: In this figure the local wave height at both sides of the tank are compared to 2 different input methods. The red line is the output generated by the external input file (the discreet input option), the green line is the output of the build-in model (the continuous input option)

2.7.2 Transfer function

In this subsection, the results of the simulation described in Section 2.6.3 are presented. In Table 5 are the results for the simulations with varying amplitude. In Table 6 are the results for the simulations with five varying frequencies. In Figure 6 are the results for the simulations with 150 varying frequencies. The plot shows the relation between the frequency [Hz] on the x-axis and the wave height [m] on the y-axis.

Amplitude [m]	**Frequency** [Hz]	**Wave height** x_1 [m]	**Wave height** x_2 [m]	**Max force** [N]	**Max pressure** [Pa]
0.03	0.5	0.252	0.243	0	0
0.06	0.5	0.269	0.261	0	0
0.09	0.5	0.288	0.283	0	0
0.12	0.5	0.299	0.298	11.85	474.05
0.15	0.5	3	0.324	60	2169
0.18	0.5	3	0.330	81	2781

Table 5: Table of the amplitude variation

Amplitude	Frequency	Average wave height x_1	#tops	Average wave height x_2	# tops	Maximum force	Maximum pressure
0.09	0.3	0.248	3	0.245	3	0	0
0.09	0.4	0.259	4	0.256	4	0	0
0.09	0.5	0.288	5	0.283	5	0	0
0.09	0.6	0.3	6	0.335	6	109	5237
0.09	0.7	0.3	7	0.463	7	324	18779
0.09	0.8	0.3	8	0.419	8	1207	66113

Table 6: Table of the frequency variation

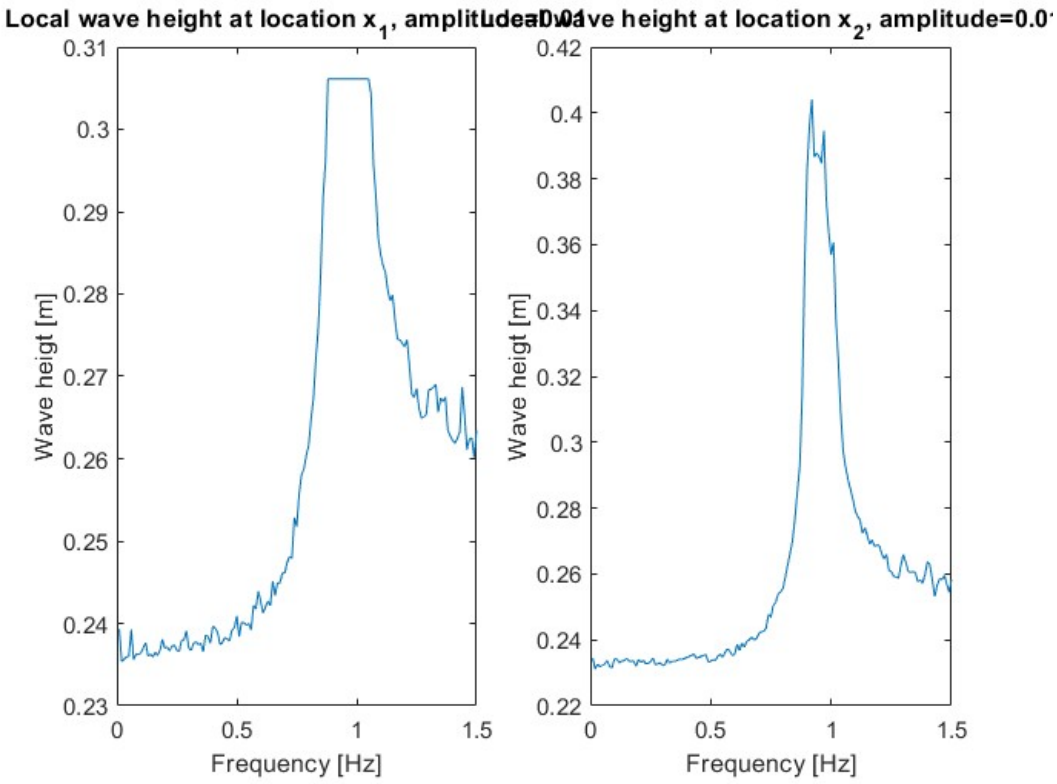

Figure 6: Transfer function of sloshing at 2 locations. (left) the location underneath the overhang. (right) the location at the empty side of the tank

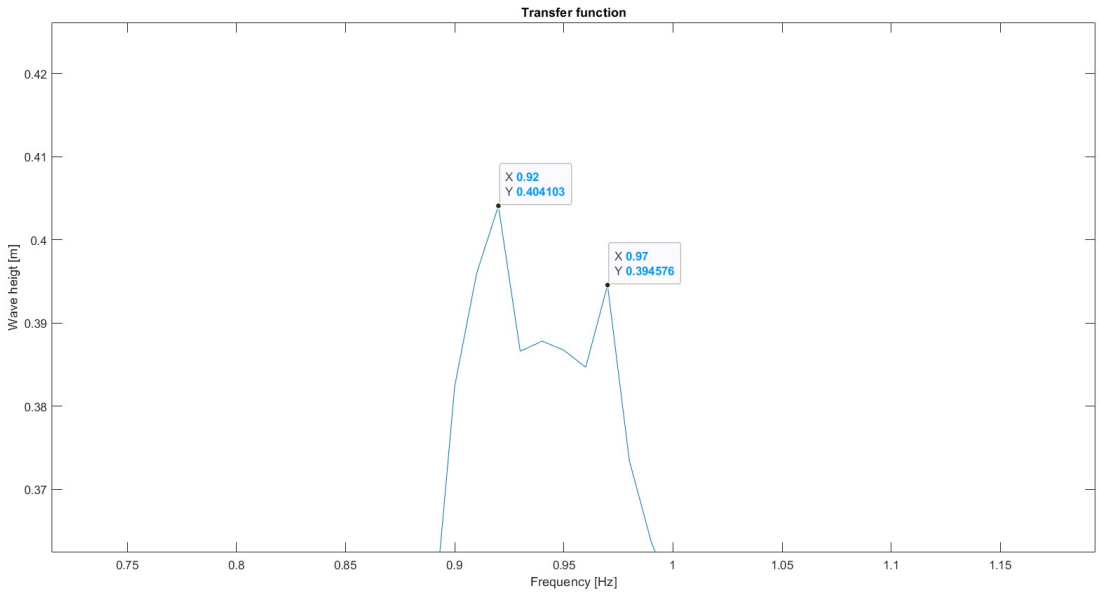

Figure 7: A high-resolution image of the zoomed-in the peak of the transfer function of Figure 6

3 Intermediate conclusion

Within this section, the conclusions drawn from the results presented in the preceding paragraph are presented. These conclusions will be utilized in the subsequent experiments conducted in this thesis.

Motion of the sloshing tank The first conclusion concerns the comparison of two different methods to define the input signal for the motion of the sloshing tank. Based on the results presented in Figure 5, it is concluded that the built-in method in ComFLOW relies on the mathematical model described in **??**. In the figure, it is clearly visible that the wave height generated by the built-in method in ComFLOW is approximately equal to the wave height generated by the external input file. Because the mathematical model for the external input file is known to rely on the theory in Figure 26b, it can be concluded that the mathematical model for the built-in method relies on the same theory.

It is important to notice the differences in the wave heights at the peaks of the waves, see for example the fourth peak in the right plot in Figure 5. The deviation in wave heights is caused by discretizing the input signal in the time dimension. When a continuous signal is discretized, the discrete results can be distorted, leading to a false representation of the real dynamics. These phenomena is called aliasing.
The external input file uses a time step of 0.1 [s], which is larger than the built-in method. A larger time step leads to a loss of detail and accuracy. Based on the plots presented in Figure 5, it is concluded that the larger time step of the external input file results in a greater effect of aliasing. This suggests that the built-in method in ComFLOW provides a better approximation of reality compared to the external input file.

Transfer function The second intermediate conclusion concerns the transfer function that relates the input frequency to the maximum wave height. The results in Figure 6 show the relation between the frequency and wave height based on the simulations. The left plot has a flattened peak due to the location of the wave height measurement and the overhang structure. To validate the transfer function, it is necessary to observe the peak. For that reason, the right plot is considered for determining the transfer function.

In Figure 7, you can see the zoomed peak corresponding to the right graph in Figure 6. The graph shows that there are two local peaks. Based on the computations in Figure 26b, the analytical natural frequency is equal to 0.92 [Hz]. This is equal to the left peak in Figure 7. This result verifies the results in Figure 6 can be used as a transfer function that relates the frequency to the maximum wave height.

Although the results in the left graph in Figure 6 can not be used to obtain the transfer function, the results are useful for another conclusion. The wave gauge x_1 is located underneath the horizontal overhang. The flattened peak implies that the maximum wave reaches the horizontal overhang. The experiment only uses an amplitude of 0.01 [m]. We can thus conclude that even with a small amplitude, the water reaches the overhang if the frequency input is chosen close to the natural frequency.

Input parameters for the other simulations The validated transfer function in Figure 6 can be used to choose the input parameters for the simulations described in Section 2.6.5 till Section 2.6.7. Based on the desired maximum wave height, the transfer function is used to obtain the corresponding input frequency for the simulations, see Table 7.

Wave	Wave height [m]	Scaled wave Height [m]	From Transfer function [m]	Error	Input frequency [Hz]
$0.90 * H_{max}$	4,16	0,2993333	0,299	0,000333	0,807
$0.95 * H_{max}$	4,39	0,3031667	0,303	0,000167	0,813
H_{max}	4,62	0,307	0,3071	-1E-04	0,818
$1.05 * H_{max}$	4,85	0,3108333	0,3106	0,000233	0,821
$1.10 * H_{max}$	5,08	0,3146667	0,3144	0,000267	0,825

Table 7: Table of input parameters for the simulation that aims to find the relation between the maximum wave height and the pressure. From left to right: the variation of the maximum wave height, the corresponding real wave height, the scaled wave height, the closest value known in the transfer function, the error between the desired scaled wave height and the known wave height from the transfer function, and the actual input frequency are given

4 Experiments

In this chapter, the method, composed of the preparation phases and the execution of the experiments will be explained. This chapter consists of the design of the experimental setup, the building of the setup, and the processing of the data. With the exception of some first results, all the results will then extensively be discussed in Section 5.

The aim of the experiments is to find what the effect of aeration will be on wave impact on a horizontal overhang. For this, a representative test setup is needed to test wave impact on the horizontal overhang and to test the difference in impact pressure with and without aeration. The gained knowledge from the previously executed numerical simulations about the expected pressures on the overhang is used for the preparation phase of the experiments. These simulations were without aeration due to the limitations of ComFLOW. Hence the experiments will be used to gain knowledge about the wave impact test with aerated water.

4.1 Experiment motivation

Using scaled experiments for testing wave impacts, in general, can prove highly beneficial in various ways. Firstly, scaled experiments allow us to replicate and observe wave conditions in a controlled environment, providing valuable insights into the behavior of waves and their impact on structures. By scaling down the size of waves, it becomes easier to study different scenarios, test hypotheses, and evaluate the effectiveness of potential mitigation strategies. Secondly, scaled experiments offer a cost-effective alternative to full-scale testing, as they require less time, resources, and funding. This makes it possible to conduct a larger number of experiments before proceeding to expensive and time-consuming full-scale tests. Furthermore, scaled experiments provide a safer testing environment, minimizing risks associated with large-scale structures and unpredictable wave conditions. In the specific situation of this research, which is about the maximum pressure of a wave impact including the effect of aeration, a scale (or full-scale) experiment is mandatory to measure the effects of the aerated wave impact, because of the limitations of the used numerical simulation program ComFLOW. The experiments conducted in this research are sloshing experiments. In this sloshing experiment, the maximum wave force will be measured at a horizontal overhang. These experiments will then be executed with and without aeration, so a conclusion can be drawn about the effect of aeration on the maximum force.

4.2 Experiment design

In the preparation of the experiments, all the preliminary steps will be discussed. The first preliminary steps are discussed in Section 2. Here the global understanding of how the sloshing water will react, and what the order of magnitude expected wave pressures is discussed. In this chapter, all the components of the experiment will be discussed as well as the used measuring equipment.

4.2.1 Experimental setup

This subsection will begin with introducing the different parts of experiments that together form the setup. It will start with treating the Sloshing rig. After the sloshing rig, the Tank Design will be dissed, and finally, the design of the Overhang construction is shown.

Sloshing rig For the experiments, the sloshing rig of the facility of 3ME will be used. This sloshing rig is designed and used by Dr. Ing. S. Schreier at Rostock University[42]. Unfortunately, after moving the sloshing rig from Rostock University to the TU Delft, it hasn't been used ever since. For testing the forces on a horizontal overhang, the sloshing rig is the perfect testing device. Before it could be used for the experiments the setup needed to be reinstalled in the basement of the towing tank facility of 3ME. This includes all the systems for the control signals and the computer that will collect all the measured data. The sloshing rig has two degrees of freedom. The transnational motion in the longitudinal direction of the tank and the rotational excitement on the transverse axis located in the middle of the tank. The longitudinal excitement has a maximum amplitude of 60[mm] and the rotational excitement has a maximum amplitude of 10[deg]. Both excitations have a maximum frequency of 1.5[Hz]. The 2 excitations are

condoled by a numerical control box. This makes it possible to vary the frequencies of both translation and rotation during the experiment. Both amplitudes can only be changed via a physical setting that can only be done in between the experiments. This is one of the main reasons that in Section 2.4 the choice was made to use the amplitude as a fixed parameter.

Tank design Preinstalled at the sloshing rig is the water tank in which the experiment will take place. This tank is made of 20 mm thick acrylic glass. The inner dimensions of the current tank setup are a length of 700[mm], a height of 496[mm], and a width of 200[mm]. The tank has a front and back plate that are preinstalled with multiple cable entrees Figure 8. The Tank is also fitted with a sealing cover. This cover prevents water from sloshing out of the tank and prevents disturbance in the tank. The cover of the tank also has preinstalled cable entries near the front and back wall. This original cover will not be used in these experiments due to the custom tank design. a new cover will be made that will only cover the part containing water, and leave the part above the overhang open. This makes it easy to gain access to the sensors and air hoses without damaging the sensors with splashing water.

Figure 8: In this figure, the cable entries are visible. These old cable entries are on both sides of the tank. For this new tank design, the cable entries will be used for supporting purposes only

Overhang construction design The novel part of the experimental setup will be the inner construction of the tank. This consists of the overhang, the back plate, and the aeration system. The internal structure is the horizontal overhang. For all the simulations with ComFlow and for all the experiments a reversed L shape (Γ) will be used. In addition to the earlier mentioned (Γ) shape that was used in the simulations, the overhang construction that will be used in the tank has two additional parts. The first added part is the back wall, in the simulations, the back wall only reached up until the horizontal overhang. Now the back wall continues to the top of the tank. This gives it more strength and a smaller chance of damaging the tank. The second added part is the gray part. This splash wall is made so the fragile sensors will not be in touch with any water at all during the experiments.

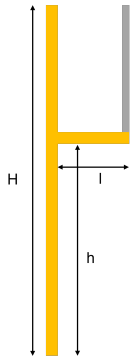

Figure 9: In this first computer drawing of the overhang construction, the dimensions and geometrics become clear.

The dimensions of the Γ in previous research were: an overhang length (l) of 20cm and a height (h) of 60cm. The inside dimensions of the tank are smaller than the previously used overhang dimensions[17]. So to fit in the tank with dimensions of H=496 mm, L=700 mm, W=200 mm the previously used overhang will be scaled with a factor $\frac{1}{2}$. Therefore, the dimensions of the horizontal overhang will be h=300 mm, L=100 mm, w=200 mm, see Figure 9. The thickness of the overhang will be 20 [mm], and will be made from PVC.

To secure the overhang structure to the tank, the old cable entries can be used. 9 openings will be used to screw the whole back plate to the tank wall. The overhang construction and the splashing plate will be glued to the back plate and therefore the whole construction is secured with those 9 screws. A detailed drawing of the overhang can be seen in Appendix A

4.2.2 Sensor selection

The selection process of the sensors will be dependent on the desired output. For this experiment, the required output with the designated sensor is shown in Table 8.

Output	**Measure**	**sensor**	**Sampling frequency**
Wave spectrum	Water level	Wave Gauges	10.000 Hz
Pressure spectrum	Local pressure	Pressure sensor	10.000 Hz
Aeration level	Added volume	Aeration float	N/A
Air pressure	Air pressure above the water	Air pressure sensor	1000 Hz
Impact visualisation	Images on impact	Digital camera	200 Hz

Table 8: In the output table, the desired output and the corresponding sensors are given

Pressure sensors For the results, the pressures will be used to compare different wave impacts. These sensors will be placed only on the horizontal part of the structure. The part that is interesting is the closed corner part at l=0. For the sensor layout, see Figure 10. Pressure Sensor 1 (PS1) is located in the closed corner. PS1, PS2, and PS3 overlap with each other to create a path to see how the pressure distributes at impact. They are not installed on the same line to get a higher resolution by overlapping them. PS4 and PS5 do not overlap, this gives the sensors far away from the closed corner the highest resolution. This is done so with a relatively low number of pressure sensors (5), both the overall pressure distributions with a low resolution as well as the area with the expected maximum pressure with a high resolution can be measured.

Besides the longitudinal location also the location in the beam direction is chosen wisely. The reason that the sensors are placed in the middle of the plate, is due to the 2D analysis. Because the analysis is 2D, the best for the sensors is to be in one line behind each other. But, for the reasons mentioned above, a high resolution is needed. So the middle of the plate is used to get as Little disturbance of the tank walls as possible. The wall-fluid interaction can create imperfections in the wave that can influence the measuring results.

Wave gauge To measure the water level in the tank, wage gauges will be used in the tank. The wave gauge will give insight into which wave will cause which pressures. There is however one main disadvantage. The wave gauges work with an electrical resistance principle, after adding water to the tank, the wave gauge can not be used for measuring water height. So the wave gauge will be placed inside the tank, but will only be used with the non-aerated experiments. The wave gauge has two main types, one is a very thin wire that is accurate but fragile. The other one is a small metal bar, which is less accurate but also way less fragile. The choice is to use option 2. The main reason for this is so the wave gauge can be placed in the tank, even if the aerated experiments will be conducted, without damaging the wave gauge.

Aeration float The level of aeration need to be known for the experiments. Hence an aeration flotation device will be fitted in the tank. A float can be used as a method to measure aeration. When air is introduced into the system, the additional volume can be accounted for by adding it to the water volume Figure 11. By observing the change in water level, one can estimate the distribution between the air and water volume. Assuming that the conservation of mass is valid. This means that no air will leave the system at any other place than at the free surface. The difference in volume can be expressed in Equation 29. This formula can be written to a formula with the water height as variable Equation 30. To calculate the percentage of the aeration Equation 31 will be used. With A the surface of the free surface at still water, V the volume and h the water height.

$$V_{\Delta} = V_{mixture} - V_{water} \tag{29}$$

$$A * \Delta_h = A * h_{mix} - A * h_{water} \tag{30}$$

$$aeration = \frac{V_{added}}{V_{mix}} * 100 = \frac{A * h_{added}}{A * h_{mix}} * 100 \tag{31}$$

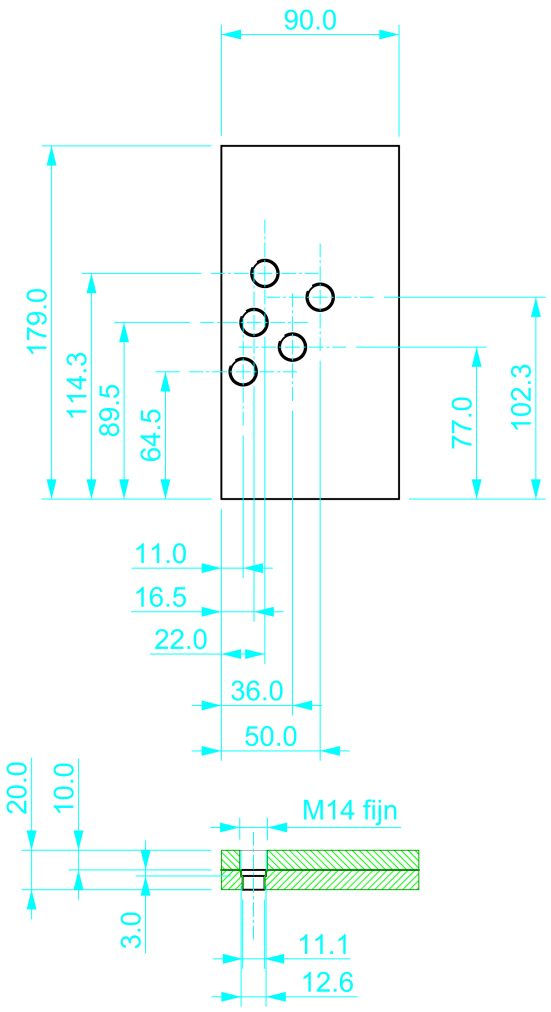

Figure 10: In this top view of the overhang, the sensor locations can be seen. From left to right: PS 1 to PS5. The left side of the overhang is the side attached to the back wall. In the bottom drawing a side view of how the sensors can be screwed in to place with a special hollow bolt.

Camera To be able to provide insights into the different pressure results, a camera was introduced into the experimental setup. This camera is used to capture certain aspects of the impact and visualize it. A camera trigger is employed for two main reasons. The primary reason is to ensure that the pictures are taken precisely at the moment of wave impact. The second reason is that the camera trigger can also generate an output signal, allowing for the exact timing of the captured photo to be correlated with the measurement data.

The camera setup can be seen in Figure 12, here it can be seen that the camera is fixed to the outer frame of the sloshing rig. The trigger itself will be on the positing sensor of the tank. Just before reaching the maximum position the camera will be triggered. The camera will then take three pictures, one before, one during, and one after impact.

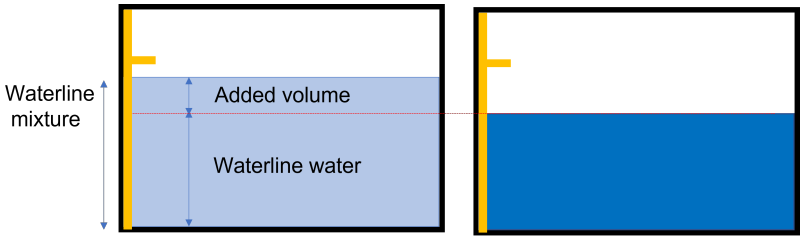

Figure 11: (right) The water level without aeration. (left) The water level with aeration. In the left figure, the added volume, in comparison with the original water level can be computed.

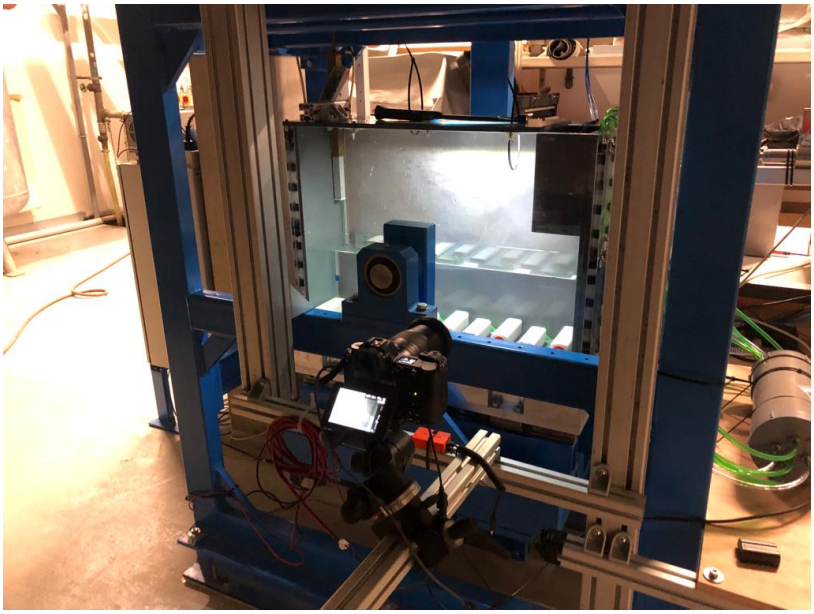

Figure 12: A Nikon Z6 camera is used to take images during the wave impact. The camera is fixed to the main frame of the sloshing rig

4.3 Experiment building

After the preparation phase of the experiments, the building design phase could start followed by the execution phase, with includes the building of the structure. All the steps that were not foreseen at the design phase, are discussed and adjusted in this section.

4.3.1 Aeration design

In the first sketches, the aeration stones were designed in the same way as the experimental setup of van der Zee [44]. Here the aeration stones covered the full width of the tank. Because this is beneficial for the homogeneous bubble flow, the first design was just like this.

However, the air hose connection of these aeration stones is an extension of the stone itself. This means that the total width of the stone, including the air connection would be wider than the tank. Two main option to solve this problem was drilling the air hoses through the tank *or* using smaller aeration stones. Due to the reusability of the tank, the decision was made not to drill in the tank walls. So instead of the 20[cm] wide aerating stones, a 15[cm] stone was ordered. The adjustment to the design was made so the air hoses could be guided underneath the bottom plate see Figure 13

This gave new limitations for the homogeneous distribution of the air. The problem and the solution is discussed in Section 4.3.3.

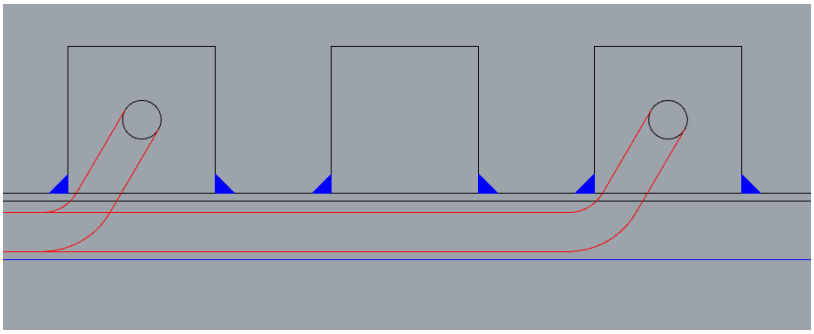

Figure 13: With the double floor construction, the air hoses (marked in red) are guided underneath the aeration stones so the air hoses will not interfere with the waves.

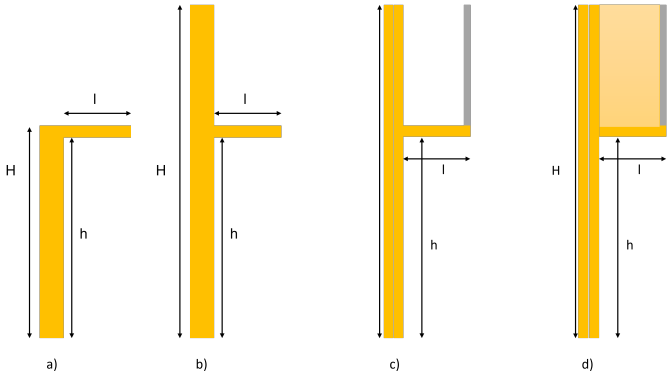

Figure 14: The first to the final design

4.3.2 Overhang design

The overhang was initial designed as a pure Γ shaped construction. Soon after the sketch phase, not only the shape and dimensions were taken into account but also the feasibility of the design was discussed. Then it became clear that the securing points on the tank were limited. So the design went from a Γ shaped to the current design shown in Figure 14. This includes a back wall that reaches from the bottom of the tank to the top of the tank. So the choice was made to bolt the back plate in place with nine m8 bolts. The bolts are directly screwed into the PVC back plate. Which has 9 tapped m8 treads. After the first evaluation from a) to b). The material had changed from plywood which was the initial design, to PVC which is in the final design. Also, the double back wall is added to the design. To guide the air hoses outside of the tank, without interfering with the waves. Also, the splash wall was introduced to prevent water damage to the sensors. The last design d) is the one that is in Appendix A on which the actual overhang is based. This includes an extra set of side panels for the strength and protection of the sensors.

4.3.3 Limitations and mitigation's

Nonhomogeneous air distribution The nonhomogeneous air distribution can have multiple reasons that this research tries to limit as much as possible. The first limitation is the stone itself. The stones do not reach across the whole tank. This means that the air will not be evenly distributed across the tank. The mitigating for this problem was to place the stones in a left Right pattern. so the air is distributed as homogeneously as possible.

The second problem is the path that the air has to travel to the aeration stone. For practical reasons, one compressed air connection will be used so one air filter and one mass flow controller will be used. The problem was how to get from 1 connection to 10 air hoses without getting an uneven air distribution. An equal amount of splits in the air hoses like in van der Zee[44] could not be done due to the number of 10 stones. So an air manifold was suggested see Figure 15. This air diffuser had 1 input of the mass flow controller at the top of the picture. On both sides, the manifold has 5 outputs to the aeration stones. This means that the air goes from a pipe with a diameter of 125[mm] to 10 individual hoses with an inner diameter of 6[mm]. This means it can be assumed that the air will be equally distributed over all the air hoses.

The next of the big problems for an equal distribution is the length of each individual hose. the last aeration stone must have a longer hose than the first stone. This means the air has to travel longer distances and the outflow will be affected by this. To compensate for this effect, each of the hoses will be the exact same length in total. So there will be compensation for the length of the hose outside of the tank.

This brings us to the last challenge, bending air hoses. When the air hoses are bent, the diameter will be likely to change. This affects the output of the stone. a view critical points for bending the air hoses are present in the current design. the first bent is from the air connection at the stone to under the floor. this is a sharp bent, that would affect the output of the stone. However all 10 stones have exactly the same bent so it will affect the output, but it will not affect the homogeneous air distribution. The same for the 90-degree bent from the double bottom to the double back wall. This sharp bent will affect the airflow, but it will do so for all the hoses. But to prevent that one bent is just different than another one, which is likely. A fixed 90-degree bent is used to add to the uniformity of the airflow.

These above-mentioned mitigations will contribute to homogeneous aerated water. Which contributes to more reliable results of the experiments.

Figure 15: A 3.2[mm] thick rainpipe with a diameter of 125[mm] is used as a air manifold. The main reason for the manifold is to distribute the air as evenly as possible over the 10 different air hoses.

Uneven bottom floor of the tank The uneven bottom of the tank has two main reasons. The first one is the stones themselves, which give a blocked pattern to the floor. The second reason is that the stones themselves do not reach the whole width of the tank. To start with the aeration stones themselves. To get aeration an air diffuser is needed. The choice of Pentair was due to the extremely small bubbles [44]. These will always come in a block-shaped design. So a mitigation to prevent an uneven bottom is to use a perforated plate. However, this mitigation does has one big downside. Due to the perforation, the small air bubbles, that we want for the experiment. Will become

significantly larger. Another option was to fill the gaps in the bottom with a 3D-printed filler. This would be an option that Helps the waves feel less of the stones. The only disadvantage of that is that part of the homogeneous air distribution comes due to the fact that the sides of the stones are open. So for now that will not be used.

The proposed mitigation is to adapt to the situation. Simulations will be used to compare the situation with and without aeration stones in the tank. This helps to understand the effect that those stones have on the wave and makes it possible to adapt the conclusion to the results. The mitigation for the fact that the stones do not reach from side to side can however be solved with a 3D printed prosthesis that fits around the air connection and the air hose sicking out of the stone. in this way, the wave will feel like a stone that reaches from side to side. This prevents turbulence in the water due to an unevenly distributed stone in the width direction. This mitigation would very help full in a 2D analyze that would be used for this experiment.

4.4 Experimental method

The Method chapter provides a comprehensive description of the experimental approach employed to investigate the effect of aeration on wave impacts. This chapter outlines the procedures, equipment, and techniques utilized to gather data and analyze the results.

4.4.1 Aerated water

One of the novel features of the sloshing tank is the possibility to create aerated water in the moving tank. The built-in aeration system in the tank consists of 10 aeration stones. The stones used are the AS15S from Pentair [38]. These stones are made from bonded silica and can provide a homogeneous divided bubble flow above the stone.

To produce aerated water in a repeatable manner, a Mass flow controller (MFC) is utilized. The MFC is controlled by the data acquisition computer. Via a 0V to 10V input signal, the MFC can adjust the amount of air sent to the diffuser Figure 15. The stones are capable of producing 15.21 L/min air each. In total 10 stones will be used in the setup. One of the big challenges was to get a homogeneous bubble flow in the tank, these challenges and mitigations of this are described in Section 4.3.3.

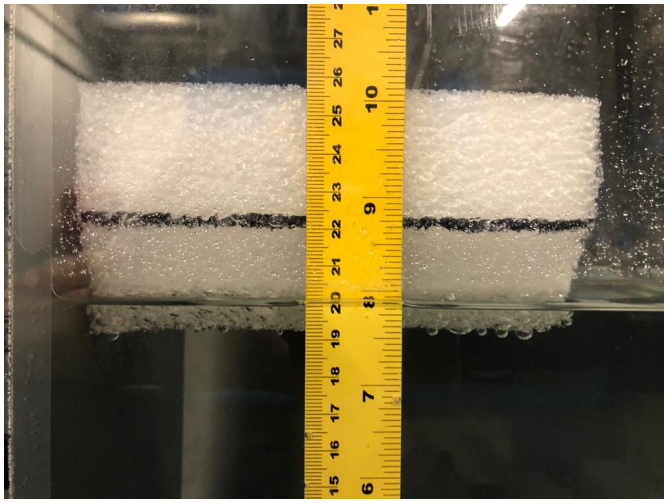

(a) The float without aeration

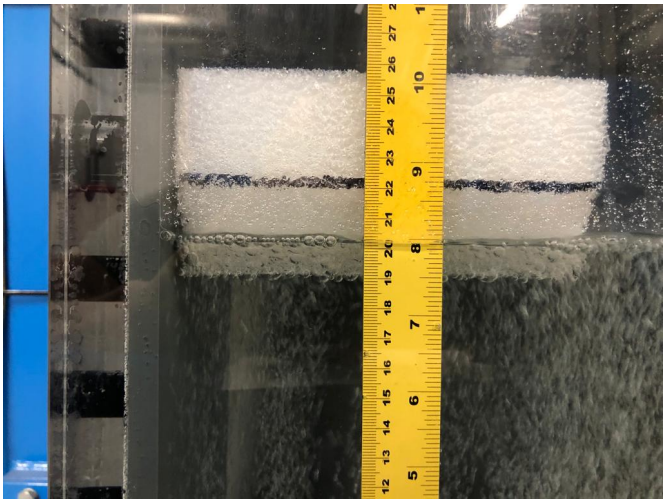

(b) The float with aeration

The desired amount of aeration for the experiments is 0, 1, 1.5, 2, and 4 percent. To get the correct input setting for the MFC, an aeration test is done by using a float Figure 16b. In steps of 0.5V, the input of the MFC is increased. During each step, the water height is measured with the float. For each step, the water height is tested at two locations. The average water height is used for the calculations.

After the water heights were taken, the percentage of added aeration can be calculated. This is done by calculating the inner dimensions of the tank, $L * B * h$ with h the normal water height. This is the default volume of the tank. But to get the amount of water in the tank, the volume of the aeration stones must be subtracted. These measured added volumes of the tank can be transferred into the percentage of air via the formulas of Figure 4.2.2.

Adding the aerated water will not only change the total volume of the mixture but the speed of sound will also be affected. Looking at the speed of sound of water $c_w = 1480[m/s]$ and the speed of sound through air $c_a = 343[m/s]$. The logical consequence of adding the two is a reduction in the speed of sound going from only water to water with aeration.

The results of the aeration test are summed up in this Table 9. In this table, the results were displayed with 1.0-volt intervals. This is the full domain of the MFC. As can be seen, the desired percentage of aeration is not matching up with the tested data point.

Input voltage [V]	**Added volume** mm^2	**Percentage aeration** %
0	0	0
1	12900	0,56812
2	268000	1,07821
3	402000	1,617316
4	536000	2,156421
5	670000	2,695526
6	804000	3,234631
7	938000	3,773737
8	1072000	4,312842
9	1206000	4,851947
10	1340000	5,391052

Table 9: Added aeration

For this reason, the desired aeration percentages, 1%, 1.5%, 2%, and 4% were linearly interpolated and extrapolated. These results are displayed can be seen in table Table 10. These will be the values used in the experiments.

Input voltage [V]	**Percentage aeration** %
0	0
1.99	1
2.98	1.5
3.21	2
7.32	4

Table 10: Desired aeration input values

4.4.2 Frequency

For the input frequency, a 0 to 10-volt range is utilized as the input signal. Hence, a conversion from the frequency of the tank movement to the input signal has been made. The input signal can be calculated by using the maximum voltage of the input signal, and the maximum frequency output of the motor. This relates to a linear ratio to each other. The voltage has a range of 0V to 10V, and the motor has a range of 0Hz to 2Hz.

4.4.3 Test matrix

To make sure that the experiments are performed in a structured way, a transformation matrix is used. this transformation matrix shows all the different tests that will be performed. The first test matrix is made for 5 different levels of aeration and 5 different levels of frequency. These levels of frequency are chosen for their relation with the natural frequency. All the different tests within the test matrix will be performed multiple times to ensure robust results.

	0%	1%	1.5%	2%	4%
0.93Hz					
0.94Hz					
0.95Hz					
0.96Hz					
0.97Hz					

Table 11: Experiment matrix 1

4.4.4 Calibration

For the pressure sensors, a translation from volts to pascals is needed before the data is of any use. The calibration values are known for each sensor, as presented in Table 12. To validate if these values are still accurate, reference is made to the paper by [19], which employed the same sensors and performed a comparison with numerical values. The comparison showed that the values were in the same order as each other.

In Table 12, it can be observed that PS3 has a calibration value that is a factor of 2 different from the other sensors. Firstly, this sensor was placed in the middle so that any strange values would be noticeable. Additionally, a test was conducted on PS3 to verify if the calibration value made sense at all. This test involved switching the pressure sensors 1 and 3 in the setup, as well as modifying the calibration value in the post-processing MATLAB file. After running a random experiment from the test matrix, the results were close to each other. Therefore, the low calibration value of PS3 appeared strange initially, but it is indeed the correct calibration value.

Pressure sensor	**Calibration value** mV/kPa
Ps 1	44.95
PS 2	44.23
PS 3	19.45
PS 4	43.37
PS 5	41.29

Table 12: Calibration values

4.4.5 Experiment Steps

For the experiments, the tests that will be performed are noted in Table 11. The procedure for each individual experiment needs to be executed in the same manner for all experiments in the test matrix. Furthermore, these experiments should be conducted on the same day to ensure consistent temperature and water quality across all test runs. The used procedure is:

- Set the tank to the start position using manual control.
- Measure the water height in the tank and refill it if necessary.

- Switch to computer control.
- Start data acquisition.
- Initiate automatic control after a 5-second delay.
- Save the run number along with the corresponding frequency and aeration level.
- Wait for the water to reach a fully calm state.
- Switch back to manual control and reset the tank position to the start position.

4.4.6 Automatic Tank Control

To ensure the repeatability of the experiments, a control file is utilized to regulate the movement of the tank. This file is created using a MATLAB script that generates and saves two columns comprising 20,000 rows each. The control program on the computer reads these files at a sampling rate of 100 Hz, resulting in an experimental duration of 20 seconds.

For the tests involving aeration, a separate file is generated to ensure that aeration is present from the moment the tank starts moving. The Mass Flow Controller (MFC) typically requires between 10 and 18 seconds to reach a steady-state aeration input signal. Therefore, the control files for all the tests consist of 20,000 values to establish aeration, immediately followed by 20,000 values representing the relevant aeration level and the corresponding tank frequency. The data acquisition will be initiated 5 seconds prior to the start of the control file, resulting in 45 seconds of measured data per test. The initial 5 seconds, during which nothing occurs in the tank, are utilized for a zero measurement.

4.4.7 Post processing

Post-processing of the data will enable the visualization of the collected data, allowing for visual analysis of the results. The computer connected to the experimental setup, as depicted in Figure 17, receives data from all the sensors. This data is organized into separate columns for each sensor. In the case of the experimental setup, there are 5 pressure sensors, 1 wave gauge, and 1 mass flow controller for the added air, resulting in 8 output signals. Each output signal has a specific starting time and time step size. By combining these two parameters, an additional column representing time can be added.

The post-processing of the data will be conducted on my personal computer using MATLAB. The data from the experimental setup is transferred to my laptop via a USB flash drive. A MATLAB script is then written to read the data from each column. Once the data from a sensor is linked with the time column, plotting the time against the pressure or wave height can be achieved using a simple MATLAB command.

4.4.8 Data visualisation

The data visualization aimed to analyze the impact of different aeration levels and sloshing frequencies on the maximum pressures achieved. To achieve this, a two-step approach was adopted. Firstly, line plots were utilized to observe the trends of maximum pressures for each frequency. This enabled a comparative analysis of the influence of various aeration levels within a specific frequency range. The line plots provided a clear representation of how the maximum pressures varied as a function of the aeration level.

Additionally, to gain a comprehensive understanding of the data, box plots were incorporated into the visual analysis. These box plots further revealed the distribution of maximum pressures across different aeration levels for each frequency. The box plots allowed for a concise summary of statistical measures such as the median, quartiles, and potential outliers. They provided insights into the central tendency and spread of maximum pressures at different aeration levels, facilitating comparisons and identifying any potential anomalies.

By combining line plots and box plots, a comprehensive visualization of the maximum pressures at various aeration levels and sloshing frequencies was achieved. This approach enabled a thorough analysis of the effects of different parameters on the system's behavior and helped identify significant trends or deviations in pressure responses.

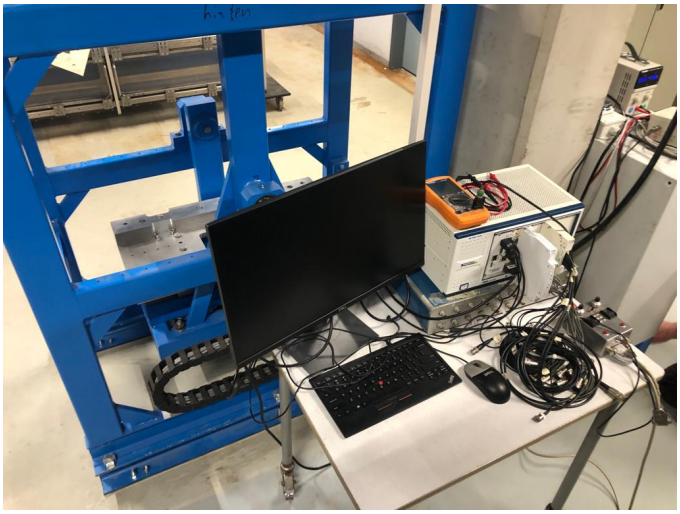

Figure 17: The computer that is coupled to the experimental setup preforms two functions. The first function is to send a control signal with the desired frequency to the drive motor of the tank. The second function is to receive all the data of the different sensors.

5 Results

This chapter presents a comprehensive analysis of the results obtained from both simulations and experiments conducted in this study. The primary objective of this chapter is to provide a detailed overview of the findings and insights gained from the investigations into the maximum wave force on a horizontal overhang, including the effect of aeration.
The results presented here encompass a range of parameters, including different excitation frequencies and different levels of aeration. These results shed light on the behavior, performance, and characteristics of the system under different conditions, offering valuable insights into its dynamics and response.

The chapter begins with an examination of the simulations, which provided a platform for modeling and analyzing the system's behavior. The simulation results unveil important trends, patterns, and correlations, offering a theoretical foundation for understanding the system's performance. Furthermore, the simulations provide a basis for comparison with the experimental results, validating the accuracy and reliability of the model.
Following the simulations, the chapter proceeds to present the results obtained from the experiments. These experimental findings provide crucial empirical data, offering real-world observations and measurements. The experiments were carefully designed and conducted to investigate the effects of various parameters, such as aeration. The outcomes of these experiments contribute to a deeper understanding of the system's behavior and provide insights into its practical implications and potential applications.

Throughout this chapter, both qualitative and quantitative analyses are employed to interpret the results accurately. Statistical analyses, visualization techniques, and relevant metrics are utilized to present and interpret the data effectively. The emphasis is on providing a comprehensive and detailed analysis of the results, supported by appropriate graphical representations and statistical measures.

5.1 Simulation results wave height variation

The results of the simulation described in Section 2.6.5 are extracted from 3 pressure sensors located near the closed corner of the overhang. In the plots in Figure 18 you see the results for five different variations of the maximum wave height. H_{max} is the maximum wave height as computed in Section 2.6.4. The scaling factors for each wave height are given below each plot. In each plot, you see the pressures for each moment in time, measured by the three pressure sensors. Additionally, the peak pressure is marked by the black dot and its coordinates.

The results are analyzed by comparing the maximum pressures over all three sensors. The maximum pressure versus the wave height is presented in Figure 19. The relation is approximated by a linear relationship, indicated by the straight red line. The dotted lines indicate the 95% confidence bounds. The conclusion thus far is that there exists a nearly linear relationship between the pressure and wave height in the vicinity of H_{max}

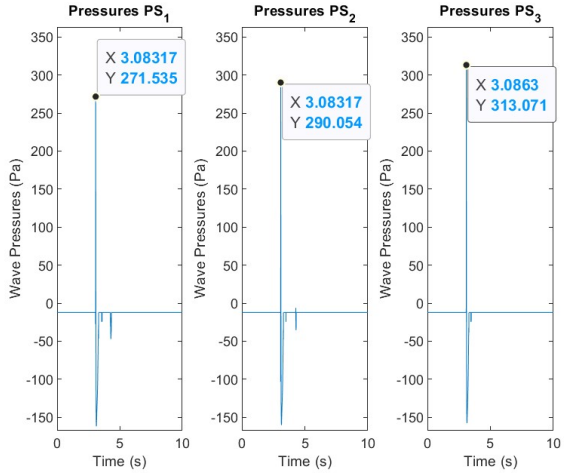

(a) Pressure peaks with $0.90 * H_{max}$

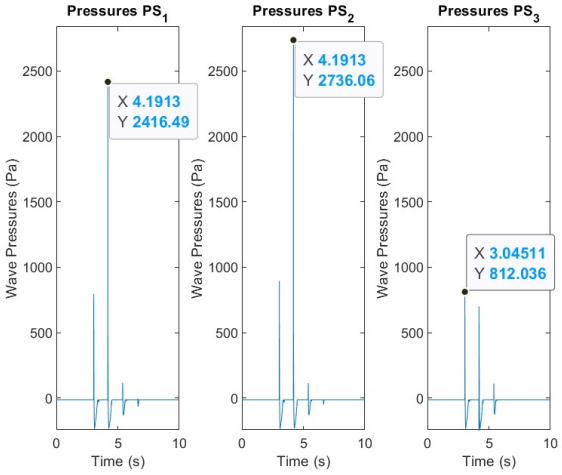

(b) Pressure peaks with $0.95 * H_{max}$

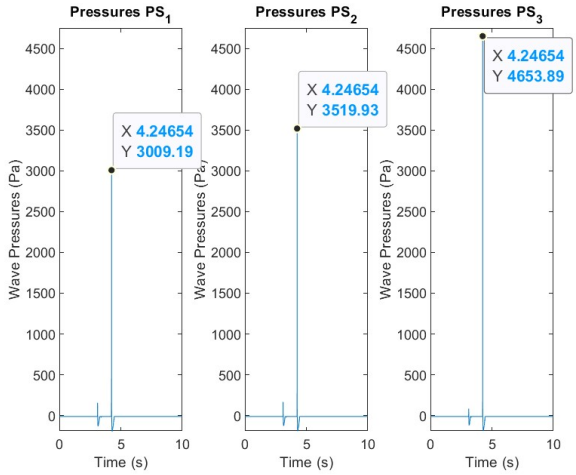

(c) Pressure peaks with H_{max}

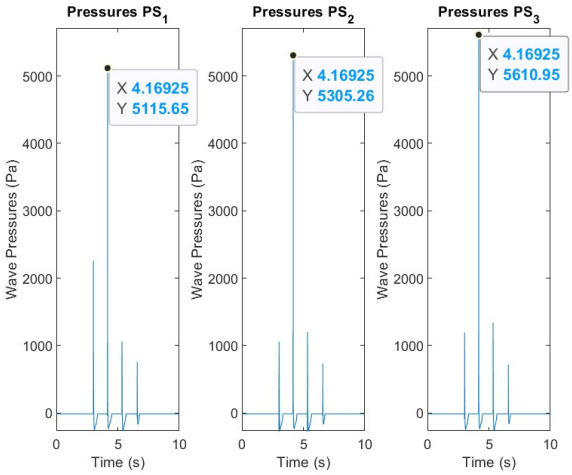

(d) Pressure peaks with $1.05 * H_{max}$

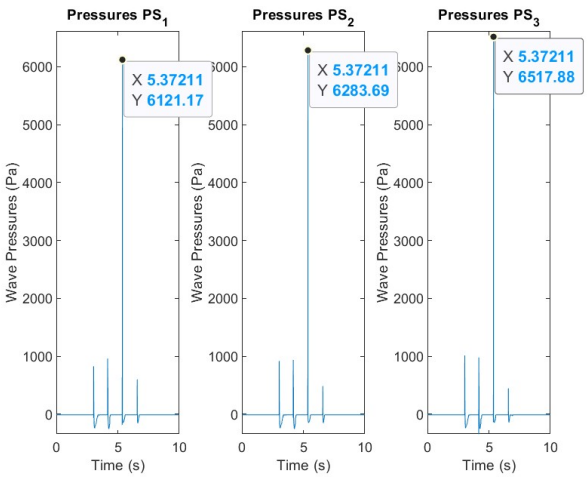

(e) Pressure peaks with $1.10 * H_{max}$

Figure 18: Maximum pressure results of a non-aerated wave impact. With the only variable the maximum wave height

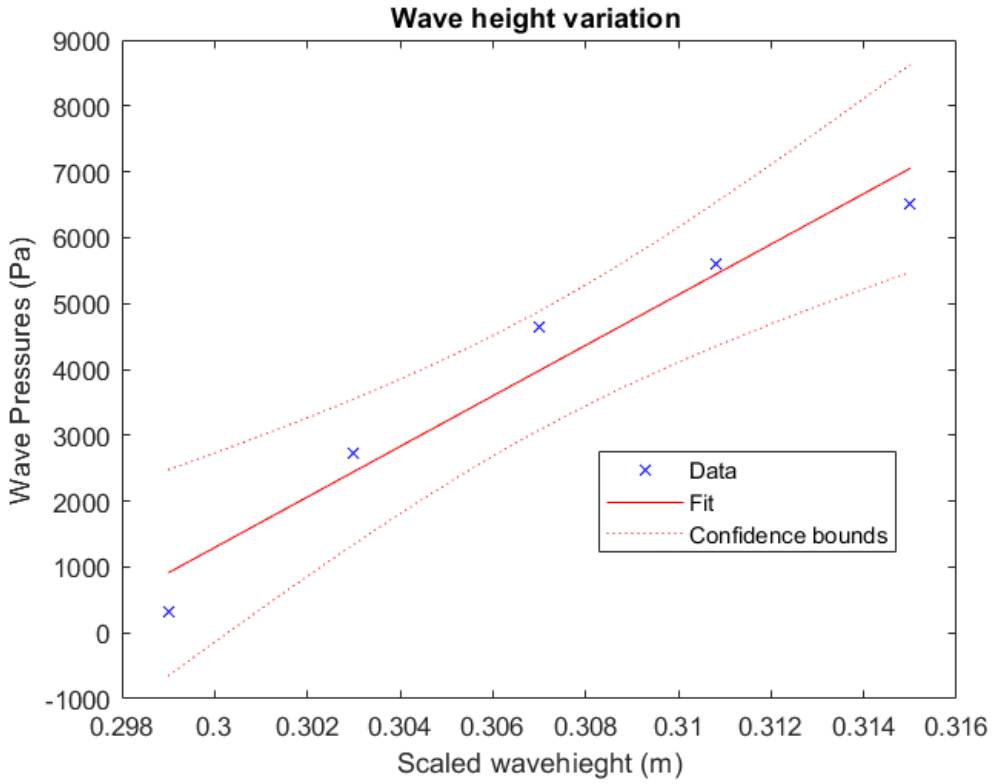

Figure 19: Linear approximation of the relationship between the wave heights and pressures

5.2 Simulation results water height variation

In Figure 20 you see the results of the experiment where we varied the water height for a constant set of input signals, where the amplitude and frequency in the input signal correspond to the maximum wave height H_{max}. The blue dots indicate the maximum wave pressure for the corresponding water height. The relation between the water height and the maximum pressure is assumed to be linear, which is represented by the red line. The red dotted lines are the 95% confidence intervals.

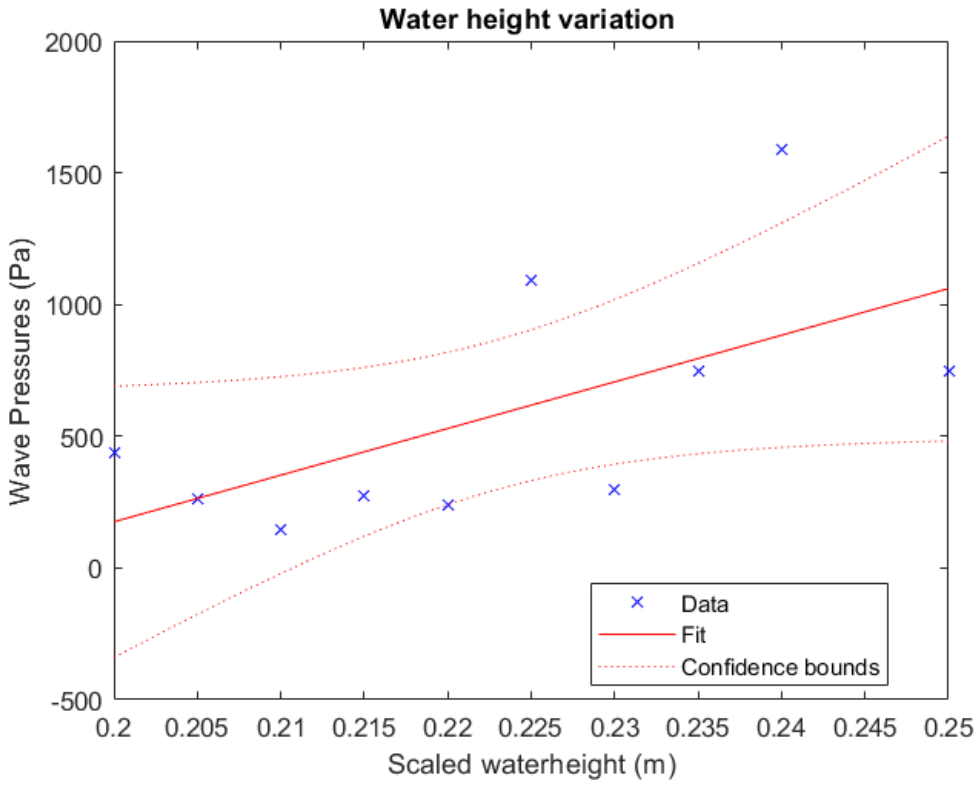

Figure 20: Linear approximation of the relationship between the water heights and pressures

5.3 Experimental setup simulations

Looking at the peak pressures of the simulation with aeration and without aeration stones. It can be seen that the (peak) pressures of the new setup are significantly larger than the old setup. This can be explained by the phenomena of a rising bottom. The waves will feel the bottom no longer at 20[cm] deep but somewhere between 20[cm] and 16.5[cm]. As Wood and Peregrine conclude in their paper[49], is that the wave pressure will increase as the water becomes more shallow. The effect measured at the simulations would therefore be likely to have the pressure magnitudes of the last simulations.

(a) Old setup, used in the simulations

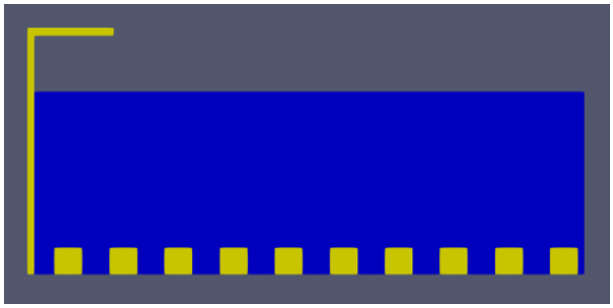

(b) New setup, used in the experiments

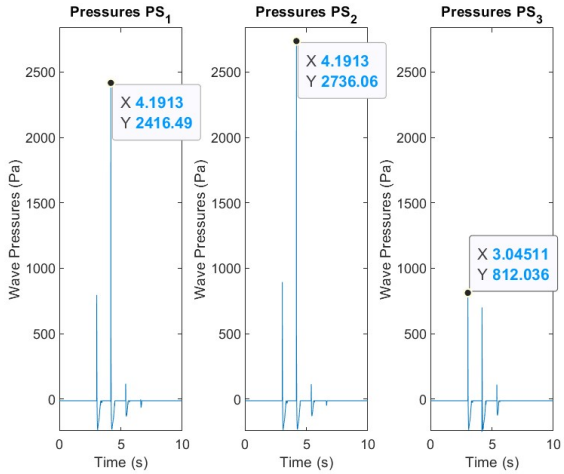

(c) The pressures of the old setup. This setup is without aeration stones

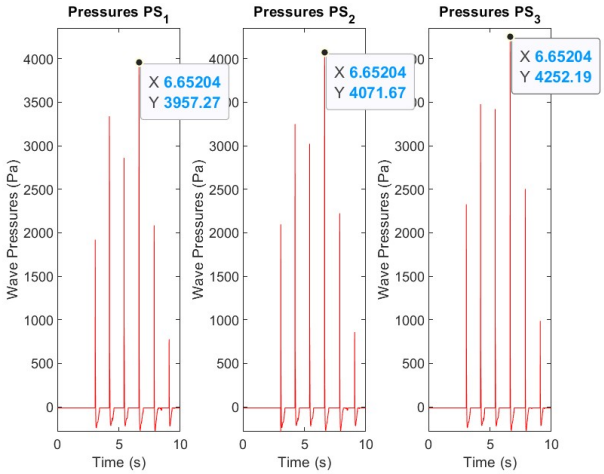

(d) The pressures of the experimental setup, with aeration stones

Figure 21: The comparison of the results of two different test setups in the simulations

5.4 Experimental results

In this section, the results of the test matrix, as displayed in Table 11, will be presented. In Figure 22-Figure 26, the pressures per aeration level for each of the sensors are presented.

In order to gain a better understanding of the results and draw a more robust conclusion, it is beneficial to use both a line plot (left plots) and a box plot (right plots) to display the results of the pressure vs. aeration experiment. A line plot enables visualization of the overall pattern or trend in the data, allowing for a clear understanding of how the maximum pressure changes at different levels of aeration at different pressure sensors, whereas a box plot provides a concise summary of the data distribution of the pressure at each aeration level. By incorporating both a line plot and a box plot, the emphasis can be placed on both the trend and the statistical summary of the data, ultimately resulting in a better understanding of the results and a more robust conclusion in Section 6.

For convenience, a brief explanation will be provided on how to interpret a box plot using the visualization presented in Figure 22. The middle line represents the median observation, which is the middle value of the dataset when it is sorted in ascending order. The lower and upper bound of the blue box represent the first quartile and third quartile respectively. These quartiles bound the middle 50% of the observations when sorted in ascending order. The horizontal lines indicate the area that is at a maximum distance of 1.5 times the interquartile range, which is the range between the first and third quartile. The points outside this range are represented by dots, which indicate that they are considered outliers.
Although each boxplot only consists of five observations, there are still a few advantages of this type of visualization. Even with a small sample size, a box plot can provide a visual representation of the distribution of your data. Furthermore, the box plots allow for a direct comparison of the results between different experiments.

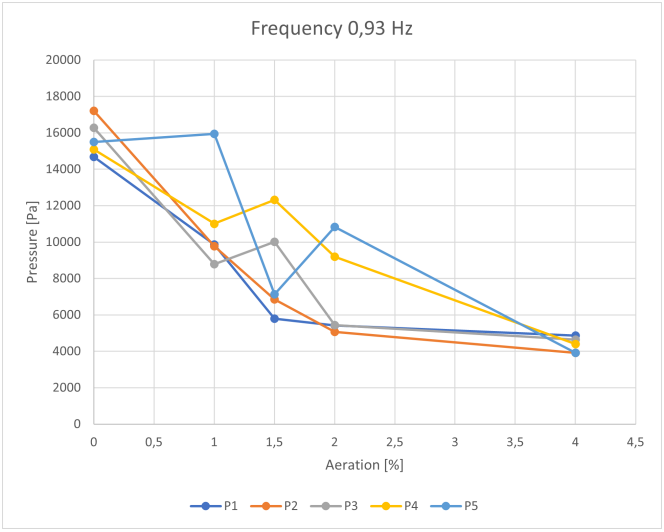

(a) Line plot of all the individual pressure results of the pressure sensors, plotted against all levels of aeration at a fixed frequency of 0.93Hz

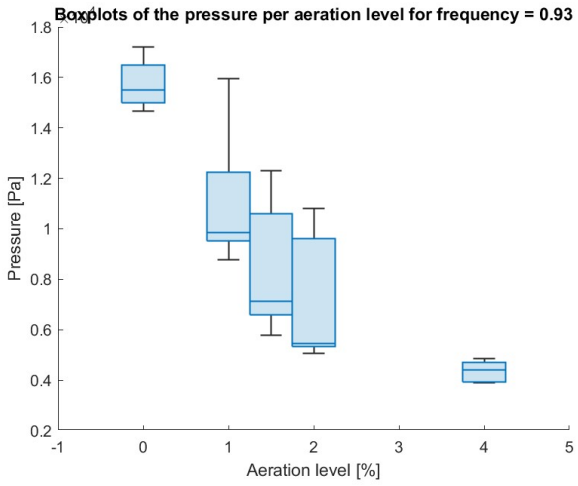

(b) Box plot of all the pressure results of the pressure sensors, plotted against all levels of aeration at a fixed frequency of 0.93Hz

Figure 22: Results of the experiments at a frequency of 0.93 Hz

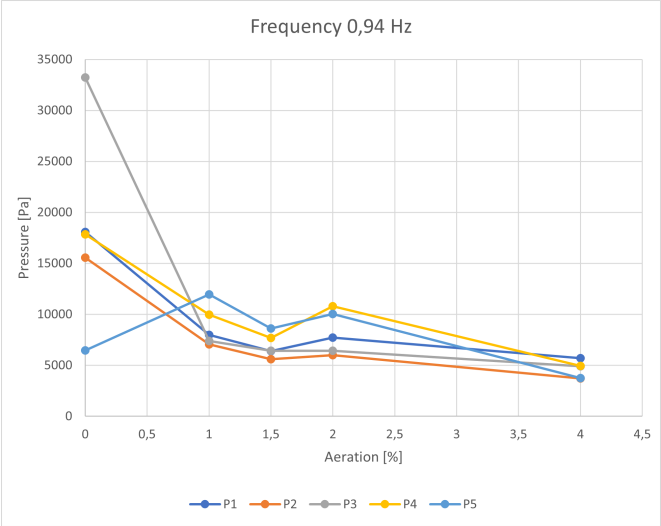

(a) Line plot of all the individual pressure results of the pressure sensors, plotted against all levels of aeration at a fixed frequency of 0.94Hz

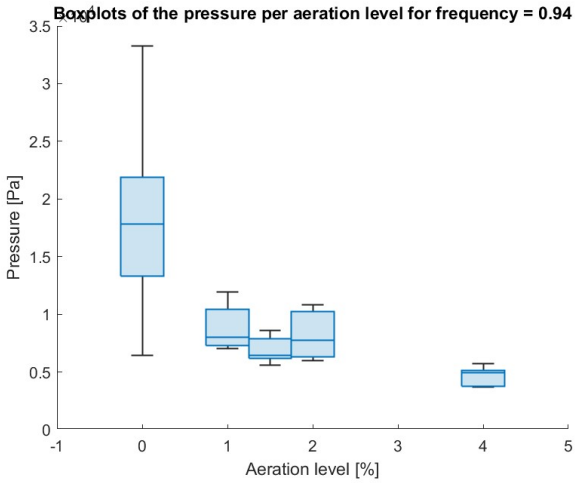

(b) Box plot of all the pressure results of the pressure sensors, plotted against all levels of aeration at a fixed frequency of 0.94Hz

Figure 23: Results of the experiments at a frequency of 0.94 Hz

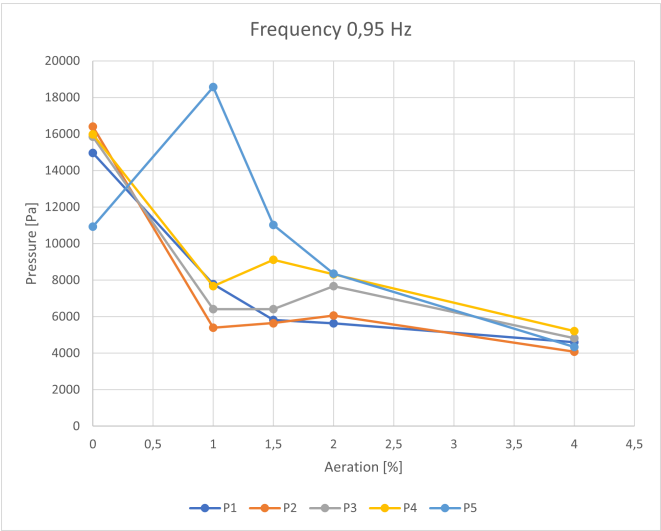

(a) Line plot of all the individual pressure results of the pressure sensors, plotted against all level of aeration at a fixed frequency of 0.95Hz

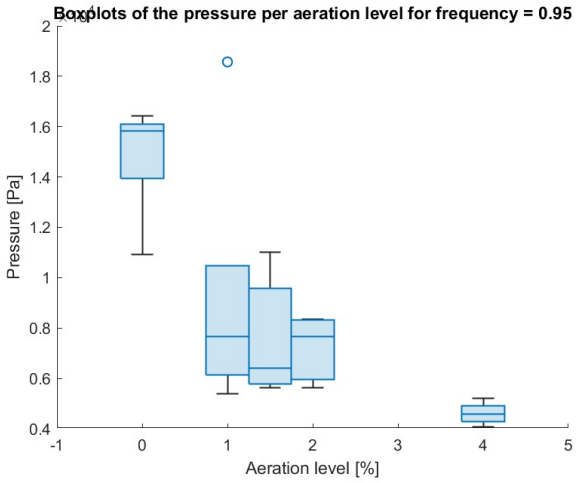

(b) Box plot of all the pressure results of the pressure sensors, plotted against all levels of aeration at a fixed frequency of 0.95Hz

Figure 24: Results of the experiments at a frequency of 0.95 Hz

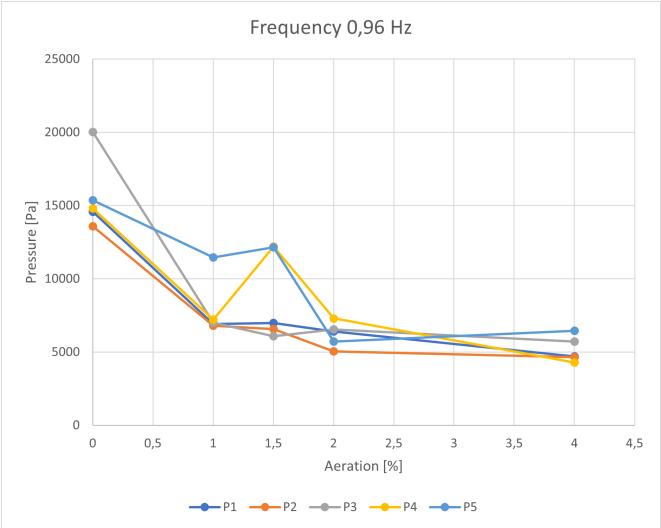

(a) Line plot of all the individual pressure results of the pressure sensors, plotted against all levels of aeration at a fixed frequency of 0.96Hz

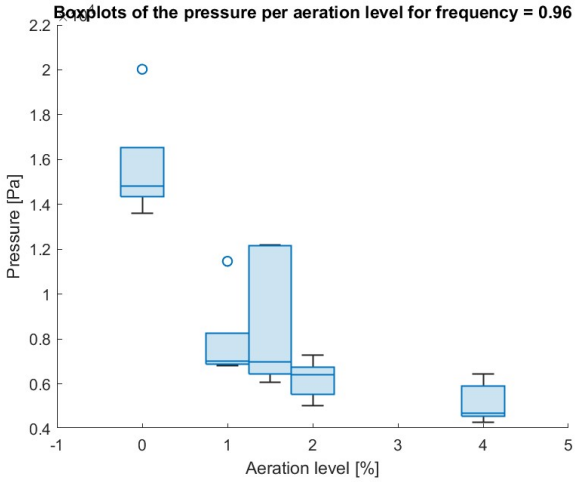

(b) Box plot of all the pressure results of the pressure sensors, plotted against all levels of aeration at a fixed frequency of 0.96Hz

Figure 25: Results of the experiments at a frequency of 0.96 Hz

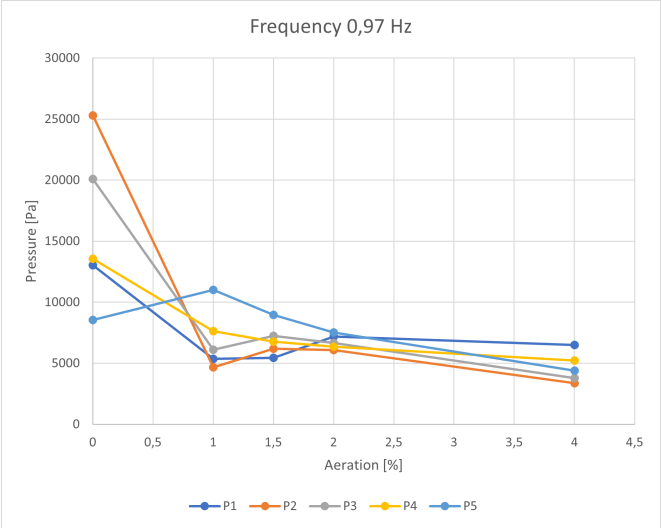

(a) Line plot of all the individual pressure results of the pressure sensors, plotted against all levels of aeration at a fixed frequency of 0.97Hz

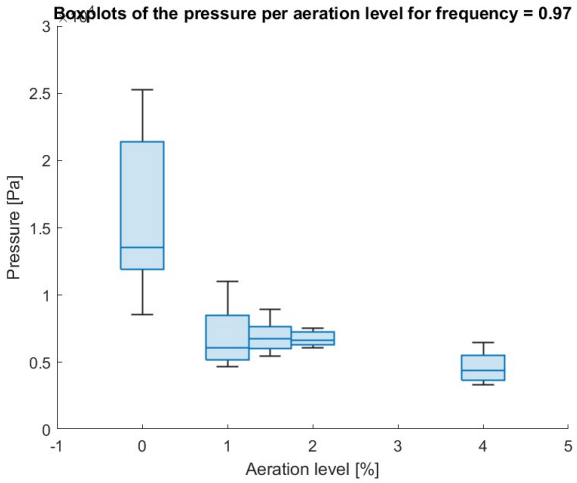

(b) Box plot of all the pressure results of the pressure sensors, plotted against all levels of aeration at a fixed frequency of 0.97Hz

Figure 26: Results of the experiments at a frequency of 0.97 Hz

5.4.1 Results aggregated over all frequencies

To check the general effect of the added aeration, the results in Figure 22-Figure 26 are aggregated over all frequencies into one set of results. These results can be used to find a trend of the effect of aeration independent of the frequency. The aggregated results for the first set of experiments are shown in Figure 27 and the results for the second set of experiments are shown in Figure 28.

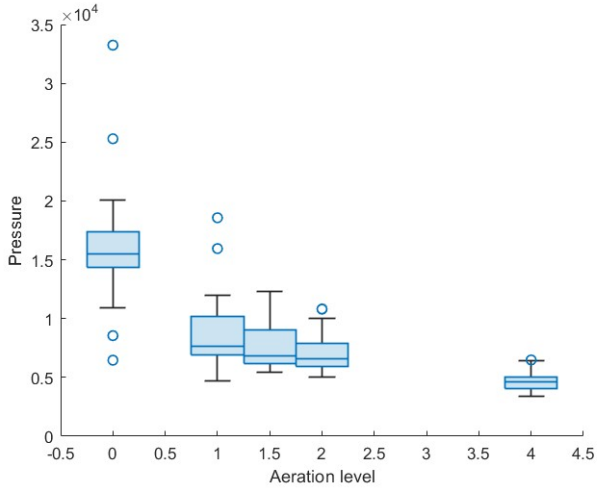

Figure 27: Box plot of the pressure per aeration level aggregated over all frequencies, first run

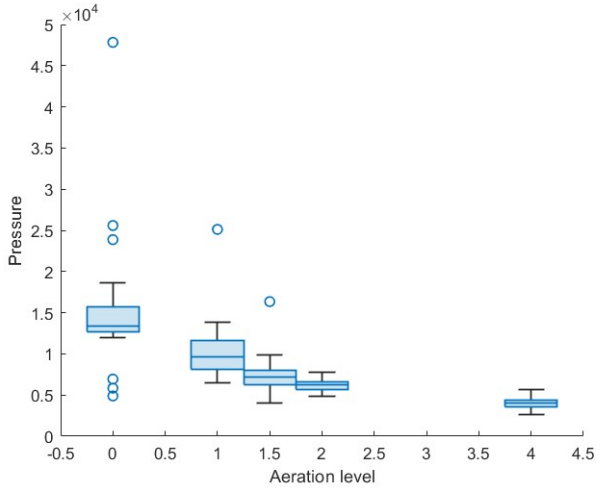

Figure 28: Box plot of the pressure per aeration level aggregated over all frequencies, second run

5.5 Wave impacts

In this section, specific air phenomena and wave types are presented through pictures captured during the experiment. The pictures corresponding to the highlighted impacts are displayed alongside the pressure time series. The subsequent Section 6.2, summarises the findings of this section. It should be noted that the pictures were taken precisely align with the displayed peaks, as explained Figure 4.2.2. The pictures are scaled down for the viability of the overall pictures. The full-scale images of the wave impact are shown in Appendix D

In Figure 29, two distinct impacts are depicted, with peak (I) noticeably lower than peak (II). Upon examining the corresponding images captured at the moment of impact, a discernible air pocket can be observed for impact (I). Notably, this air pocket is situated in the central region of the overhang. Conversely, impact (II) exhibits smaller air pockets, which are primarily absent (or minimal) in the middle section of the overhang where the sensors are located. These findings confirm the damping effect exerted by an air pocket during a wave impact. This observation aligns with earlier research conducted by C. Lugni, confirming the presence of a damping effect [30].

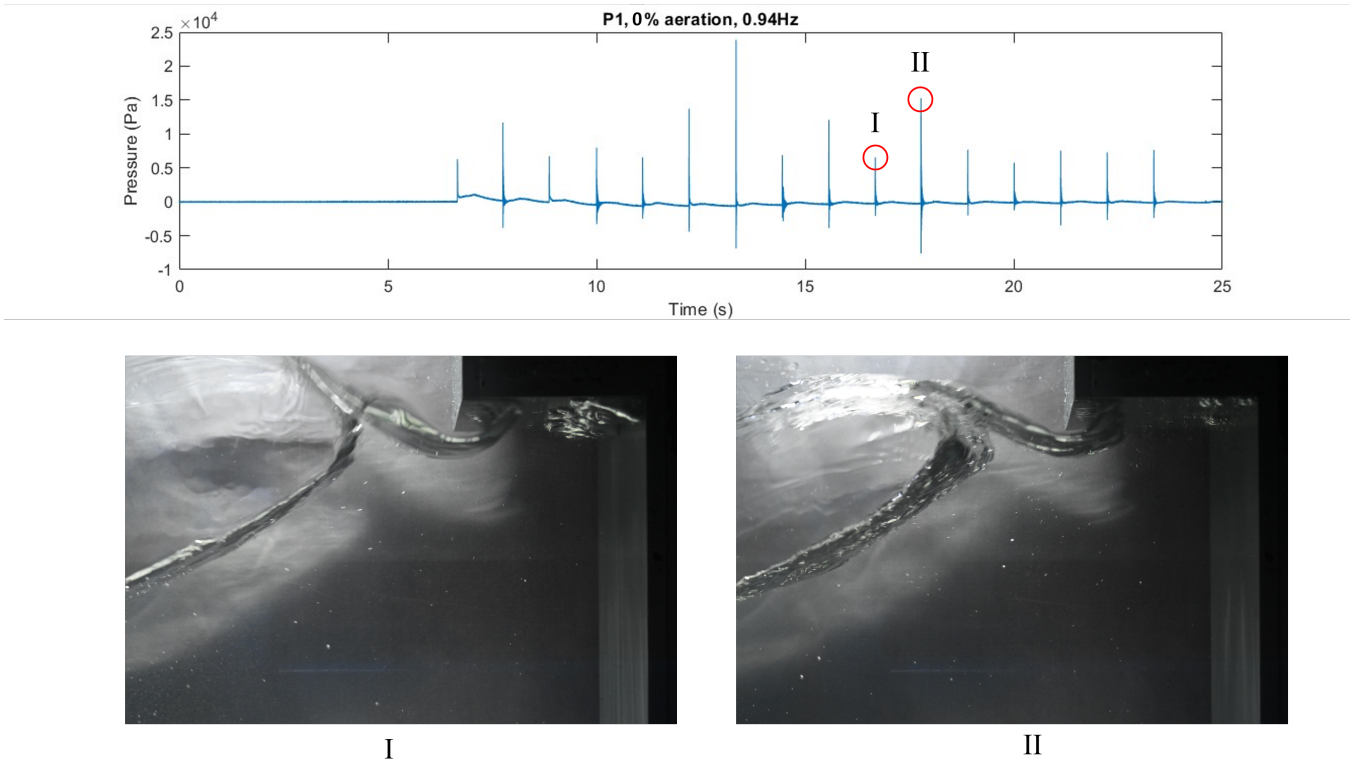

Figure 29: The time series of the pressure sensor 1 of an experiment with 0% aeration at 0.94Hz. Two pictures of the moment of impact are shown below, corresponding to the labeled and marked peaks. In picture I, an air pocket near the pressure sensors is visible. In picture II, almost no air entrapment is visible.

In Figure 30, two distinct aerated wave impacts are depicted, with impact (I) exhibiting significantly higher intensity compared to impact (II). Upon examining the accompanying images captured at the moment of impact, it is evident that air pockets are visible in picture (II), in addition to the presence of aeration. Conversely, in picture (I), the absence of air pockets is notable. The pressure measurements corresponding to these images corroborate the conclusion drawn in the previous point: the presence of air pockets during a wave impact has a damping effect. This implies that even in cases of wave impacts with homogeneous aeration distribution, the formation of air pockets can still occur, resulting in a further reduction of peak pressure.

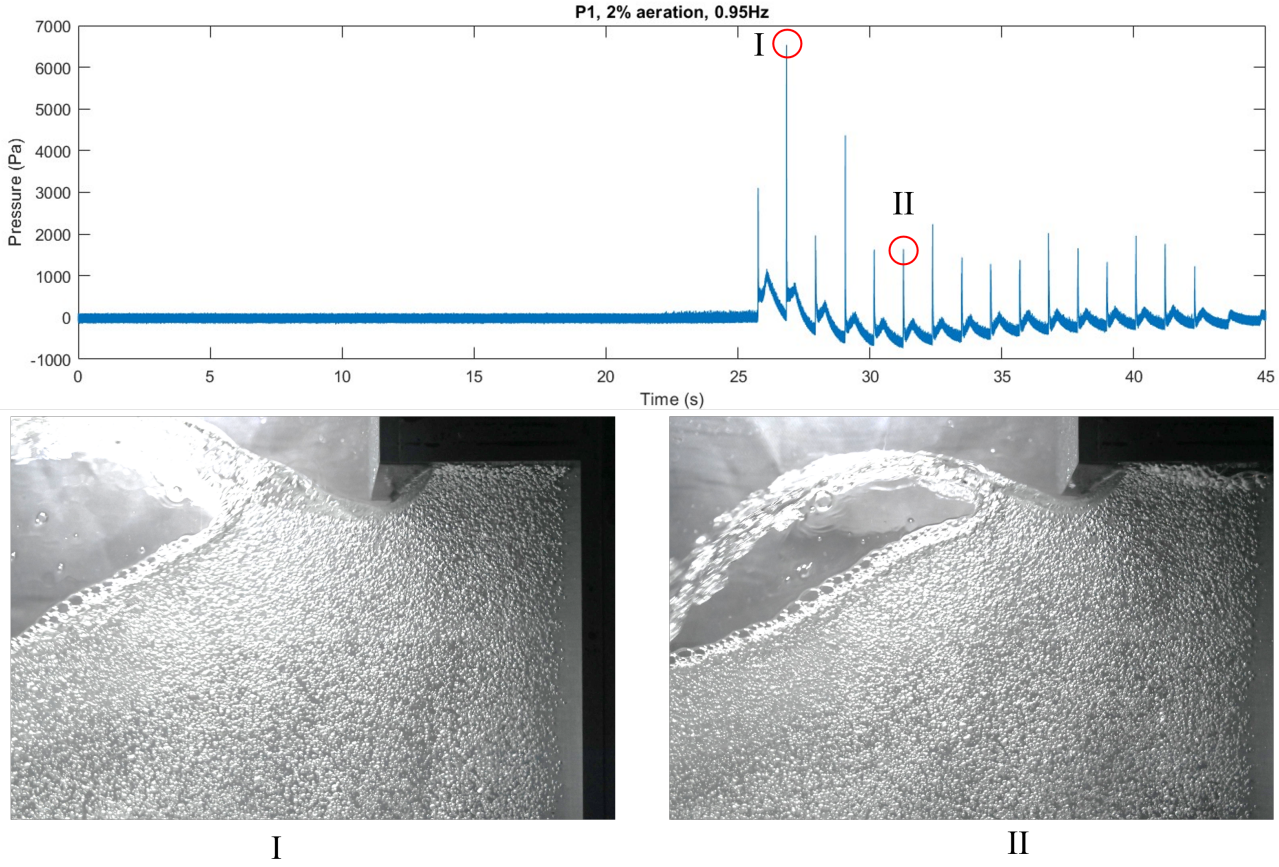

Figure 30: The time series of the pressure sensor 1 of an experiment with 2% aeration at 0.95Hz. Two pictures of the moment of impact are shown below, corresponding to the labeled and marked peaks. In picture II, an air pocket near the pressure sensors is visible. In picture I, almost no air entrapment is visible.

In Figure 31, two wave impacts are depicted through images captured at the first moment of impact and immediately after the impact. The time series plot reveals that wave impact (II) represents the largest impact observed in this experiment. Analyzing the characteristics of the wave types, the impact displayed in Figure (II) exhibits the characteristics of a flip-through wave. Such wave types are known to cause the most severe impact on vertical walls, leading to extreme pressure levels and high jet speeds, as discussed in the literature [30]. Conversely, wave impact (I) yields one of the lowest pressures. Notably, Figure (I.b) shows the presence of an air entrapment, which accounts for the low pressure measured during this peak.

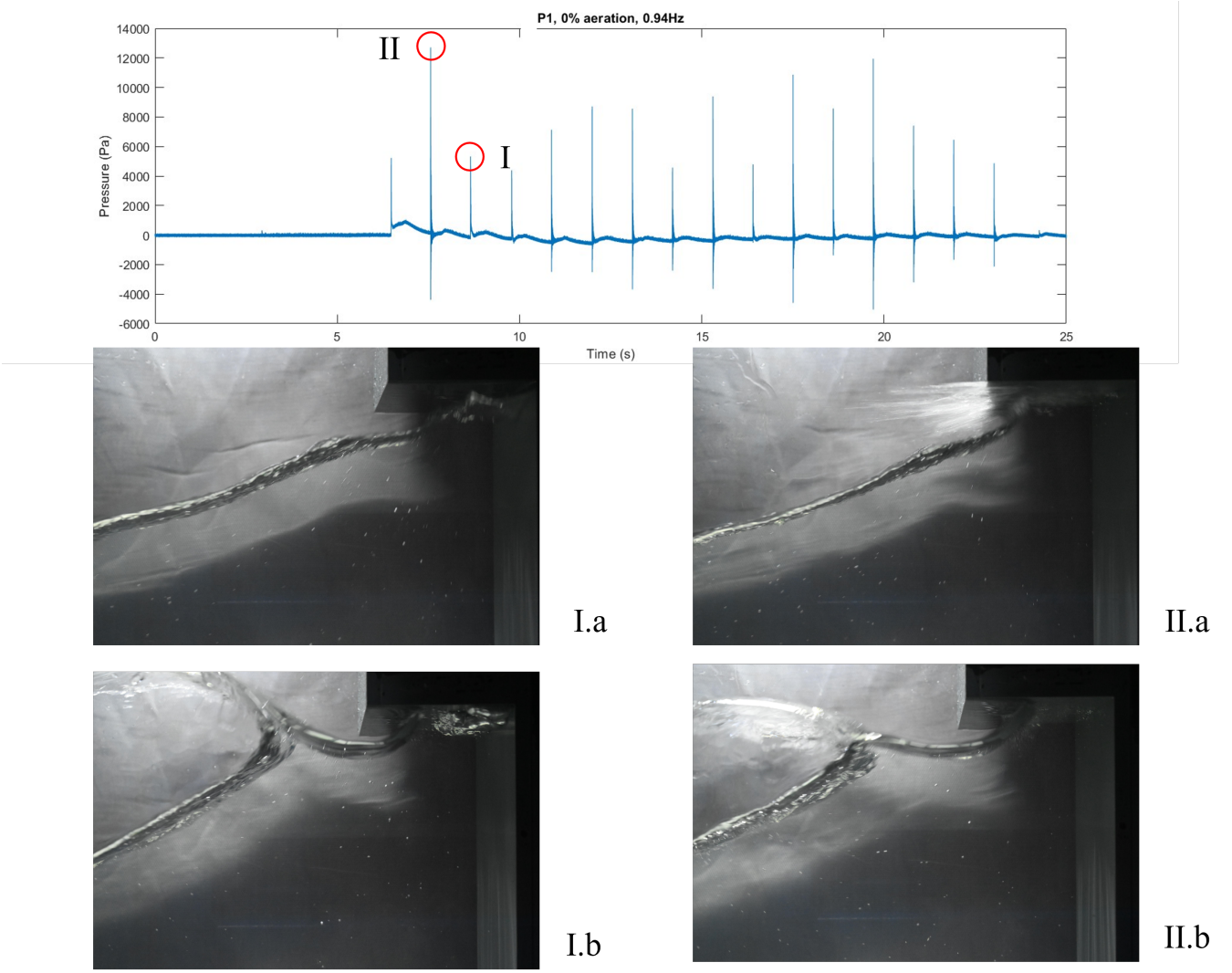

Figure 31: The time series of the pressure sensor 1 of an experiment with 0% aeration at 0.94Hz. Two pictures per pressure peak are shown below. Picture I.a is the first picture in time taken at peak I. Picture I.b is the follow-up picture of I.a. In I.a an upward moving wave can be seen. This wave has a peak halfway through the overhang. In picture I.b a large air pocket can be seen near the pressure sensors. In picture II.a an upward-moving wave can be seen with minimal clearance between the top of the wave and the bottom of the overhang. In picture II.b the moment after impact can be seen. Here it is visible that there is no air entrapment or air pockets visible.

In Figure 32 2 different wave impacts are shown. Resulting in two different pressures. Analysing these impacts, it was noticeable that the motion of the aeration bubbles was different in two impacts. Where it looks like impact (I) has less rotational movement in the bubble cloud than impact (II). This can be the cause of the impact difference on the horizontal overhang. The conclusion of this observation is that the movement of the wave matters to the impact measured on the horizontal overhang.

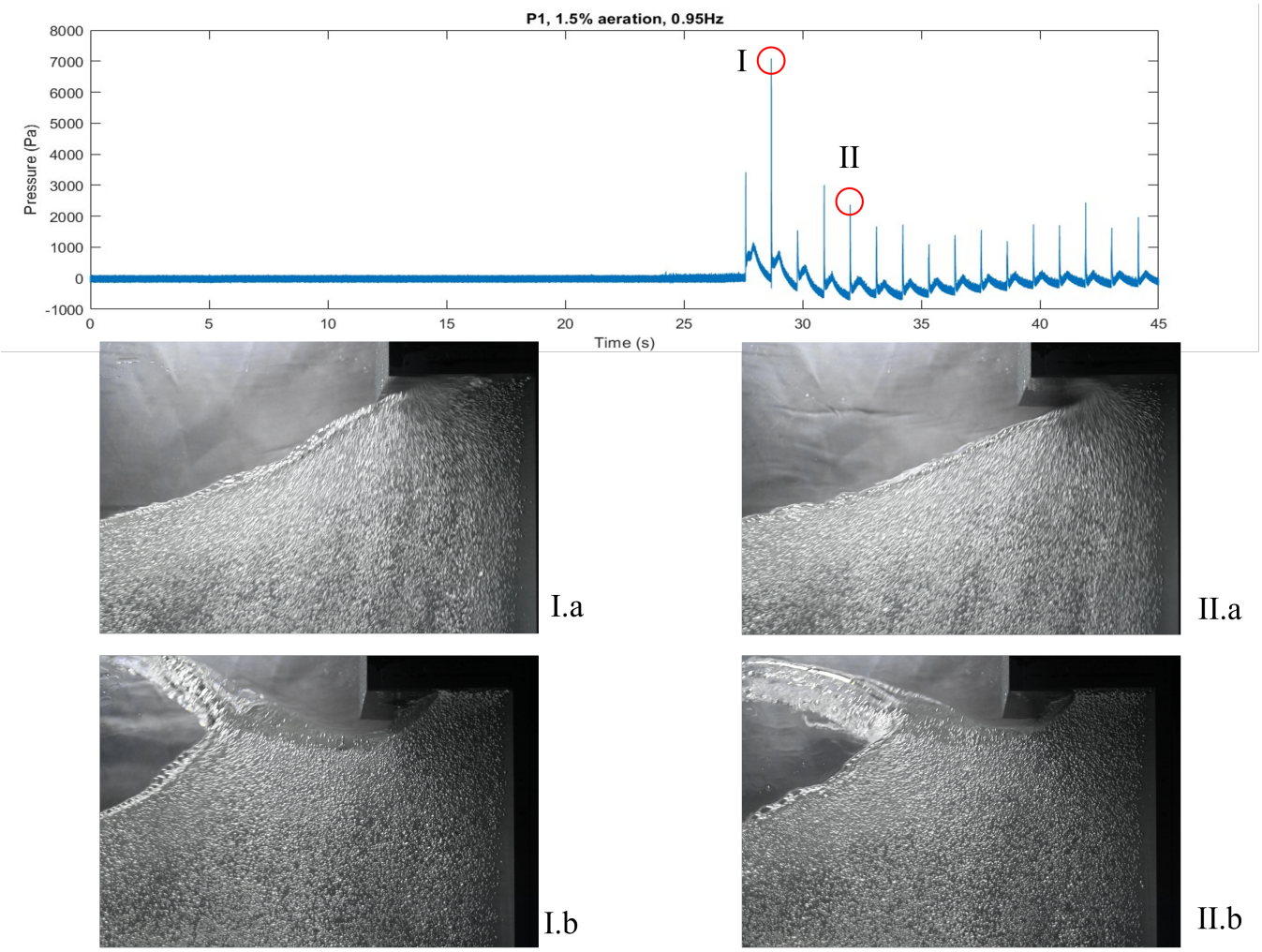

Figure 32: The time series of the pressure sensor 1 of an experiment with 1.5% aeration at 0.95Hz. Two pictures per pressure peak are shown below. Picture I.a is the first picture in time taken at peak I. Picture I.b is the follow-up picture of I.a. In Figure I.a the direction of the water movement can be by the arrangement of the air bubbles. In I.a the arrangement near the back wall is mostly in a vertical direction. Whereas in picture II.a, the arrangement of the air bubbles in both vertical and horizontal movement, resulted in a more circular motion of the air bubbles near the overhang.

6 Conclusion

After all simulation and experimental results are finalized, a conclusion can be drawn. In this section, the aim is to answer the research questions. The research question of this thesis is *What is the effect of aeration on the maximum vertical force on a horizontal overhanging cantilever slab, caused by wave impacts?*

6.1 Conclusion based on the sub-questions

To answer this question in a structured manner, multiple sub-questions are formulated in Section 1.4.1. These questions will be addressed individually, and collectively, they provide an answer to the main research question.

6.1.1 How are the frequency, water height, wave height, and wave pressure related to each other?

We only take into account the relations that we think are relevant for the experiment setup or the conclusions for the main research question. The relation between the parameters can be answered with the results of the simulations. In the numerical simulations, multiple different tests were performed to answer this sub-question. The conclusion of these different tests is divided into the next paragraphs.

Relationship between the wave heights and pressure In Figure 19, the relationship between the wave height and pressure is approximated with a linear relationship. In the plot, it can be seen that all five data points lie within the 95%-confidence intervals. This suggests that indeed the relation between the wave height and wave pressure is linear. Based on the assumption that a minimum of five data points provides a reliable result for the linear approximation, we conclude that the relation between the wave height and pressure is linear.

Relationship between the water height air gap and pressure In Figure 20 we approximated the relation between the water height and the pressure by a linear relationship. In this plot, three out of ten data points lie outside the confidence bounds. Therefore, we reject the suggestion that there is a linear relation between the water height and pressure. The water height will not be used as an input variable and therefore we do not investigate the relation further.

Natural frequency The natural frequency calculation knows 2 approaches. The first one is with a plotted transfer function, the second one is with the dispersion relation. In Figure 6 are the results for the plotted transfer function, which shows two peaks. From the results of the transfer function, it was not clear if the natural frequency of the sloshing was at 0.92[Hz] or at 0.97[Hz].
The second method is the dispersion relation, which is the theoretical method to compute the natural frequency. The computations in Section 2.6.3 imply a natural frequency of 0.97[Hz].

	Natural frequency
Transfer function	0.92[Hz]-0.97[Hz]
Dispersion relation	0.97[Hz]

The dispersion relation confirms that the natural frequency of the transfer function showed in the peak of Figure 7 is more towards the high end of the interval between 0.92[Hz] and 0.97[Hz]. However, the dispersion relation does not include any resistance of the horizontal overhang. This means that the overhang it self has clearly been an obstacle as can be seen in the left part of Figure 6. Implement dampening mechanisms: Installing a horizontal overhang, consequently lowering the natural frequency. This means the 0.97[Hz] of the dispersion relation would likely be an overestimation. The other conclusion that can be drawn from the combination of the conclusion about the natural frequency and Figure 2, is that the calculated natural frequency, used in the simulations, would most likely not be the same for the experiments with the aeration stones permanently secured to the test setup.

The natural frequency of both methods is approximately equal. As the transfer function has been validated at the natural frequency, it is assumed that the entire transfer function can be utilized to describe the relationship between the frequency and the wave height.

6.1.2 What is the expected maximum pressure on the overhang without the effect of aeration based on the simulations?

The expected pressures at the overhang were first summarised in Section 5.1. At H_{max} the expected pressures were in the order of magnitude of 2700[Pa]. With the variations of wave height, the maximum pressure measured at the overhang increased to around 6500[Pa]. However, as explained in Section 5.3, all the simulations were done without the aeration stones modeled into the simulation. In Section 5.3 the difference in maximum pressure is shown. For the situation of H_{max} the maximum pressure is again in the order of 2700[Pa]. However, the maximum pressure in the case of a simulation including aeration stones, the maximum pressure becomes 4250[Pa]. This is a 66.6% increase in pressure. It is not expected that for each simulation a 66.6% increment is needed to get a reliable estimate. But it is good to notice that the previous simulations would be likely to give an underestimation as a result of the forgotten aeration stones.

6.1.3 What is the maximum pressure on the overhang without the effect of aeration?

The answer to this sub-question can be found in the experimental results. In this chapter, experiments have been performed for 5 different levels of aeration. This includes tests with 0% aeration, which are specifically relevant to this sub-question. Looking at the results that are independent of the frequency, see Figure 27 and Figure 28, the boxplots show that the median of all experiments will be around 15 [kPa].

In Figure 27 and Figure 28, the observed pressures exhibit a broad distribution across the measured data. This is indicated by the dots in the boxplots, which represent the outliers in the data set. Based on this, the maximum pressure on the overhang can be more than 3 times higher than the median pressure of 15 [kPa], which results in a maximum pressure on the overhang of 47.3 [kPa] without the effect of aeration.

This concludes that maximum pressures above 47[kPa] can happen. But that the most likely maximum wave impact is within the order of magnitude of 15[kPa]

One of the contradicting parts of these results is the location of the maximum peak pressure. Looking at different literature [18] [29], the maximum wave pressure should be located in the closed corner. Meaning that PS1 should give the highest pressure. Looking at the results, it can be seen that different pressure sensors give at different moments the maximum peak.

6.1.4 What is the effect of aeration on the maximum pressure on the overhang?

In the first experiment the maximum wave impact for different frequencies and for different levels of aeration are tested. The different tests are displayed in Table 11. The conclusion will be based on the experiment of Table 11, which has been performed twice. Here, the effect of aeration will be evaluated via the pressure results, observation by the camera, and visual observation during testing. This brings us to the following conclusions, that are drawn from the experiments with aeration:

- In the box plots Figure 22-Figure 26 it can clearly be seen that the median of the experiments without aeration, is higher than the median of the observed pressures with aeration. Furthermore, the third quartiles of the observations with aeration are below the median of the observations without aeration for all experiments. This means that 75 % of the lowest pressures including aeration take lower values than 50% of the highest pressures excluding aeration. Based on this observation, it is concluded that the wave impacts without aeration result in the highest pressures on the overhang. This is consistent with the results obtained by Van der Zee [44] as was explained in Section 1.1.3.

- In the box plots Figure 22-Figure 26, it can also be seen that in the case of 4% aeration, the median is below all the medians of the experiments with another level of aeration. This is valid for all five tested frequencies. It can be concluded that 4% aeration has a damping effect on the wave impact on the overhang, and it is the biggest damping effect that is tested. This is consistent with the results obtained by van der Zee [44] and H. Bredmose [6] as is explained in Section 1.1.3

- When plotting all the frequencies per aeration against the maximum pressures, see Figure 27 and Figure 28, a downward trend can be seen. So the visible trend, independent of the frequency, is a downward trend. This concludes, for aeration levels from 0% to 4%, that when the aeration increase, the maximum pressure decreases.

- There is a significant decrease in variability of the measured pressures for the 4% aeration level, see Figure 27, where the interquartile range is much smaller for the 4% aeration level, compared to the other aeration levels. This variability effect is also mentioned in the results of H. Bredmose [9]. Also, there are significantly fewer outliers for the measurements of the 4% aeration level compared to the measurement with 0% aeration level.

- Throughout all the wave impacts, the researcher was positioned in close proximity to the test setup. One of the initial noticeable aspects of the experiments was the sound emitted by the impacts. A discernible variation in sound was observed, transitioning from a test with 0% aeration to a test with 1% aeration. The sound of the first test was high in tone and was loud. The second test was much less high in tone and also less loud. Hereby, it can be concluded that the decrease in the speed of sound when adding aeration cannot solely be explained by the difference in speed of sound between the two mediums, as depicted in Section 4.4.1, but is also discernible by listening to the impact. The same vocal effect was also observed by Van der Zee [44].

6.2 Wave impacts

- In Figure 29 two different impacts are shown, where peak (I) is clearly lower than peak (II). Looking at the difference in the picture taken at the moment of impact, it can be seen that an air pocket is visible for impact (I). This air pocket is also located in the middle part of the overhang. At impact 2, some small air pockets are present. But (almost) not near the middle part of the overhang, where the sensors are located. This concludes the damping effect of an air pocket during a wave impact. This confirms earlier found results of the damping effect by C. Lugni[30]

- In Figure 30, two aerated wave impacts are visible, with impact (I) significantly higher than impact (II). Looking at the two pictures taken at the moment of impact, it can be seen that, besides aeration, also air pockets are visible in picture (II). In picture (I), the air pockets are absent. The pressures corresponding to the pictures confirm the conclusion in the previous point: air pockets have a damping effect during a wave impact. This means that even for a wave impact with homogeneous divided aeration, an air pocket still can be formed, resulting in an even larger reduction of the peak pressure.

- In Figure 31, two wave impacts are visualized by a picture taken at the first moment of impact and at the moment just after the impact. As can be seen in the time series plot, wave impact (II) is the largest impact of this experiment. Looking at the different wave types, the impact of Figure (II) looks just like a flip-through wave. At vertical walls, this type of wave will cause the most severe impact. As described in literature [30], this type of flip-through event can lead up to an extreme level of pressure on the wall and extreme jet speeds. Looking at the impact (I), the impact gives one of the lowest pressures. In Figure (I.b), an air entrapment can be seen. This air entrapment causes the low pressure measured at this peak.

- In Figure 172, two distinct wave impacts are depicted, resulting in different pressures. Upon analyzing these impacts, a notable difference was observed in the motion of the aeration bubbles. Impact (I) exhibited less rotational movement in the bubble cloud compared to impact (II). This discrepancy in bubble motion could potentially account for the variation in impact on the horizontal overhang. Thus, the conclusion drawn from this observation is that the motion of the wave plays a significant role in determining the measured impact on the horizontal overhang.

In summary, by addressing the main question, *What is the effect of aeration on the maximum vertical force on a horizontal overhanging cantilever slab, caused by wave impacts?* The effect that aeration has on the maximum pressure, can be summarised as a cushioning effect. This effect is in line with the literature on vertical walls, inclined walls, and falling objects [4] [44], [9], [19]. This means that the effect of aeration on the maximum pressure can be treated the same as the effect of aeration on walls or falling objects. The effect of the amount of aeration on a horizontal overhang can be summarised with the relationship that a higher level of aeration results in more damping.

7 Recommendations

In this section, the recommendations will be discussed. All recommendations are based on the results in Section 5 or on the conclusions in Section 6. Based on the knowledge gained up until now, the following recommendations are formulated.

- In the paragraph Relationship between the wave heights and pressure it can be seen, that the confidence interval bound is set at 95%. Looking at the conclusion, the relationship between the points is approximated as linear. Because all points are in the confidence interval. The recommendation, based on the results and conclusion would be to decrease the interval bounds by looking at a relation of this type, or by investigating the error distribution.

  A better and more useful way of displaying the results would be a box plot. Unlike a trend line with a certain interval bound, that primarily focuses on illustrating the overall trend or relationship between variables, a box plot is better suited for comparing multiple groups or categories, allowing for quick comparisons of central tendency, dispersion, and potential differences or similarities among the groups. For this reason, a box plot is used for all experimental results.

- Also in Relationship between the wave heights and pressure, the number of data points is mentioned to be 5. The recommendation for this is to use more data points, with the side note that looking for a relation, the transfer function, must be taken into account to see if the selected points are not at 2 sides of the natural sloshing frequency.

- In paragraph relationship between the water height gap and pressure, a variation in water height and in air gap reduction were tested together in one single experiment. The original plan was to check what the effect of the water depth was on the impact pressure. Earlier literature [49], stated that shallower water, would most likely result in more severe wave impacts. This research wanted to confirm this.

  Unlike earlier research, this test did not only include a variation in the water depth but also changed the air gap. Increasing the water dept resulted in less severe wave impact due to the added water depth, but also increased due to the reduction of the air gap. The recommendation is to do both tests individually. In this way, the effect can be determined separately.

- In paragraph natural frequency, the difference between the transfer function, obtained from the numerical simulations is discussed. The damping mechanism in the simulations, the overhang, can not be included in the dispersion relation. The other main difference between the calculated transfer function and the final setup, are the aeration stones. This should be taken in to account for determining the natural frequency of the simulations and the experiments.

  Here the advice is to 2 identical tests to determine the likelihood of the transfer function. The advice would be to determine the transfer function with the simulations and with the experiments, both with the overhang and aeration stones in place. If determining this for the experiments it self is to time consuming, at least the transfer function based on the simulations must include all objects placed in the test setup.

- In the conclusion about the maximum pressure on the overhang based on the simulations, there is a large difference between the maximum pressure with and without aeration stones. This difference was a 66.6% increase.

  The first recommendation based on the results of Table 2.3 is to include the imperfections caused by the aeration stones in all the simulations. The second recommendation is to invest in a new way of installing the aeration system. This can be done by including more aeration stones, and wider aeration stones. Both with the effect of creating a smoother bottom of the tank.

- In the Section 1.4.1, the sub-questions are separated in numerical simulations without aeration, and experiments with aeration. If a numerical program will be used that can simulate both with and without aeration, the conclusion Section 6 can be based on 2 methods for all conclusions. This has added value to this research.

ComFLOW is very use full to understand the problem and get results that can be compared to the experiments. But a numerical simulation program that can replicate homogeneous aerated water, would have added value to compare it to the experiments with aeration.

- Based on the Section 4.2, the water used in the tank is (fresh) tap water. This is most likely not always the case looking at real hydraulic structures. As Wemmenhoven [46] describes, air bubbles are more likely to dissipate faster in seawater than in freshwater.
- In the conclusion of Section 6.1.3 the maximum pressure is based on two box plots, which have only 50 observations for the case of 0% aeration. In the conclusion it was explained that the measured pressures exhibit a broad distribution, where the maximum pressure could be 3 times higher than the median of the observed pressures. The maximum pressure in this thesis is thus based on a few extreme observations. Since the maximum pressure is our main interest, it is important to collect more observations in order to have a better approximation of this maximum pressure.
- In the conclusion of Section 6.1.3 it was concluded that the variability of the observed pressures decreases for the measurements with 4% aeration, compared to the experiment with 0% aeration. In the conclusion of Section 6.2, it was concluded that various air phenomena caused pressure reduction. These phenomena happen less often and are less significant for experiments with aeration. These conclusions combined suggest that there could be a relationship between air phenomena and extreme wave pressures.
- In the conclusion of Section 6.1.3, a contradicting results was observed. For this reason, additional research is advised for the pressure distribution on the horizontal overhang.
- In wave impact with pictures a conclusion based on the shape of the wave is made. This is done based on the images with a range of only the last quarter of the tank, so 77% of the wave and therefore the wave developing is not visible. The other limitation of the image is the rate at which the pictures are taken. For each run, three pictures are taken with 200Hz. To draw a conclusion on solid results, an other camera must be used. The recommendation for the follow-up research is to use a (high-speed) camera with a higher shutter frequency. And focus not only on the air phenomena but also on the wave type and shape.
- In almost all the pictures taken just after impact after impact Figure 29 - Figure 30, a horizontal water jet can be observed. With the knowledge of this thesis, these observations will not lead to a conclusion. In [21], the numerical results are compared to the experimental results. Resulting in a comparison of the water jets between the two methods. The recommendation would therefore be, to implement such a method to learn more about the impact types of the simulations.
- In Figure 32 the aeration can clearly be seen in all 4 pictures. What is assumed in this thesis, is a homogeneous aerated wave impact. But what can be seen from the results, is that lower in the tank, the aerated water is less homogeneous than at the top. The recommendation based on this observation would be to use more water above the aeration stones to guarantee homogeneous aerated water for all impacts.

References

[1] R. G. Bea, R. Iversen, and T. Xu. Wave-in-deck forces on offshore platforms. *Journal of Offshore Mechanics and Arctic Engineering*, 123:10–21, 2001.

[2] C. E. Blenkinsopp and J. R. Chaplin. Void fraction measurements and scale effects in breaking waves in freshwater and seawater. *Coastal Engineering*, 58:417–428, 5 2011.

[3] H. Bredmose, G. N. Bullock, and A. J. Hogg. Violent breaking wave impacts. part 3. effects of scale and aeration. *Journal of Fluid Mechanics*, 765:82–113, 2 2015.

[4] H. Bredmose, G. N. Bullock, and A. J. Hogg. Violent breaking wave impacts. part 3. effects of scale and aeration. *Journal of Fluid Mechanics*, 765:82–113, 2 2015.

[5] H. Bredmose, A. Hunt-Raby, R. Jayaratne, and G. N. Bullock. The ideal flip-through impact: Experimental and numerical investigation. *Journal of Engineering Mathematics*, 67:115–136, 6 2009.

[6] H. Bredmose, D. H. Peregrine, and G. N. Bullock. Violent breaking wave impacts. part 2: Modelling the effect of air. *Journal of Fluid Mechanics*, 641:389–430, 2009.

[7] G N Bullock, A R Crawford, P J Hewson, M J A Walkden, and P A D Bird. The influence of air and scale on wave impact pressures, 2001.

[8] G. N. Bullock, C. Obhrai, D. H. Peregrine, and H. Bredmose. Violent breaking wave impacts. part 1: Results from large-scale regular wave tests on vertical and sloping walls. *Coastal Engineering*, 54:602–617, 8 2007.

[9] G. N. Bullock, C. Obhrai, D. H. Peregrine, and H. Bredmose. Violent breaking wave impacts. part 1: Results from large-scale regular wave tests on vertical and sloping walls. *Coastal Engineering*, 54:602–617, 8 2007.

[10] Xuexue Chen, Bas Hofland, Wilfred Molenaar, Alex Capel, and Marcel R.A. Van Gent. Use of impulses to determine the reaction force of a hydraulic structure with an overhang due to wave impact. *Coastal Engineering*, 147:75–88, 5 2019.

[11] M J Cooker and D H Peregrine. A model for breaking wave impact pressures, 1990.

[12] Mark J Cooker and D H Peregrine. Wave impact pressure and its effect upon bodies lying on the sea bed, 1992.

[13] Mark J. Cooker and D. H. Peregrine. Pressure-impulse theory for liquid impact problems. *Journal of Fluid Mechanics*, 297:193–214, 1995.

[14] Giovanni Cuomo, William Allsop, Tom Bruce, and Jonathan Pearson. Breaking wave loads at vertical seawalls and breakwaters. *Coastal Engineering*, 57:424–439, 4 2010.

[15] Giovanni Cuomo, Ken ichiro Shimosako, and Shigeo Takahashi. Wave-in-deck loads on coastal bridges and the role of air. *Coastal Engineering*, 56:793–809, 8 2009.

[16] Peregrine D and L. THAIS. The effect of entrained air in violent water wave impacts. *J. Fluid Mech*, page 3177397, 1996.

[17] Ermano de Almeida and Bas Hofland. Validation of pressure-impulse theory for standing wave impact loading on vertical hydraulic structures with short overhangs. *Coastal Engineering*, 159, 8 2020.

[18] Almeida E and Hofland B ;. Standing wave impacts on vertical hydraulic structures with overhangs for varying wave fields and configurations. 2021.

[19] M Van Der Eijk. Numerical modelling of homogeneous aerated-water wave impacts, 2018.

[20] Martin Van Der Eijk and Peter R. Wellens. A compressible two-phase flow model for pressure oscillations in air entrapments following green water impact events on ships. *International Shipbuilding Progress*, 66:315–343, 2020.

[21] Martin Van Der Eijk and Peter R Wellens. Experimental and numerical 2d wedge entry in water with entrained air, 2021.

[22] Martin Van Der Eijk, Peter R Wellens, and Reinier W Bos. Aerated wave impacts on floating bodies, 2021.

[23] Bas Hofland, Miroslaw Lech Kaminski, and Guido Wolters. Large scale wave impacts on a vertical wall, 2010.

[24] Leo H. Holthuijsen. *Waves in oceanic and coastal waters.* cambridge university press, 2007.

[25] Jianjun Huang and Guoping Chen. Experimental study on wave impulse and characteristic pressure of a vertical wall with overhanging horizontal cantilever slab. *Ocean Engineering*, 217, 12 2020.

[26] Dogan Kisacik, Peter Troch, and Philippe Van Bogaert. Breaking wave impact on a vertical wall with an overhanging horizontal cantilever slab: Irregular waves, 2011.

[27] Dogan Kisacik, Peter Troch, and Philippe Van Bogaert. Description of loading conditions due to violent wave impacts on a vertical structure with an overhanging horizontal cantilever slab. *Coastal Engineering*, 60:201–226, 2 2012.

[28] Dogan Kisacik, Peter Troch, and Philippe Van Bogaert. Experimental study of violent wave impact on a vertical structure with an overhanging horizontal cantilever slab. *Ocean Engineering*, 49:1–15, 8 2012.

[29] Dogan Kisacik, Peter Troch, Philippe Van Bogaert, and Robby Caspeele. Investigation of uplift impact forces on a vertical wall with an overhanging horizontal cantilever slab. *Coastal Engineering*, 90:12–22, 2014.

[30] C Lugni, M Brocchini, and O M Faltinsen. Wave impact loads: The role of the flip-through. *Phys. Fluids*, 18:122101, 2006.

[31] Z. H. Ma, D. M. Causon, L. Qian, C. G. Mingham, T. Mai, D. Greaves, and A. Raby. Pure and aerated water entry of a flat plate. *Physics of Fluids*, 28, 1 2016.

[32] marin. Marin, 2022. 23,05,2023.

[33] Author Name. Comflow, 2018. 04,03,2023.

[34] Charlotte Obhrai, Geoffrey Bullock, Guido Wolters, Gerald Müller, Howell Peregrine, Henrik Bredmose, and Joachim Grüne. Violent wave impacts on vertical and inclined walls: Large scale model tests. pages 4075–4086. World Scientific Pub Co Pte Lt, 4 2005.

[35] H Oumeraci, P Klammer, and H W Partenscky. Classification of breaking wave loads on vertical structures, 1993.

[36] overheid. overheid offshore wind data, 2022. 26,04,2023.

[37] David Pavilons, Vera Hengelmolen, D ´ Esireesiresiree Plenker, Niek Bruinsma, Luc Biermans, Alfons Smale, and Peter Wellens. Hydrodynamic loading of breaking waves on offshore inspection platforms, 2022.

[38] Pentair. Pentair, 2023. 20,06,2023.

[39] D H Peregrine. Water waves, nonlinear schrodinger equations and their solutions. *Math. Soc. Ser. B*, 25:16–43, 1983.

[40] D. H. Peregrine and S. Kalliadasis. Filling flows, cliff erosion and cleaning flows. *Journal of Fluid Mechanics*, 310:365–374, 3 1996.

[41] Bagnold R. Interim report on wave-pressure research, 1939.

[42] Sebastian Schreier and Bernhard Mehl. *Experimental Investigation of 3D Sloshing Effects in Thin Rectangular Tanks.* International Society of Offshore and Polar Engineers, 2012.

[43] Francesco Serinaldi and Giovanni Cuomo. Characterizing impulsive wave-in-deck loads on coastal bridges by probabilistic models of impact maxima and rise times. *Coastal Engineering*, 58:908–926, 9 2011.

[44] T van der Zee. The influence of aeration and deadrise angle on impact, 2022.

[45] von Karman. The impact on seaplane floats during landing. 1929.

[46] Rik Wemmenhove, Roel Luppes, Arthur E.P. Veldman, and Tim Bunnik. Numerical simulation of hydrodynamic wave loading by a compressible two-phase flow method. *Computers and Fluids*, 114:218–231, 7 2015.

[47] J D Wheeler. Method for calculating forces produced by irregular waves, 1970.

[48] windenergie. Offshore wind data, 2020. 26,04,2023.

[49] D J Wood and D H Peregrine. Wave impact beneath a horizontal surface, 1996.

[50] J. Wood and Peregrine D. Wave impact on a wall using pressure impulse theory trapped air, 2000.

A APPENDIX A

Appendix A, consist of the detailed drawings of the tank, overhang and the total experiment setup

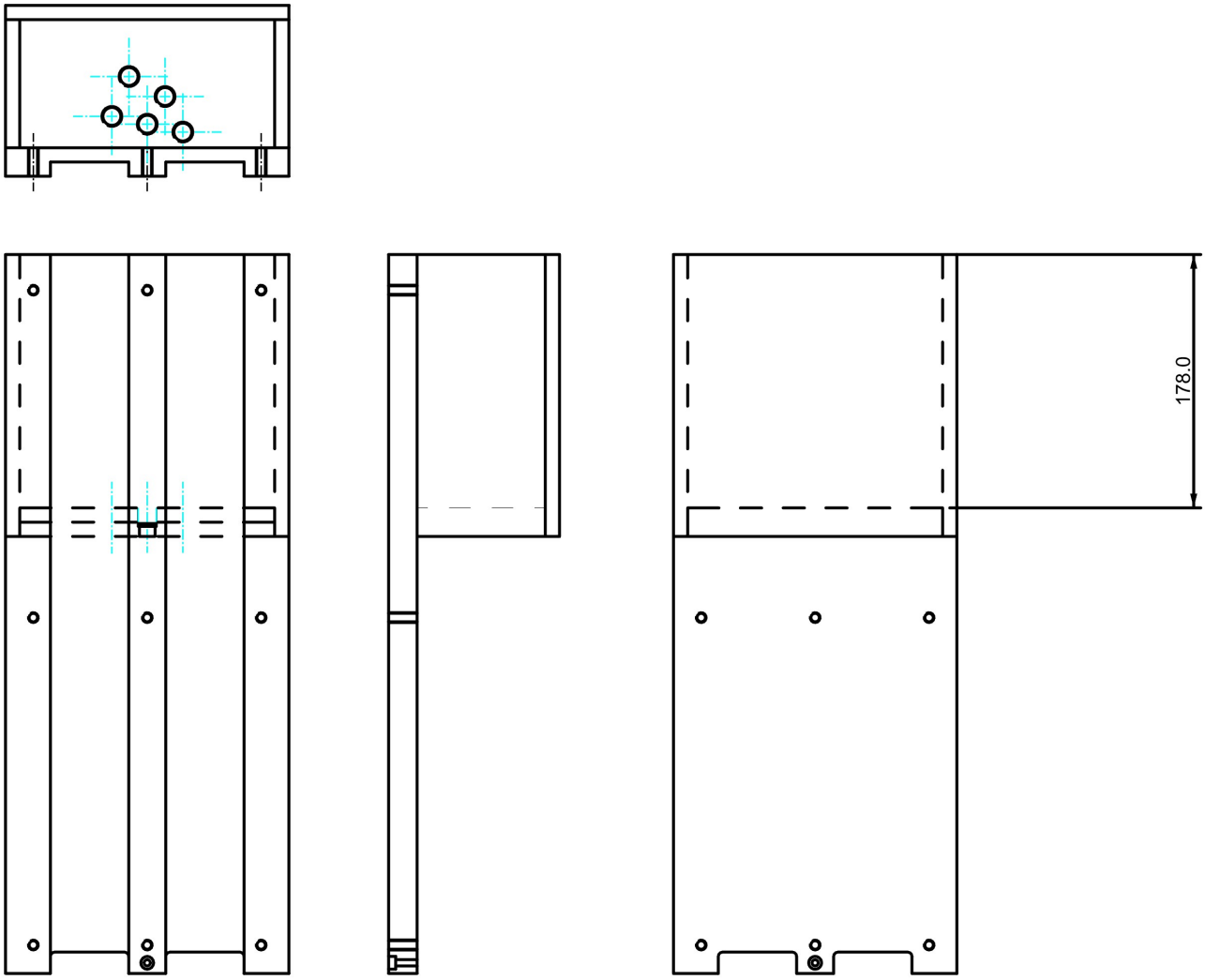

Figure 33: Overhang construction; This overhang construction is made of Polyvinyl chloride (pvc) of 10mm thick. In the top, back, side and frond view (top left to bottom right) the shape can be seen. Besides the shape, also the sensor locations, the attach points and the cable entries can be seen.

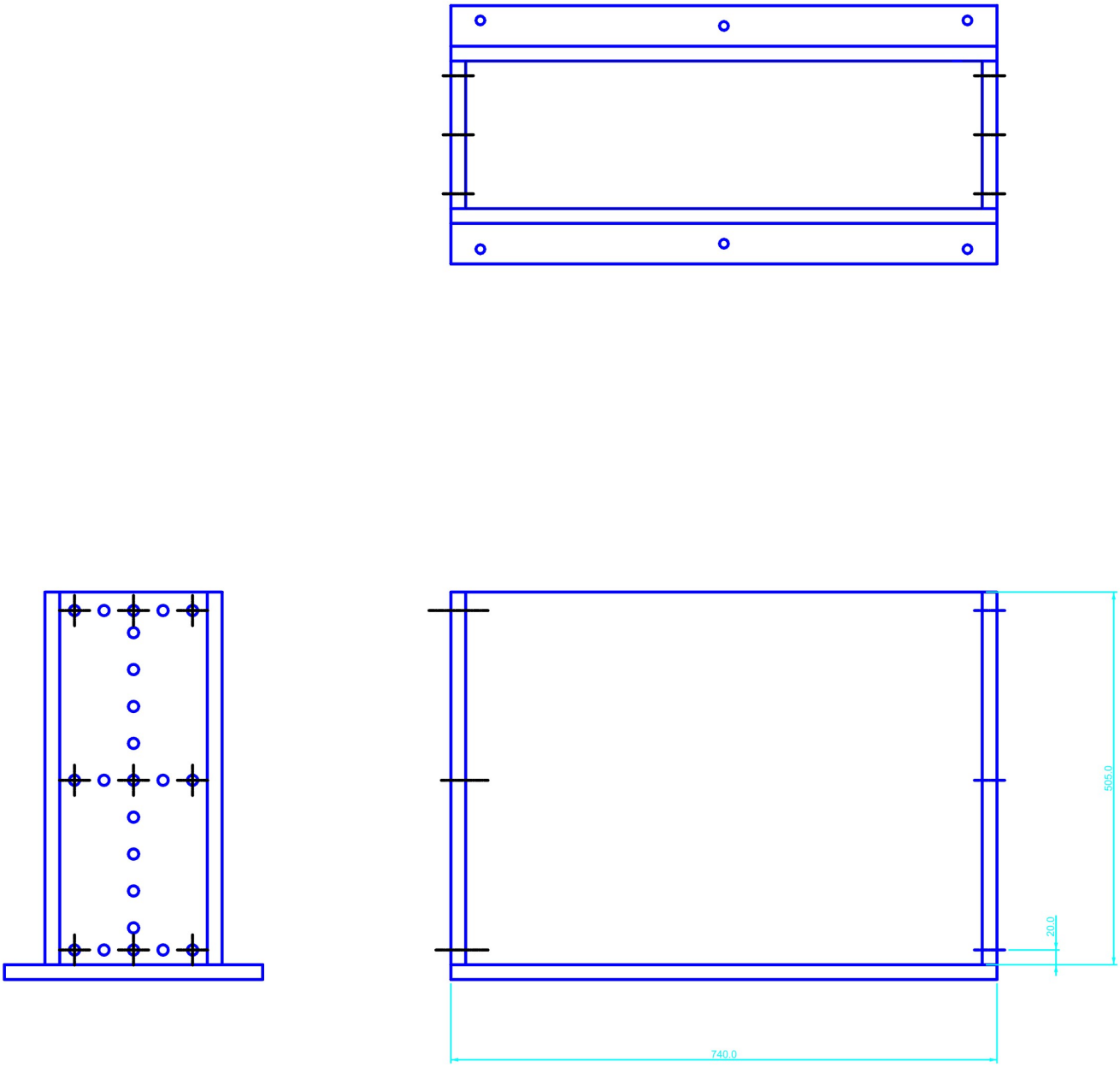

Figure 34: Tank dimensions; The tank that is used for the experiments is the designated tank of the sloshing rig. This tank is made of 20[mm] acrylic. In the tank, sensor openings are present that were used in previous experiments. These openings are now closed with blind bolts. 9 of those openings, marked in the drawing are used to secure the overhang construction to the tank.

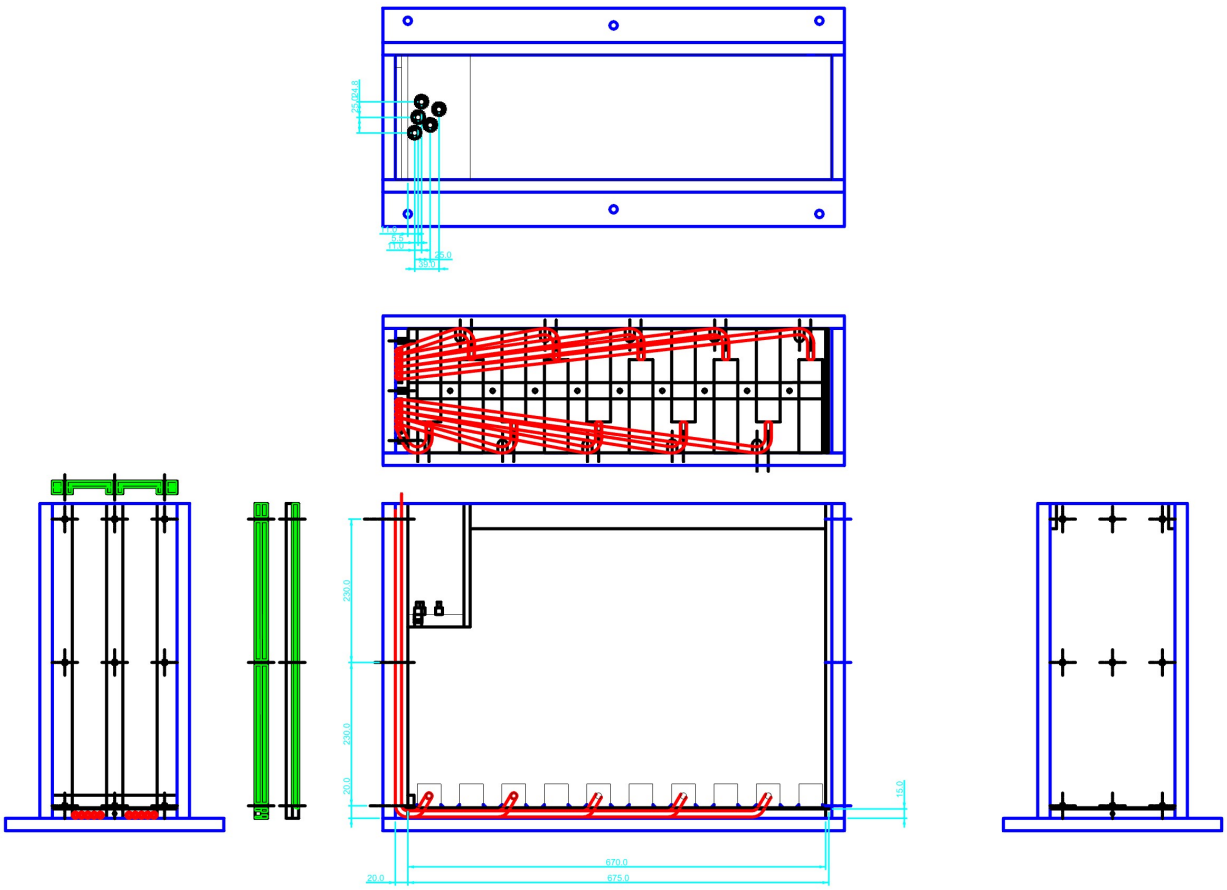

Figure 35: Experiment setup overview

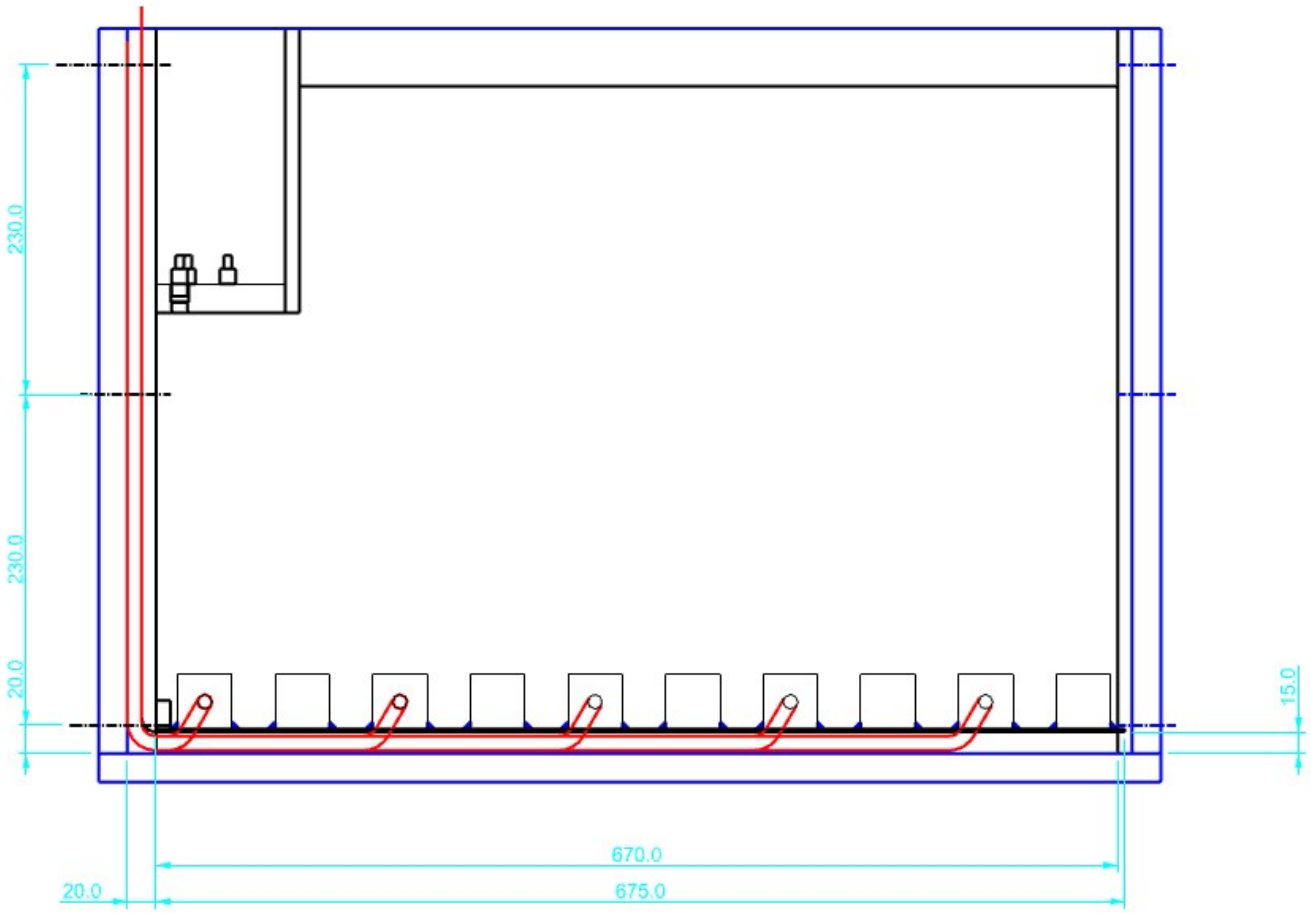

Figure 36: Experiment setup side view; the tank is designed in such a way that all the air hoses can be guided out side of the tank without letting the sloshing water feel a disturbance of the air hose it self. This means a dubble bottom must be created as wall a dubbel front wall. The air hoses are guided underneath the bottom plate and behind the front wall.

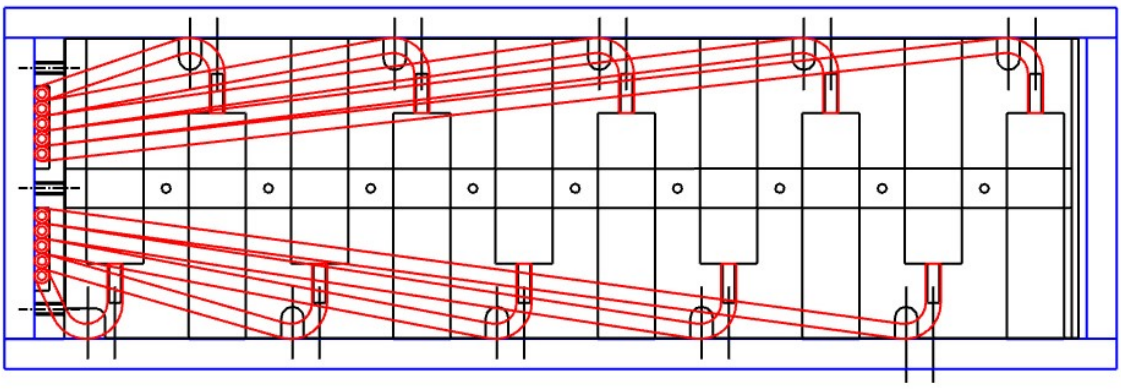

Figure 37: Experiment setup bottom view; The earlier mentioned bottom plate has 2 main reasons. The first one is that the air hoses can be guided outside of the tank with no interference with the sloshing water. The second reason is so the aeration stones can be glued to the structure without damaging the tank it self

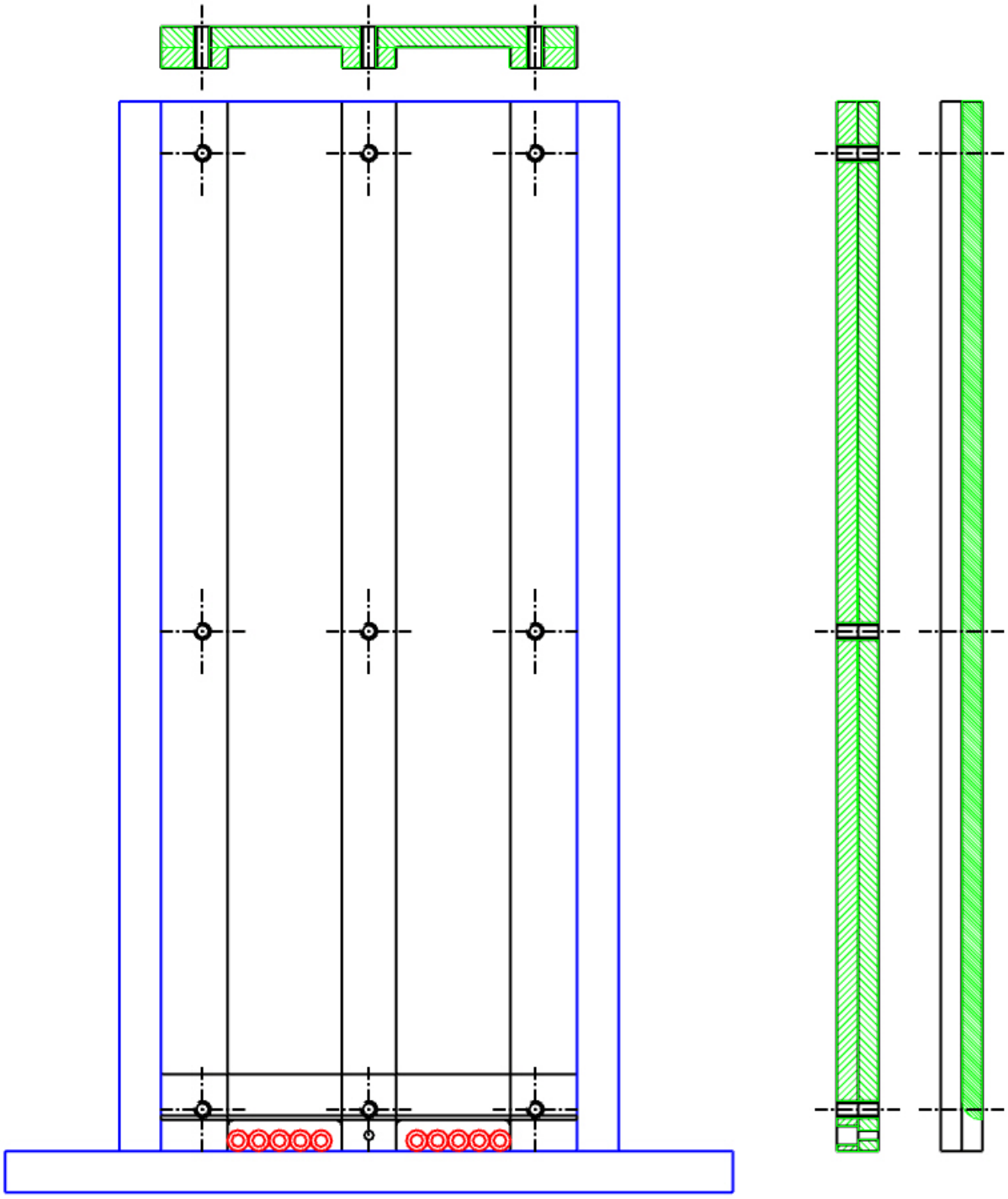

Figure 38: Experiment setup front view; In the front view the double front wall can be seen. The front wall is made of two 10mm thick pvc plates. The whole construction is secured with nine m8 bolts to the tank wall. Individual, the two plates are glued together with specialised pvc glue

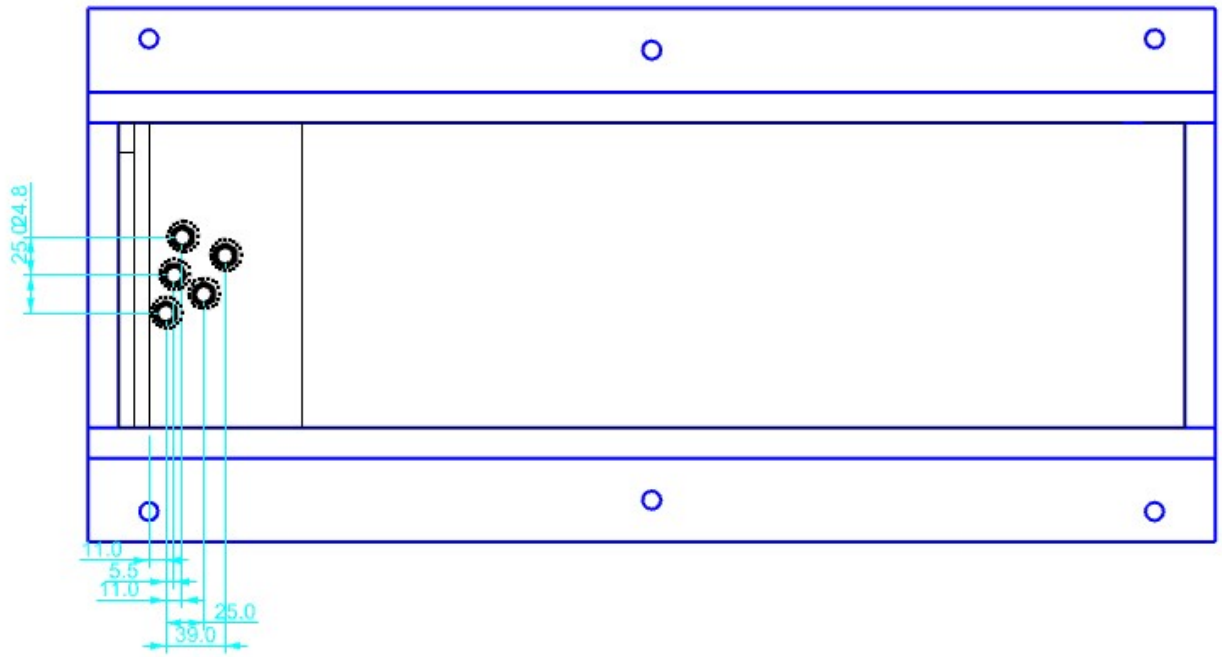

Figure 39: Experiment setup top view; In the top view the location of the sensor on the overhang can be seen. Also the 6 securing points of the tank at the side of the tank can be seen. With these securing points, the tank will be secured to the sloshing rig.

B Appendix B

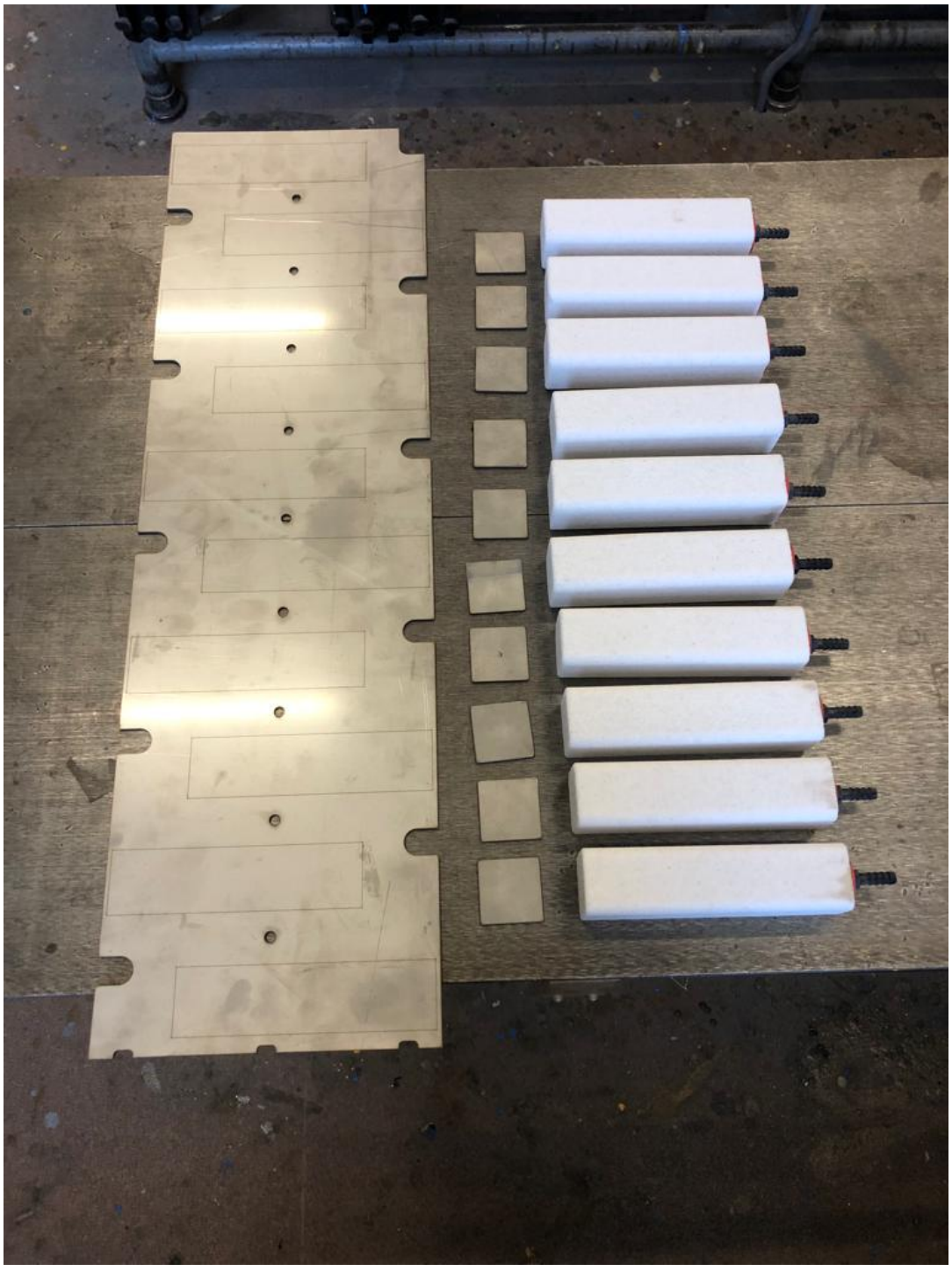

Figure 40: The bottom plate of the structure is made from a 2[mm] thick stainless steel plate. This plate is laser cut in the workshop of 3ME. In the bottom plate, openings for the air hoses (openings at the side of the plate), and openings for the bolts (the holes in the center line of the plate) are also cut with the laser cutter. On the locations where the aeration stones need to bee, a thin line is lasered in to the plate, so the installation will be more accurate. Besides the bottom plate, also ten 35[mm]x35[mm] plates are cut at the same time, these small plates will be glued to the aeration stones to prevent air from leaking from the side of the stones.

Figure 41: The overhang construction is made from Polyvinyl chloride. This was ordered as a 1[m]x2[m] plate with a thickness of 10[mm]. The first plan was to laser cut this plate as well. This would be very accurate and time efficient. But due to unforeseen limitations of the laser cutter, the construction must be saw by hand with the table saw.

Figure 42: With no accurate measuring system of the saw it self, all the measuring must be double checked by hand.

Figure 43: For smaller saw cuts, the bandsaw was used. Cutting in a straight line is more difficult, so only the small cuts where done here

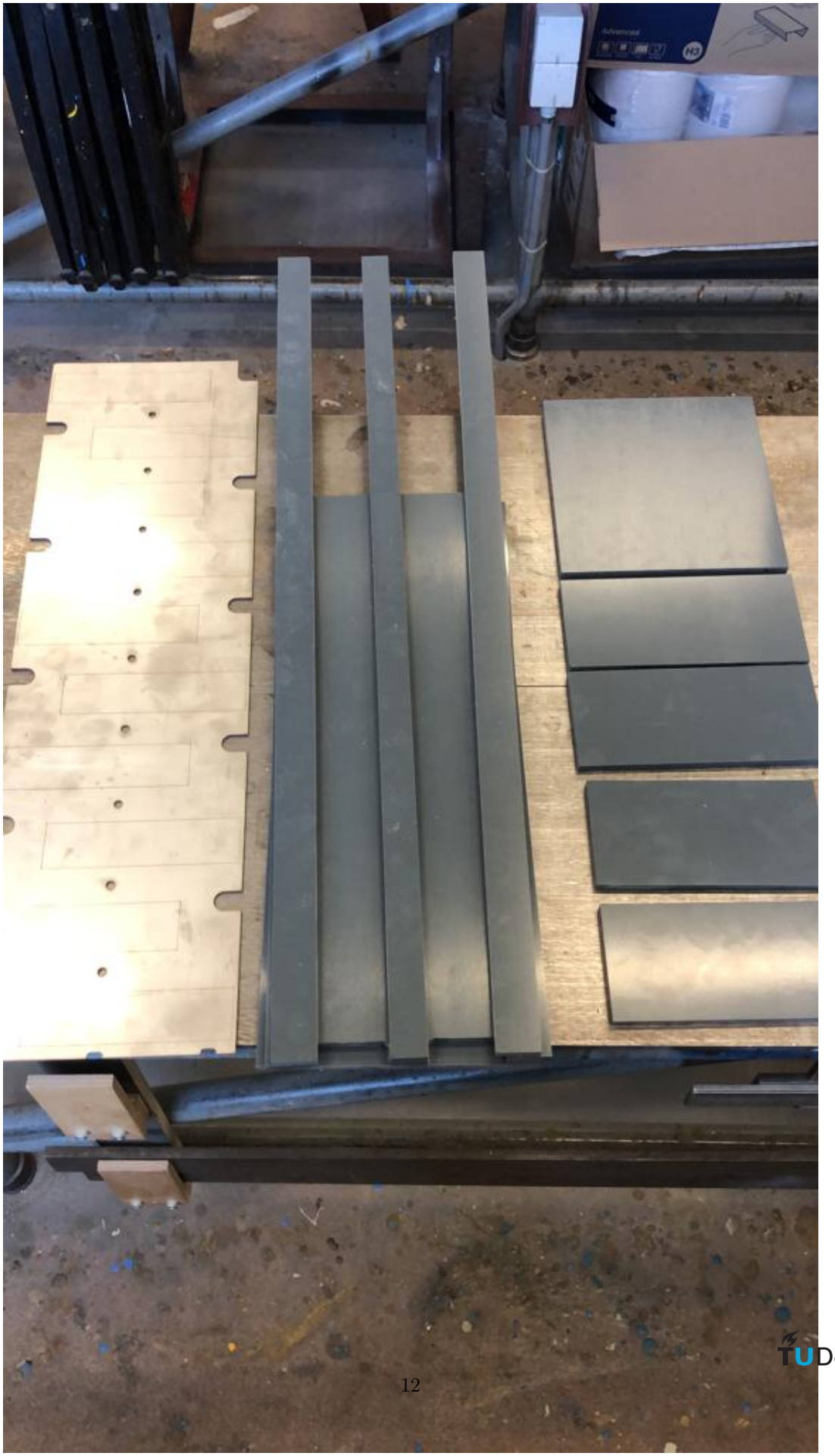

Figure 44: All the components for the construction are now finished. From here the assembly process can start. Before starting the assembly process, all individual pieces were measured again. From this measuring process, 2 pvc plate did not have the correct accuracy and therefore must be cut again.

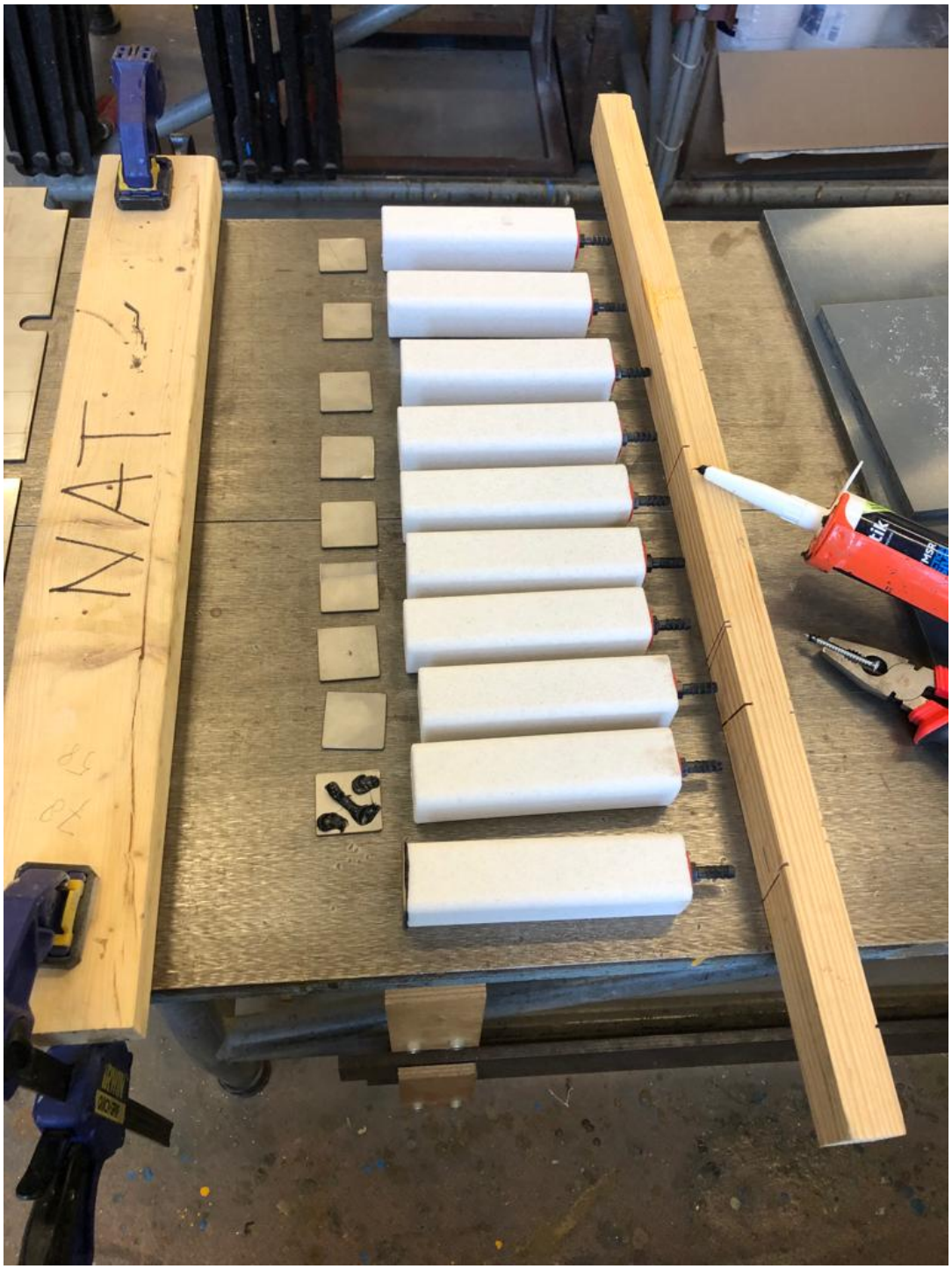

Figure 45: To prevent air from leaking close to the tank wall, and therefore blocking the visibility. end plates are glued at the end of each stone to prevent this from happening

(a) The glue is evenly distributed at the plate and at the stone, at all times there is one line of glue at the outside border of where the stone will be, this so any air leak will be sealed off.

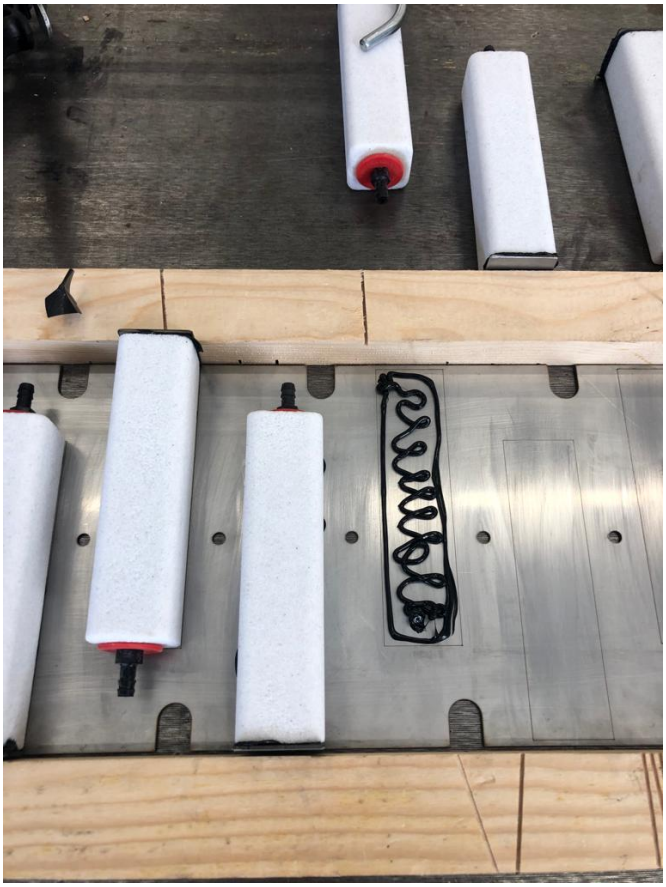

(b) On both sides of the bottom placed a wooden support is places so the aeration stones wouldn't accidentally move during the glue process. When the stone would move and will be sticking out at the outside border, the bottom plate will not fit in the tank any more

(a) The bottom part of the aeration stone is sealed with a extra fillet of glue. This to prevent air escaping from the bottom side of the stone

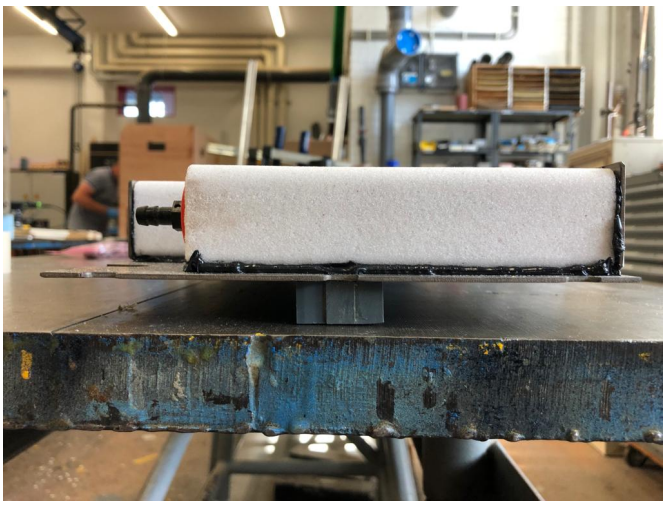

(b) The fillit only seals the bottom, and does not seal the side of the stone

Figure 48: The end result of all aeration stones glued to the bottom plate. The advice of the glue manufacture was followed, and the stones were not loaded with any force for 48 hours

(a) The drilling of the holes of the sensor is done at the milling machine. This is done because the 2 plates need the center of the sensor holes exactly on the same location.

(b) Because the second plate needs a m14 fine tread, the plates could not be glued first and drilled after. This is the reason that it is done at a milling machine with a digital measuring system with a accuracy of 1/1000 mm

(a) The bottom part of the sensor plate is a plate with a precise fit for the bottom part of the sensor. This has extra edge cut out of the material so the sensor will fit in perfectly. This extra edge is designed so the sensor can not fall trough the object.

(b) The top plate has a m14 fine tread in the material so the sensor can be screwed in to place. This special hollow bolt, is designed for the sensor and prevent the sensor from moving upwards when a wave hits the overhang and the sensor.

Figure 51: The gluing process started with the back plate and the 2 side walls, these were supported by 2 exactly 90 degrees objects so the construction did not become wider than the tank.

Figure 52: Secondly the most important plate was glued in to place

Figure 53: When gluing the horizontal overhang plate in to place, the angle of the overhang must be 90 degrees over the whole width of the tank.

(a)

(b)

(c) The end result of all the lose components build in to the tank.

C Appendix C

Appendix C consist of the pressures during the experiments. Each figure has 5 sub figures, representing pressure sensor 1 until 5. All the subsections have 5 figures, these figures represents the 0, 1.0, 1.5, 2 and 4% aeration during the experiments. The 5 sub sections represents different frequency that are used for the experiment.

C.1 Frequency 0.93 Hz

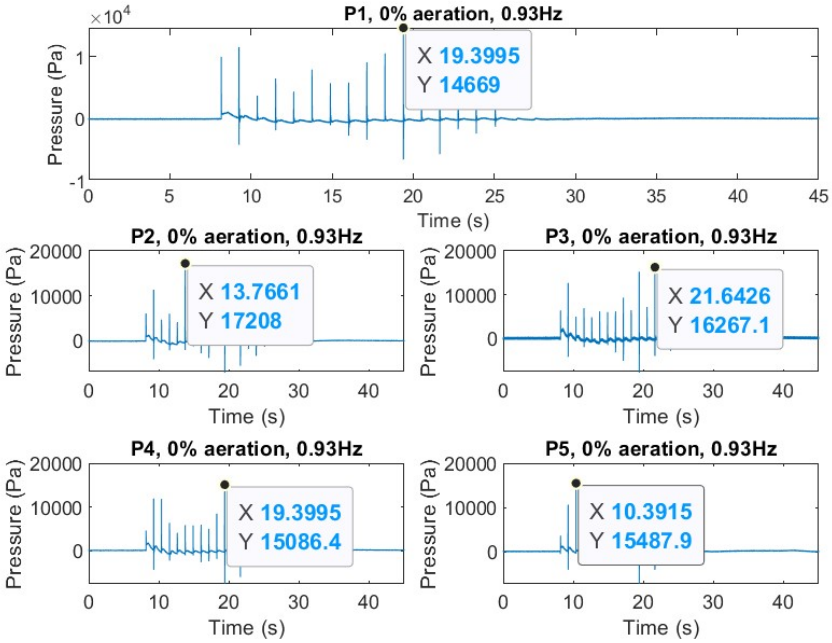

Figure 55: Pressures of all 5 sensor

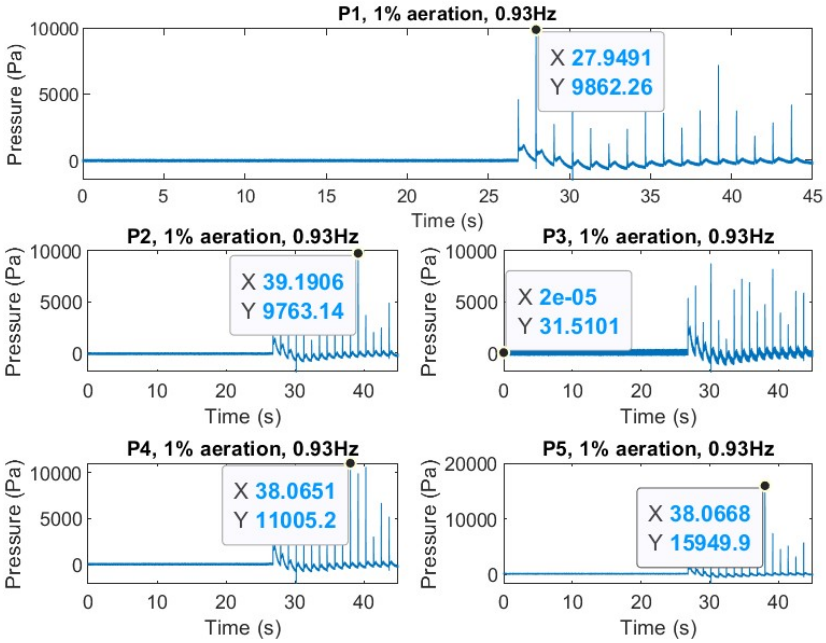

Figure 56: Pressures of all 5 sensor

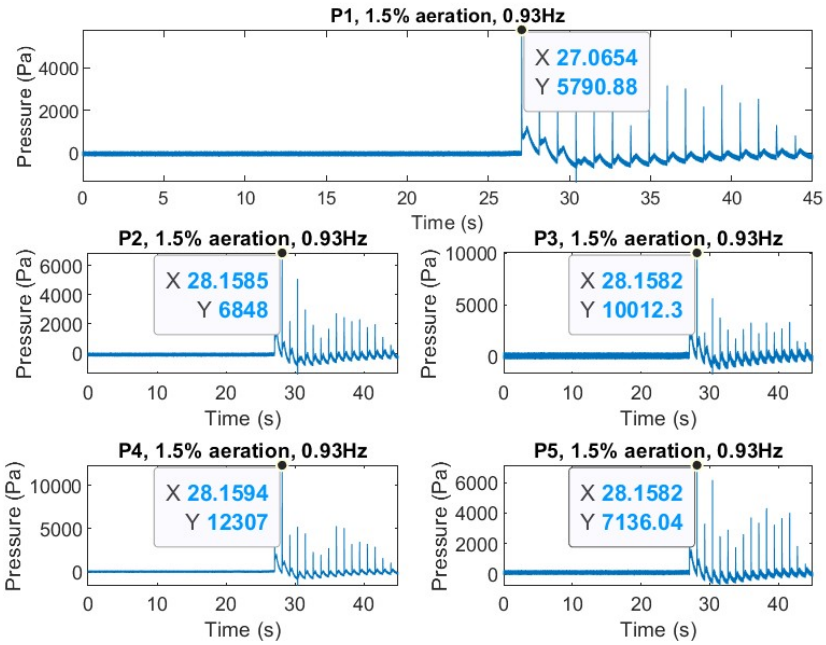

Figure 57: Pressures of all 5 sensor

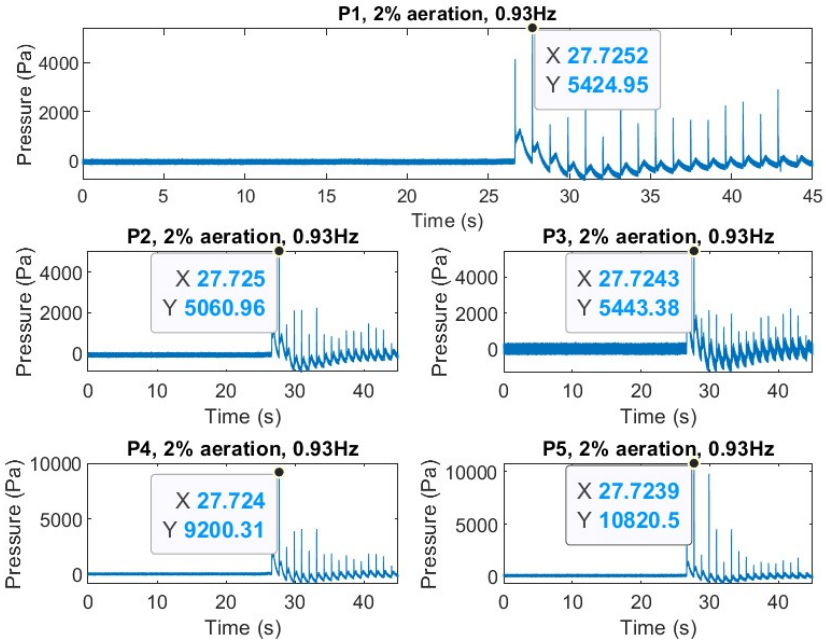

Figure 58: Pressures of all 5 sensor

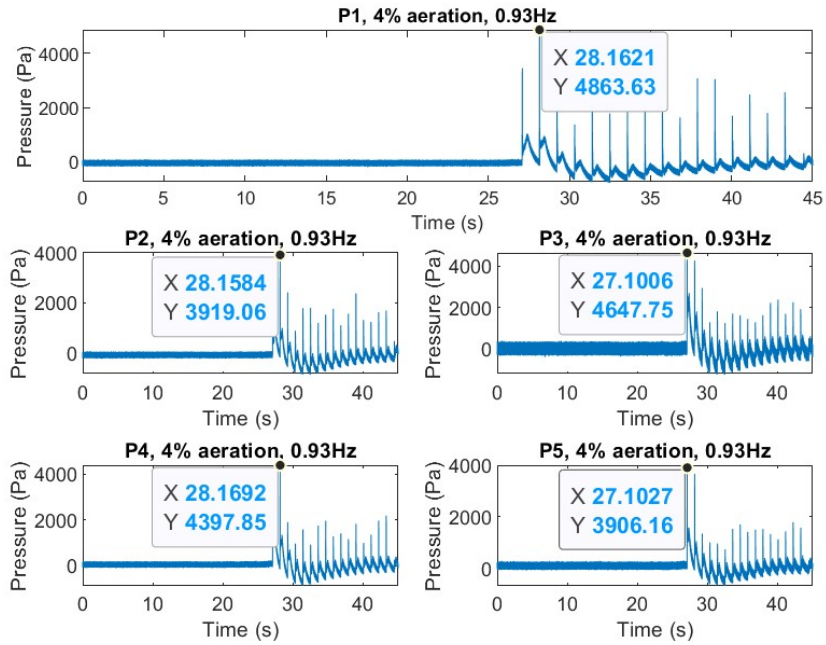

Figure 59: Pressures of all 5 sensor

C.2 Frequency 0.94Hz

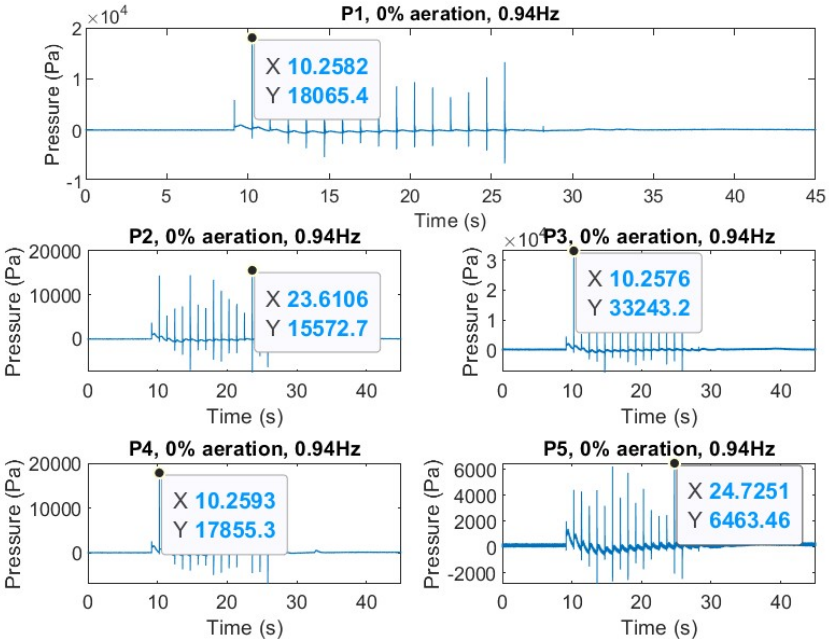

Figure 60: Pressures of all 5 sensor

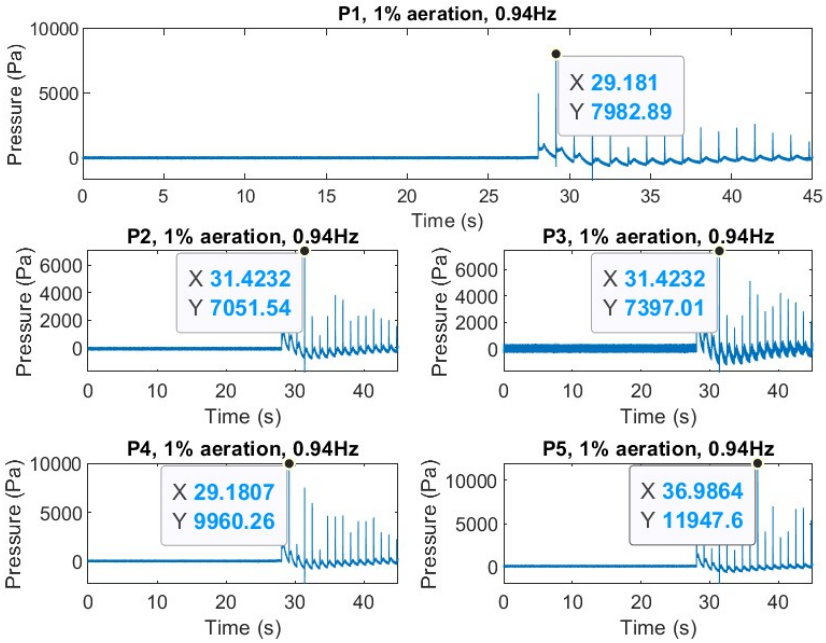

Figure 61: Pressures of all 5 sensor

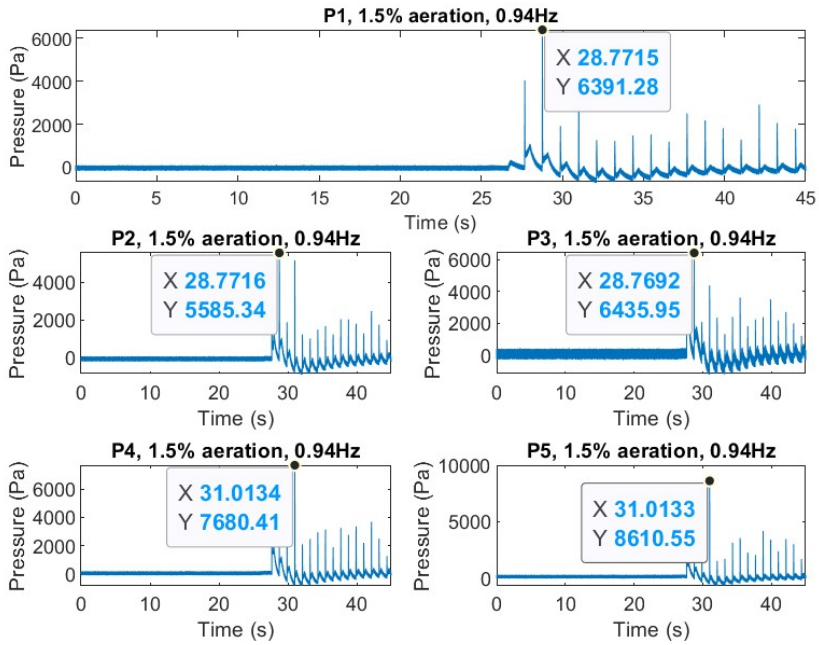

Figure 62: Pressures of all 5 sensor

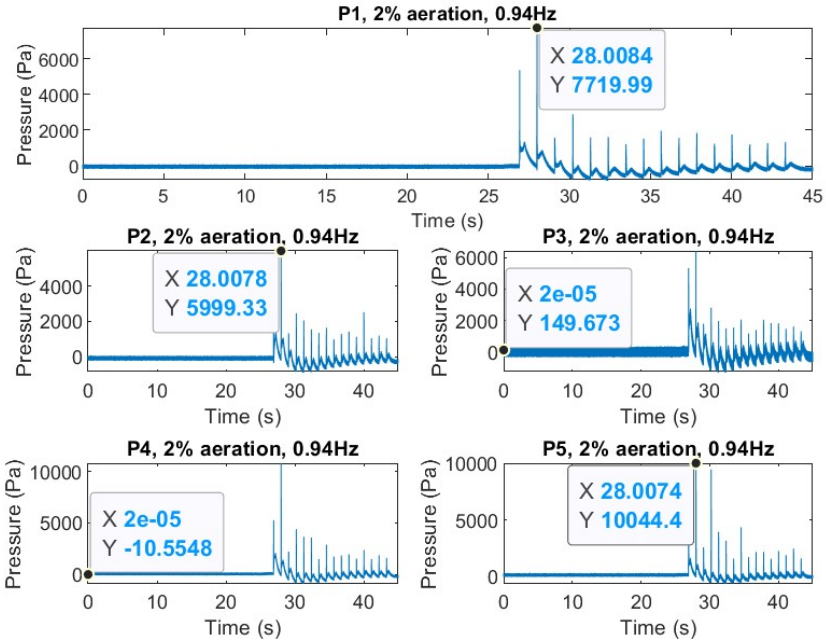

Figure 63: Pressures of all 5 sensor

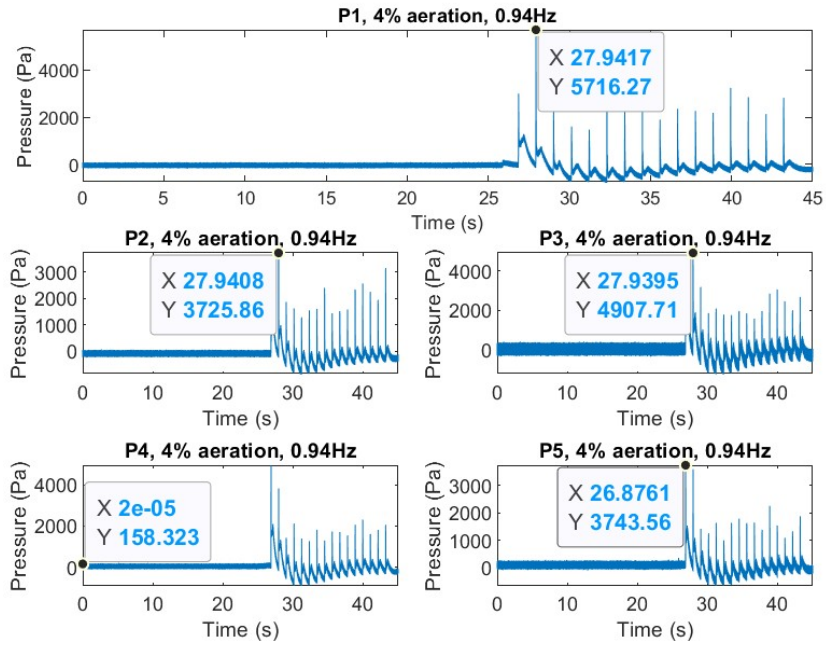

Figure 64: Pressures of all 5 sensor

C.3 Frequency 0.95Hz

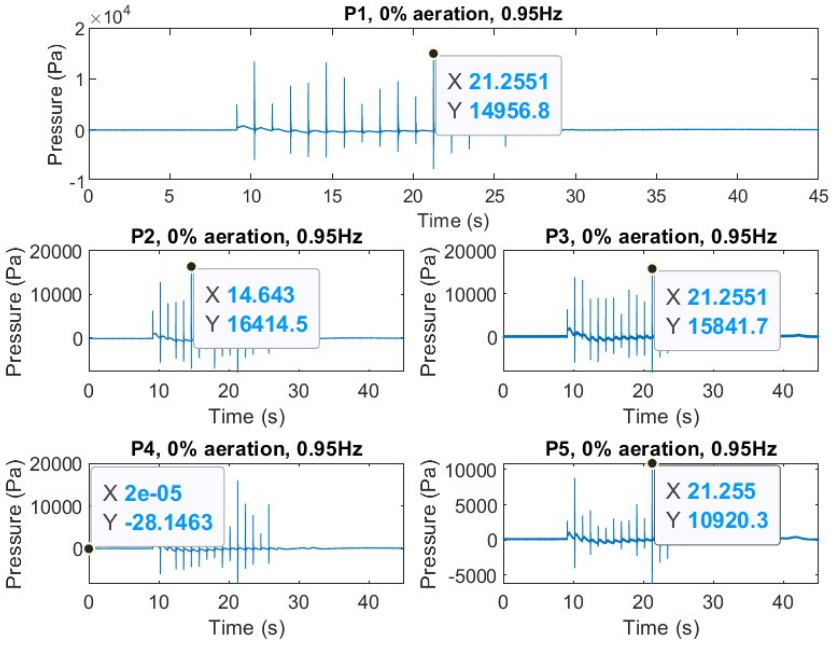

Figure 65: Pressures of all 5 sensor

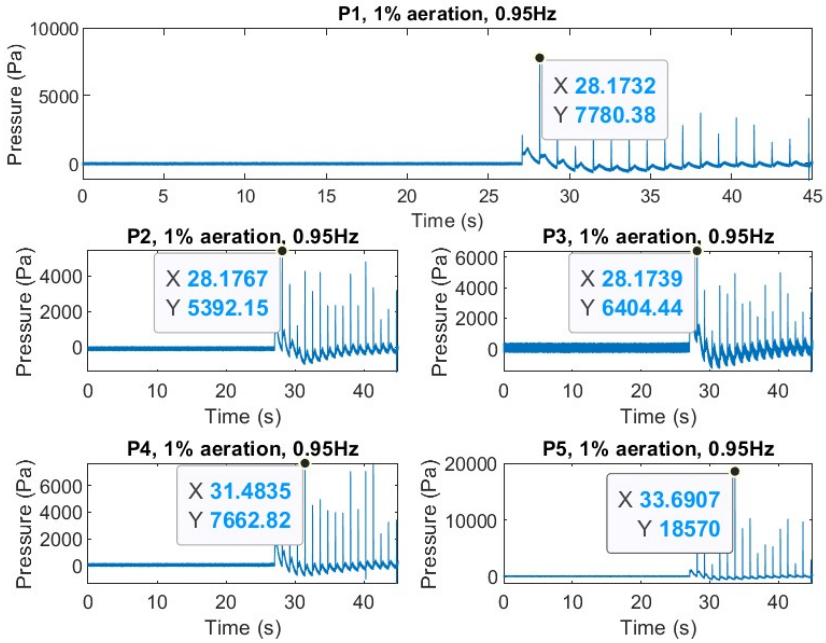

Figure 66: Pressures of all 5 sensor

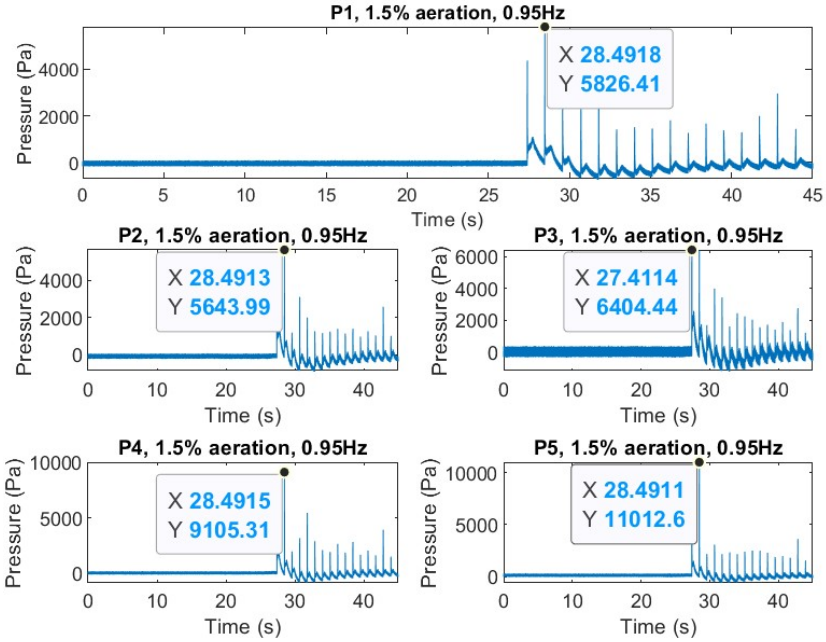

Figure 67: Pressures of all 5 sensor

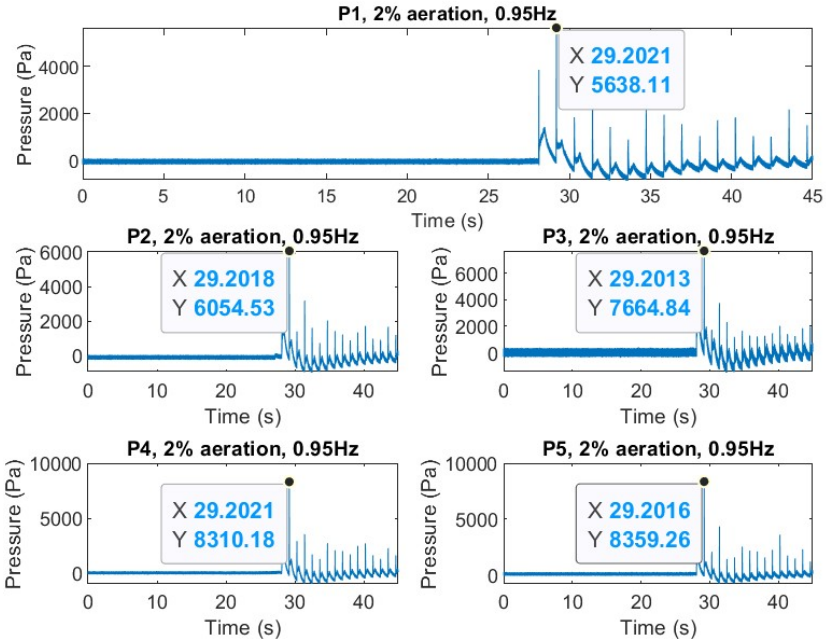

Figure 68: Pressures of all 5 sensor

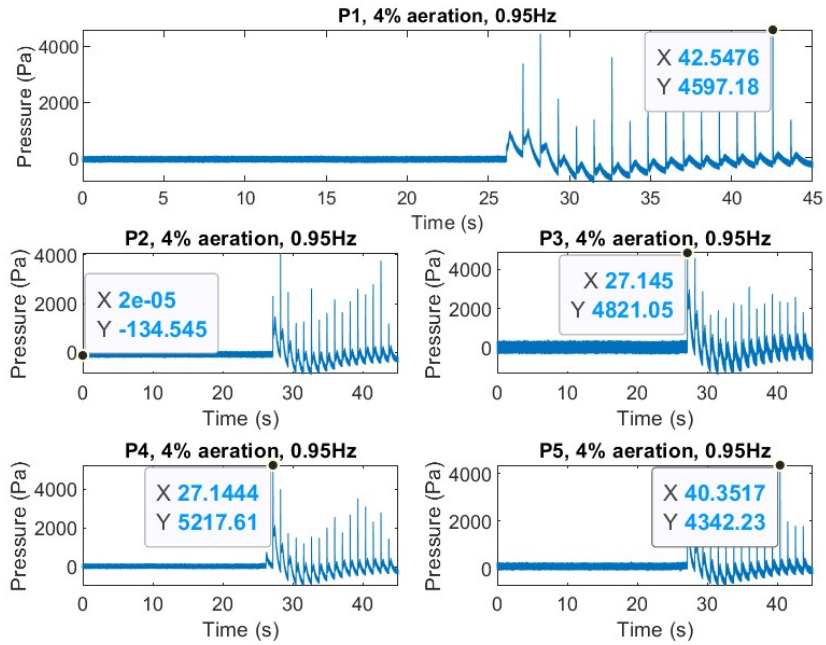

Figure 69: Pressures of all 5 sensor

C.4 Frequency 0.96Hz

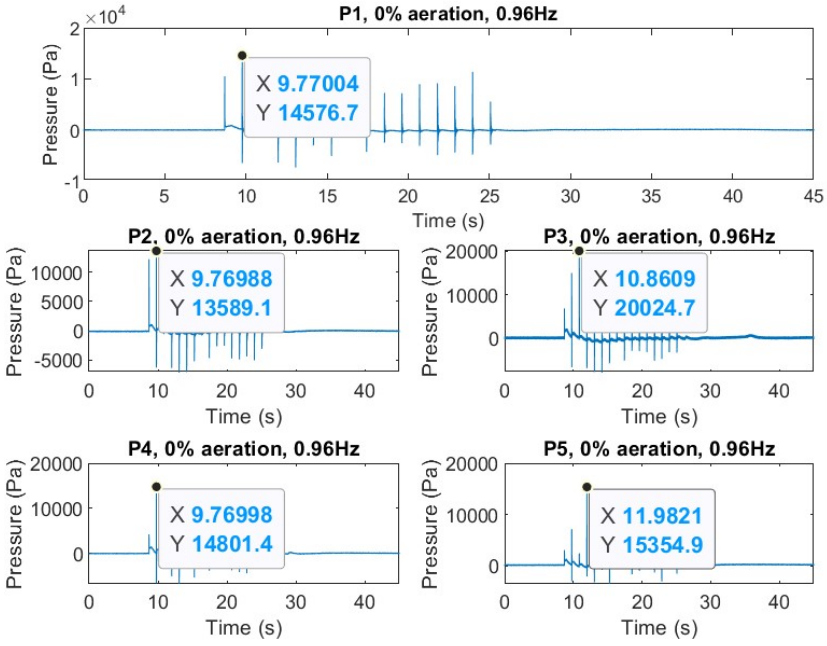

Figure 70: Pressures of all 5 sensor

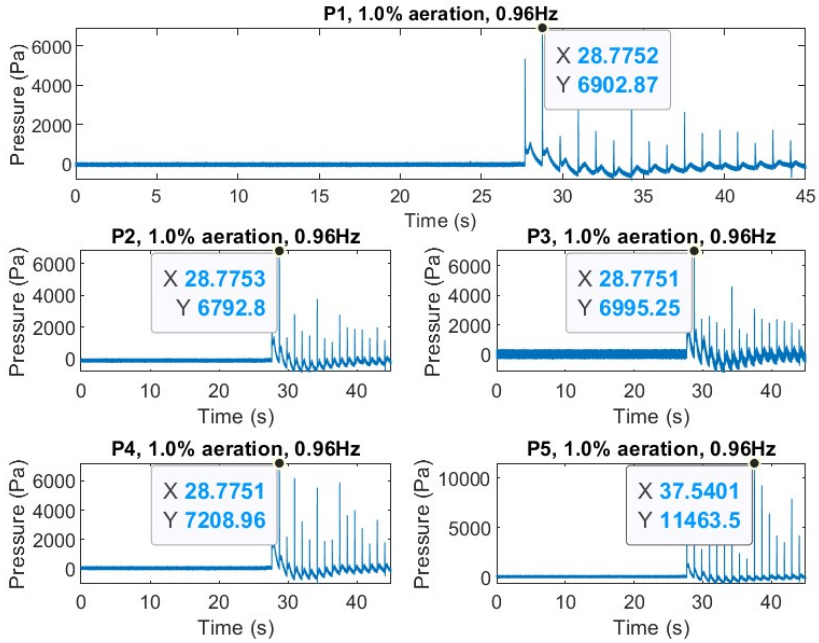

Figure 71: Pressures of all 5 sensor

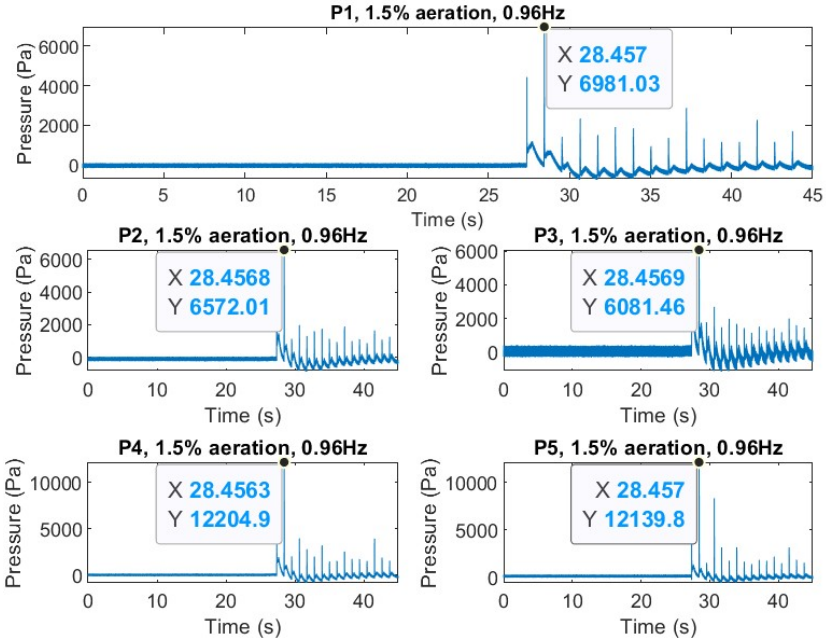

Figure 72: Pressures of all 5 sensor

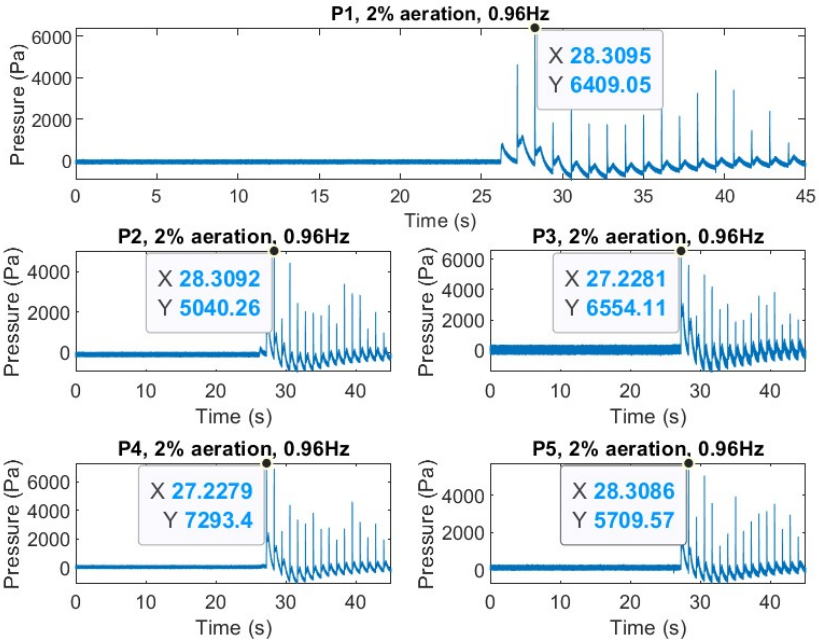

Figure 73: Pressures of all 5 sensor

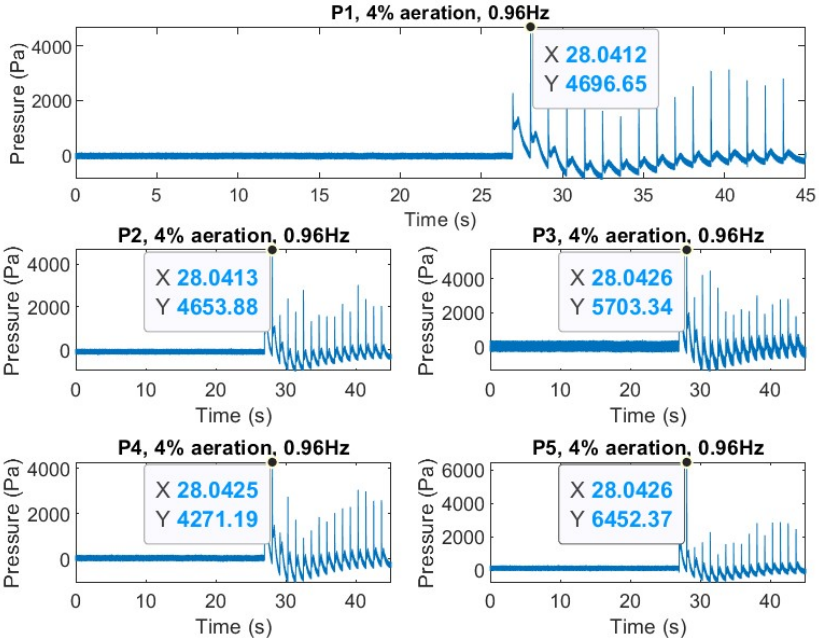

Figure 74: Pressures of all 5 sensor

C.5 Frequency 0.97Hz

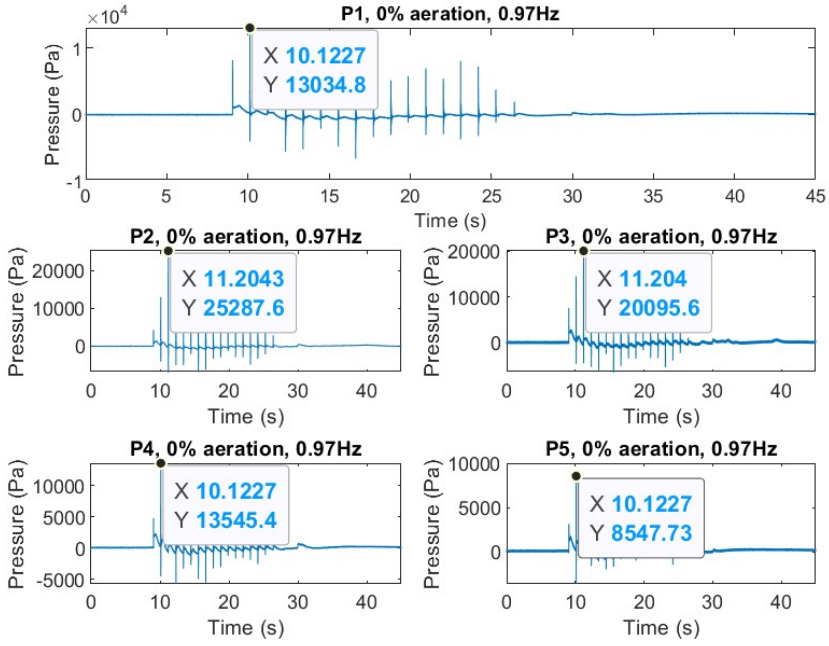

Figure 75: Pressures of all 5 sensor

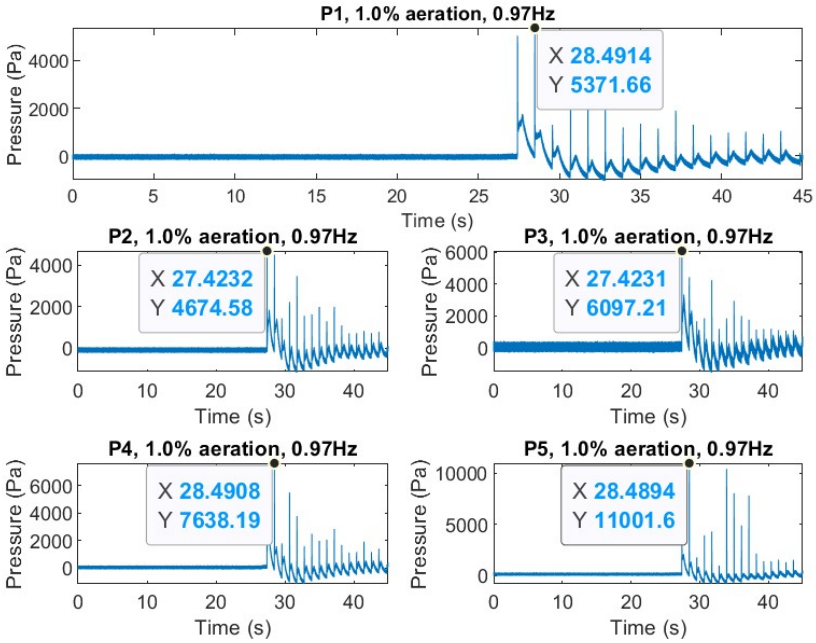

Figure 76: Pressures of all 5 sensor

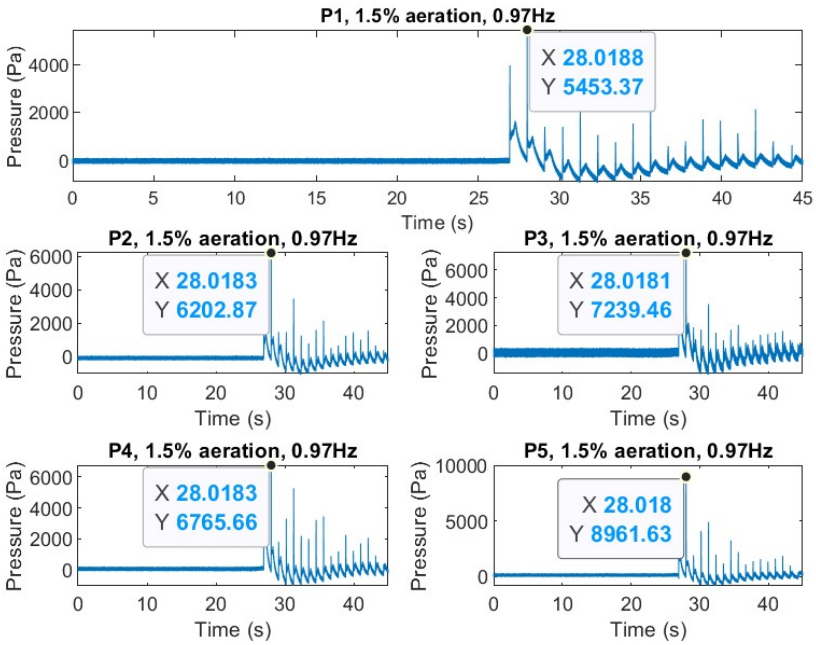

Figure 77: Pressures of all 5 sensor

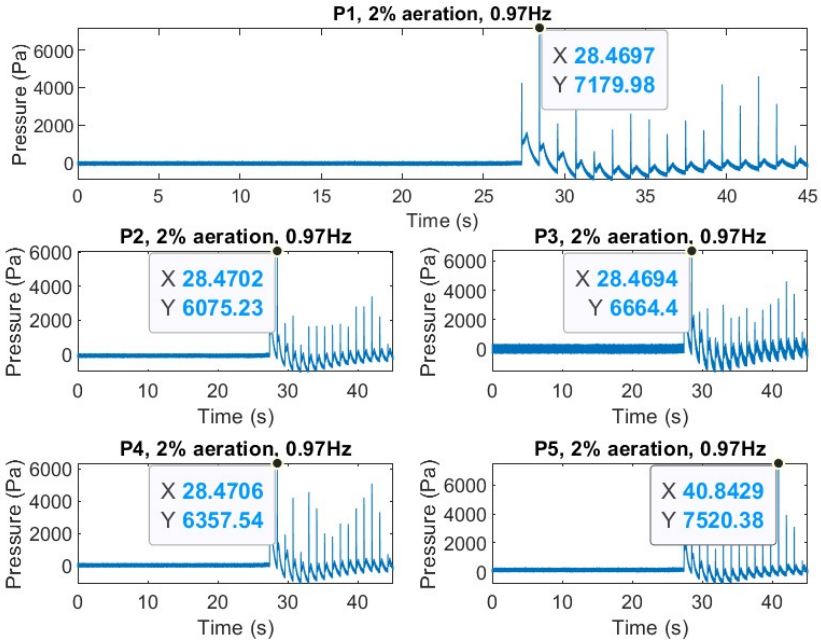

Figure 78: Pressures of all 5 sensor

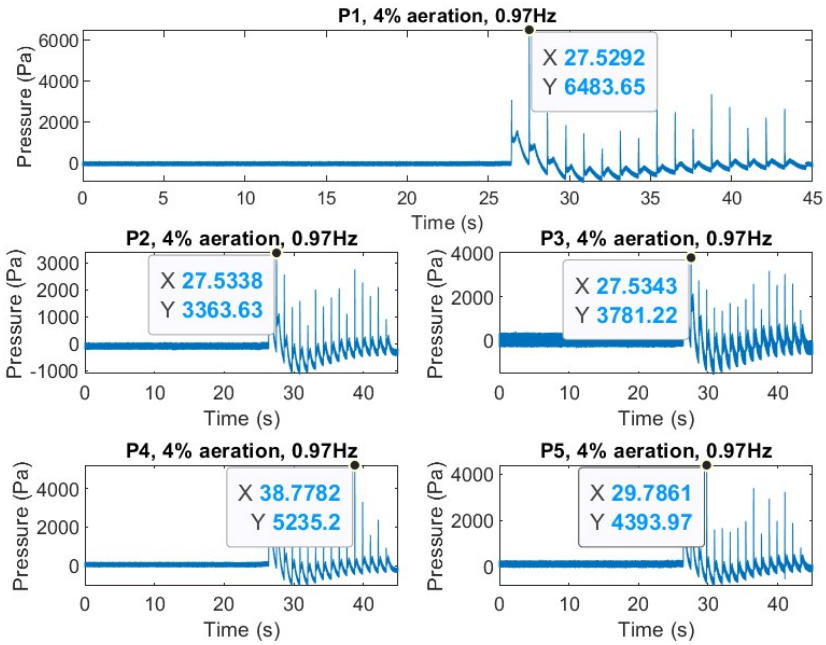

Figure 79: Pressures of all 5 sensor

D Appendix D

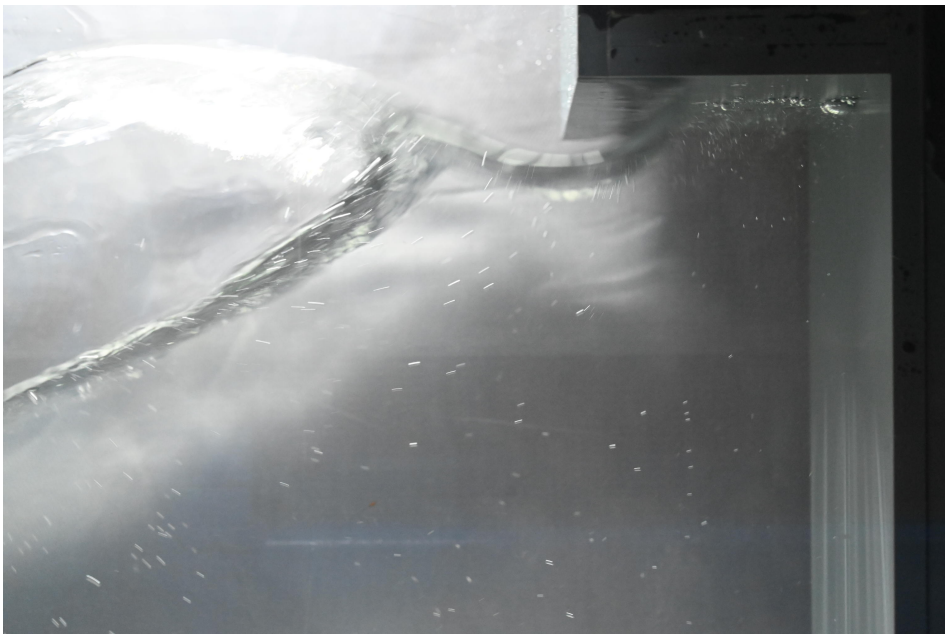

Figure 80: These full scale pictures corresponding to Figure 29

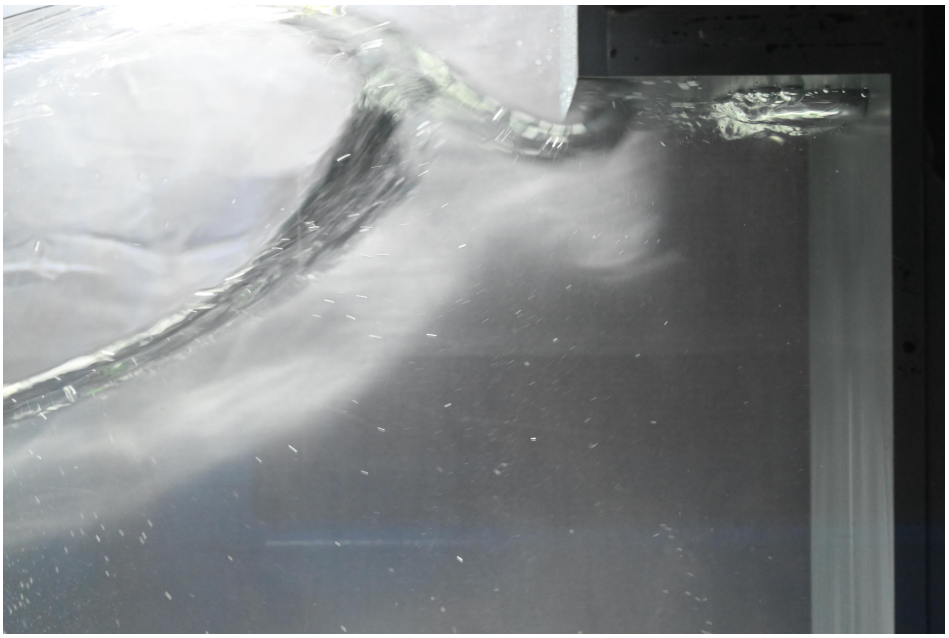

Figure 81: These full scale pictures corresponding to Figure 29

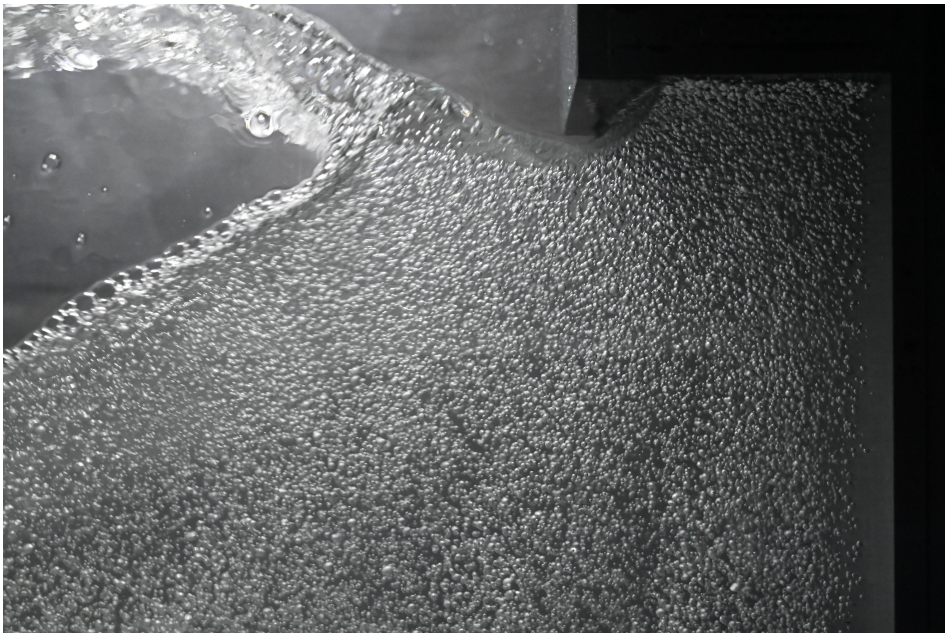

Figure 82: These full scale pictures corresponding to Figure 30

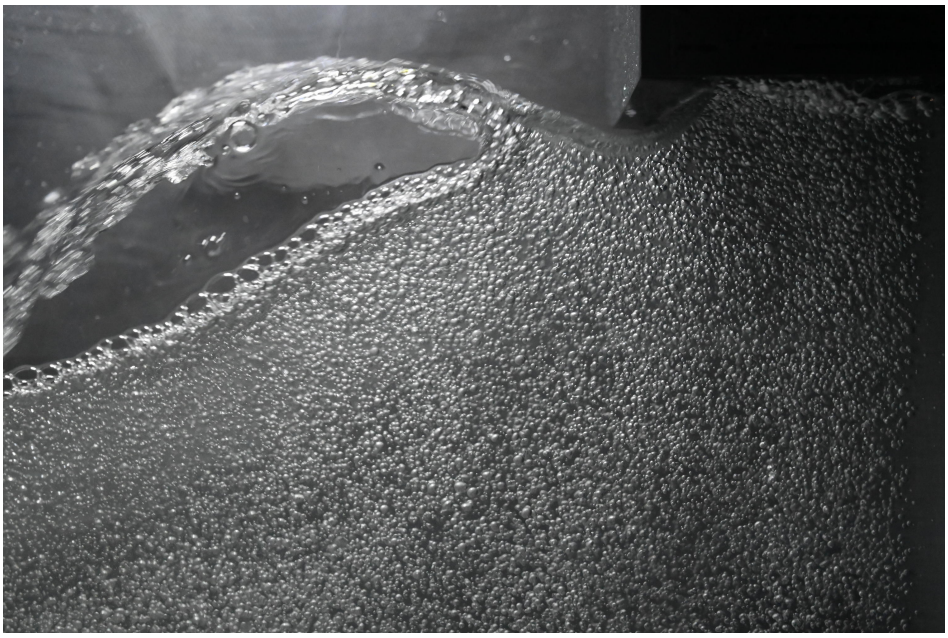

Figure 83: These full scale pictures corresponding to Figure 30

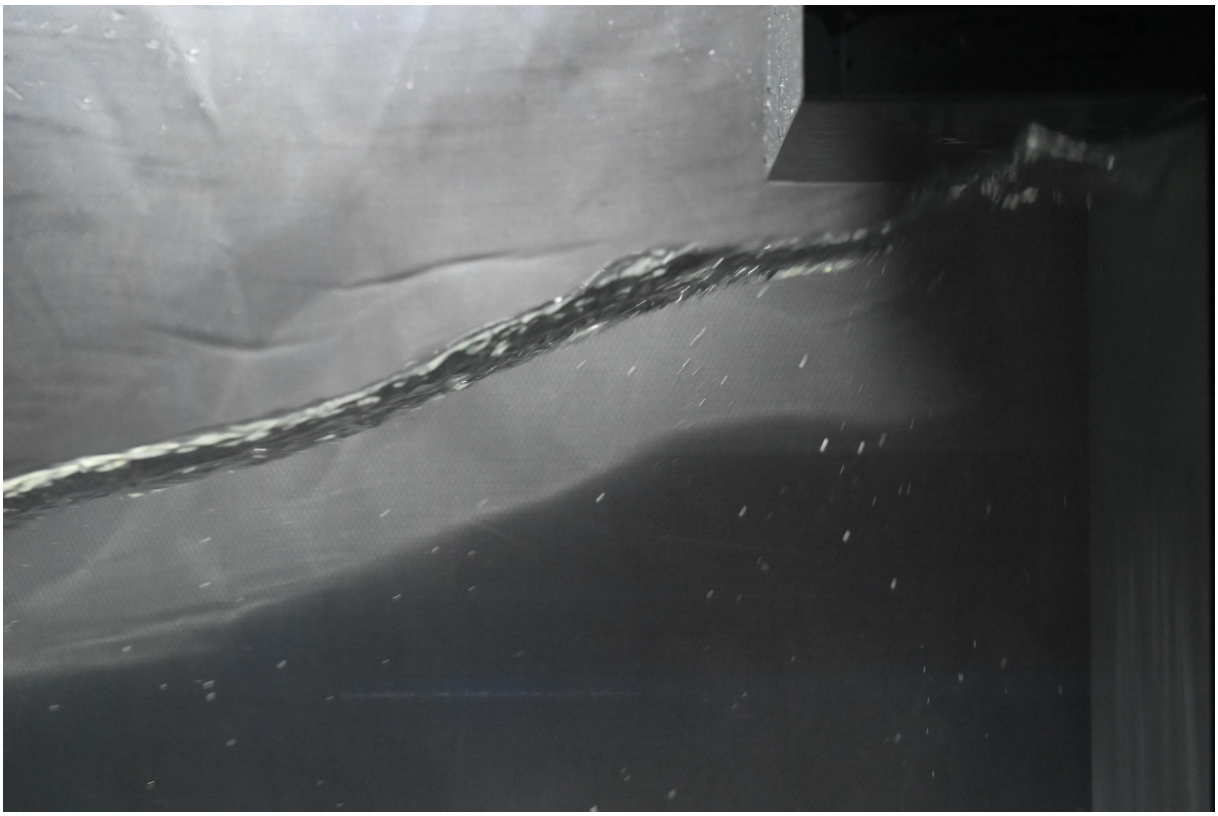

(a) These full scale pictures corresponding to Figure 31

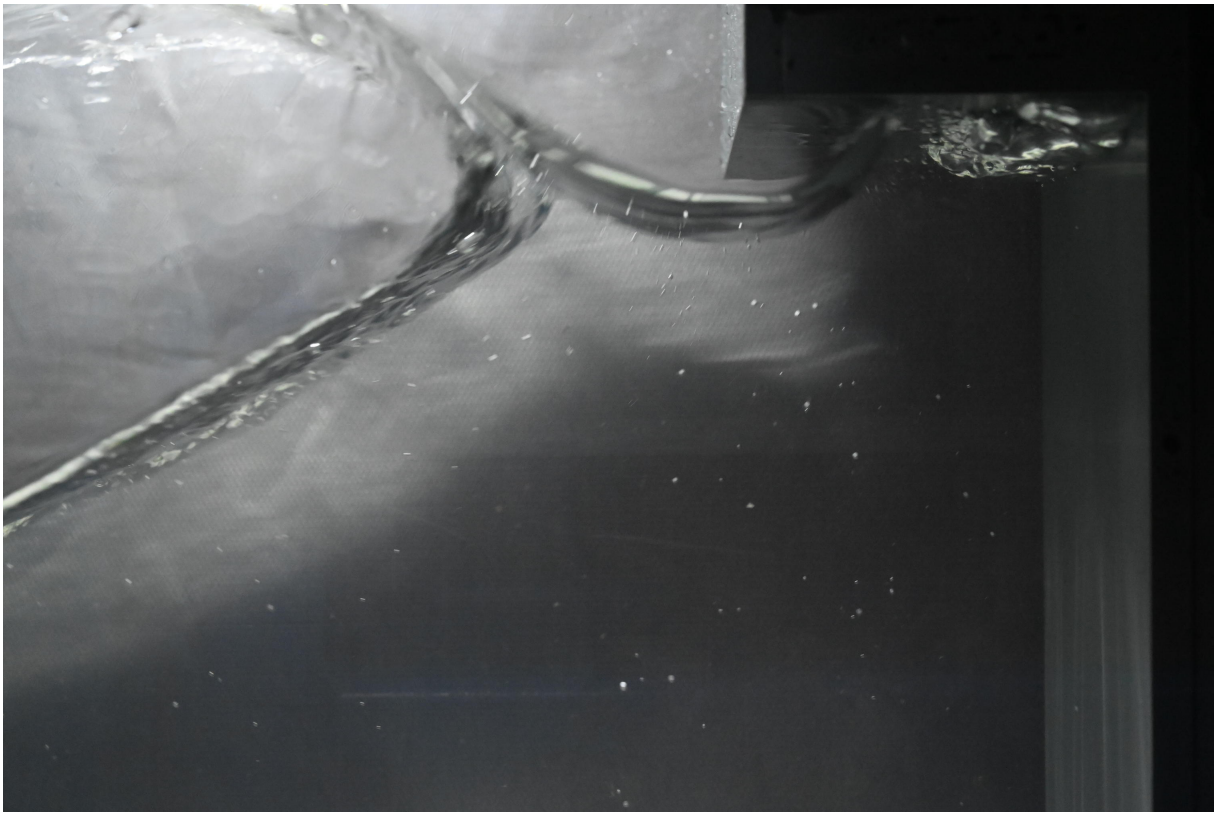

(b) These full scale pictures corresponding to Figure 31

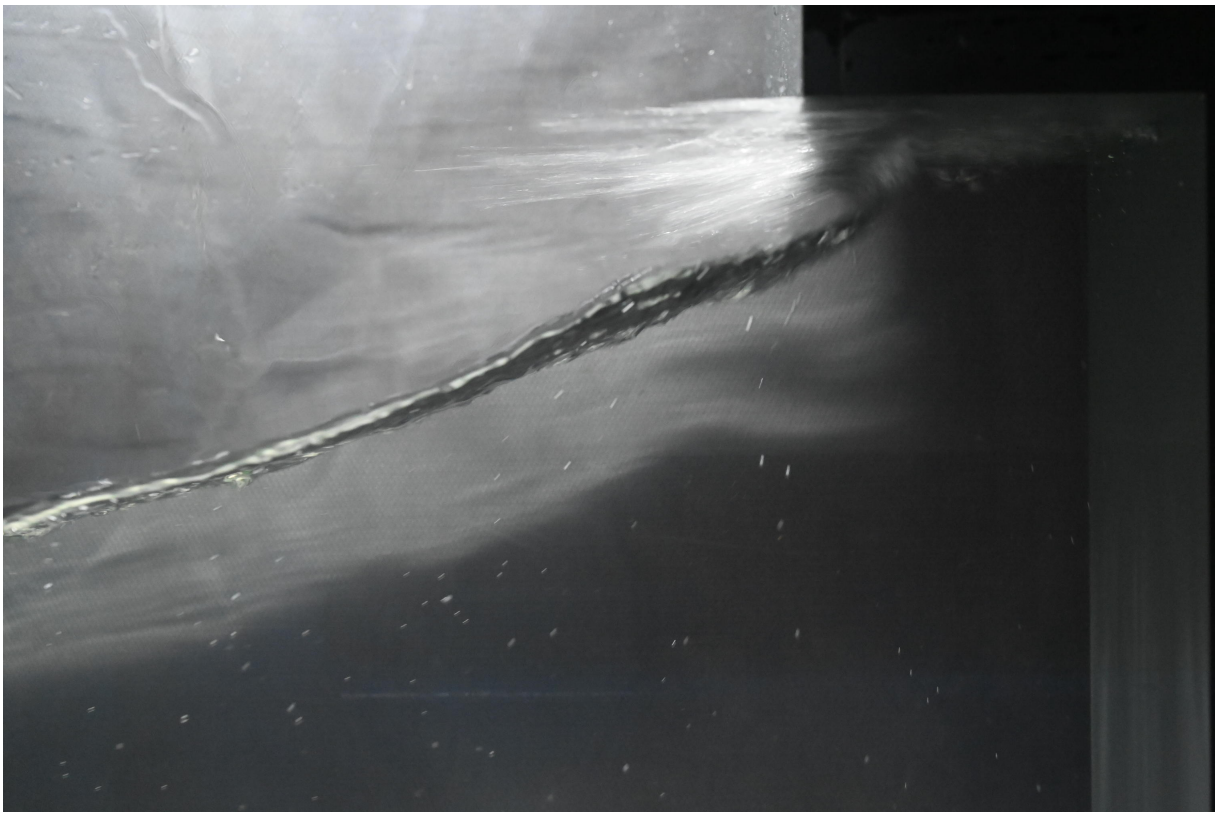

(a) These full scale pictures corresponding to Figure 31

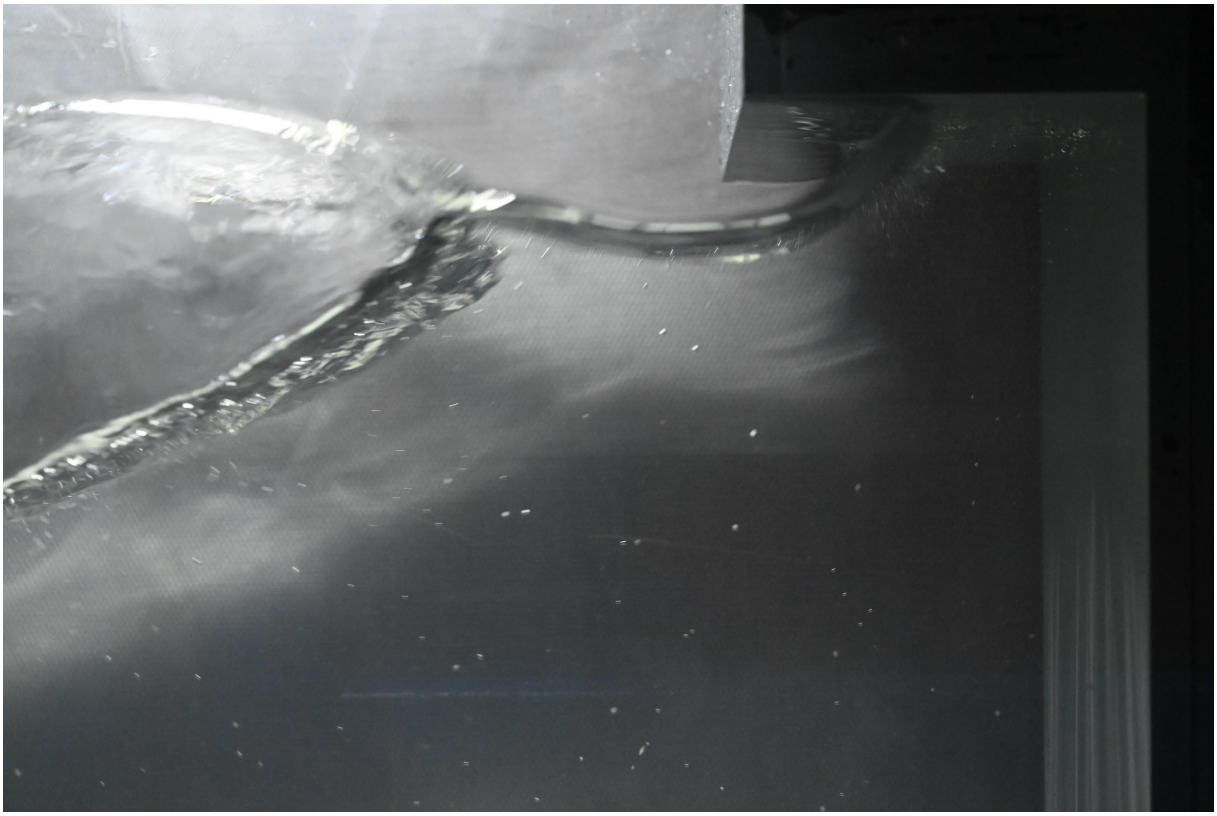

(b) These full scale pictures corresponding to Figure 31

(a) These full scale pictures corresponding to Figure 32

(b) These full scale pictures corresponding to Figure 32

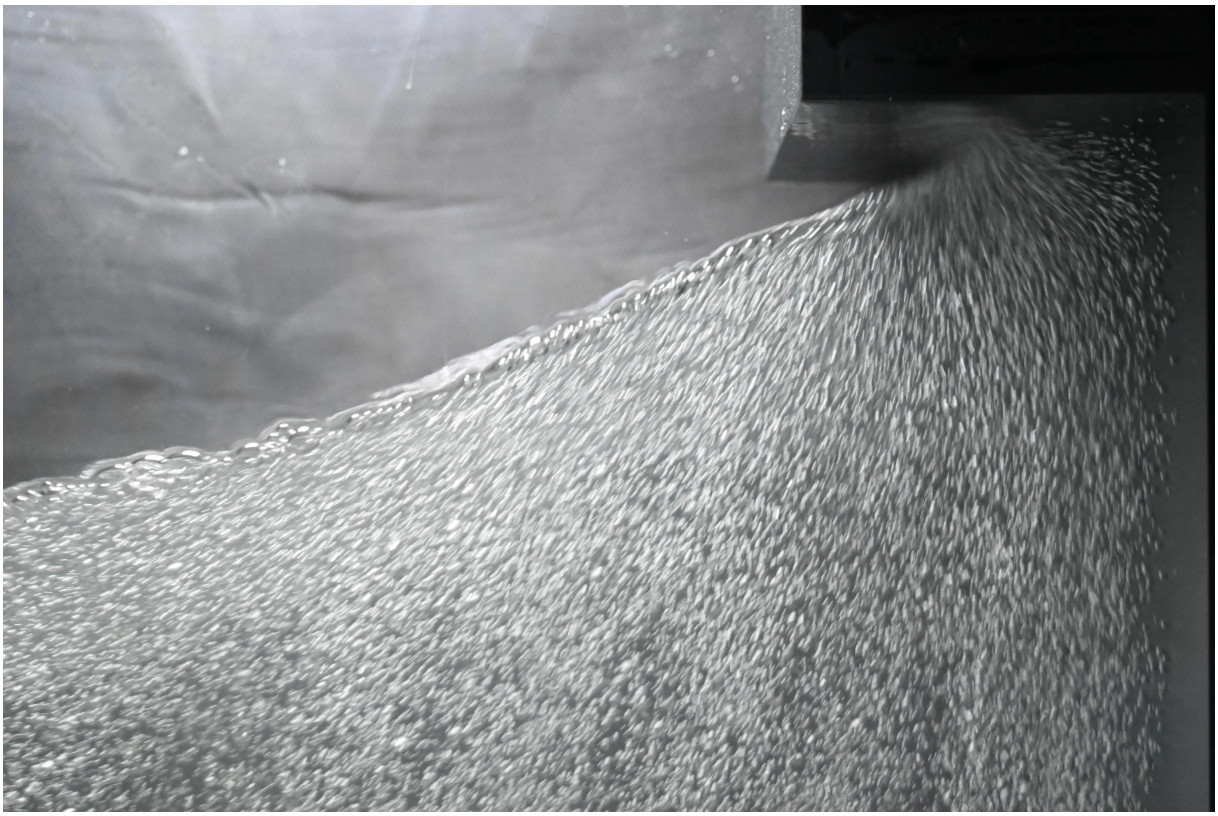

(a) These full scale pictures corresponding to Figure 32

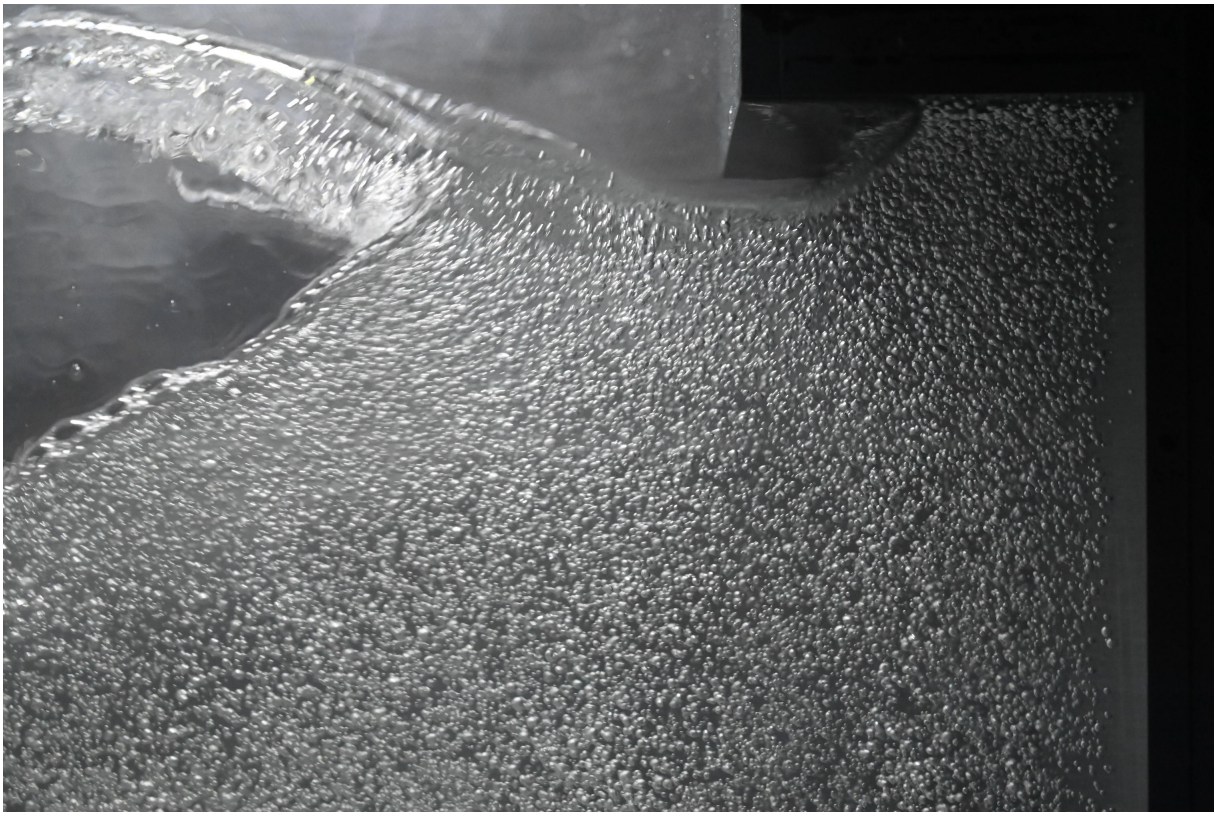

(b) These full scale pictures corresponding to Figure 32